Universitat Autònoma de Barcelona

Novel digital neuropathology methods applied to neurodegenerative diseases

Marta Querol Vilaseca

ADVERTIMENT. L'accés als continguts d'aquesta tesi queda condicionat a l'acceptació de les condicions d'ús establertes per la següent llicència Creative Commons: http://cat.creativecommons.org/?page_id=184

ADVERTENCIA. El acceso a los contenidos de esta tesis queda condicionado a la aceptación de las condiciones de uso establecidas por la siguiente licencia Creative Commons: http://es.creativecommons.org/blog/licencias/

WARNING. The access to the contents of this doctoral thesis it is limited to the acceptance of the use conditions set by the following Creative Commons license: https://creativecommons.org/licenses/?lang=en

Doctoral thesis

Novel digital neuropathology methods applied to neurodegenerative diseases

Marta Querol Vilaseca

Dr. Alberto Lleó Bisa, Thesis Director and Tutor

Neurobiology of dementia Unit – Memory Unit

Institut d'Investigació Biomèdica Sant Pau

Hospital de la Santa Creu i Sant Pau

Programa de Doctorat en Neurociències

Institut de Neurociències

Universitat Autònoma de Barcelona

Novembre 2020

Certificate of Direction

Dr. Alberto Lleó Bisa, , who obtained his PhD in Medicine at the Universitat de Barcelona , Head of the Memory Unit in the Neurology Department in Hospital de la Santa Creu i Sant Pau and aggregate professor in the Universitat Autònoma de Barcelona

Certify:

That the work entitled **"Novel digital neuropathology methods applied to neurodegenerative diseases"**, presented by **Marta Querol Vilaseca**, candidate of the PhD program in Neurosciences, has been done under my direction and meets all the requirements to be presented and defended in front of the corresponding Thesis Committee.

Dr. Alberto Lleó Bisa

Thesis Director and Tutor

Head of the Memory Unit, Department of Neurology

Hospital de la Santa Creu i Sant Pau

List of contents

Abstract

Every 3 seconds someone in the world develops dementia. Neurodegenerative diseases (NDDs) with Alzheimer's disease (AD), Parkinson's disease (PD) and frontotemporal dementia (FTD) as the most prevalent forms are a group of disorders affecting millions of people worldwide. Neuropathology of post-mortem human samples is still needed to elucidate the underlying altered mechanisms of NDDs.

This doctoral thesis highlights the importance of digital neuropathology as a tool for research purposes and clinical interpretation. We applied classical immunoassays, light microscopy techniques including super-resolution microscopy and developed automated computational tools in order to investigate neuroinflammation and abnormal protein accumulation related with disease progression in AD and other tauopathies.

We first performed a detailed neuropathologic characterization of YKL-40 expression in human brain tissue. Combining confocal microscopy and the application of a semi-automated method to quantify pathology burden, we have shown that the immunoreactivity pattern of YKL-40 in AD and other tauopathies is mainly astroglial. YKL-40 is expressed by a subset of astrocytes that do not contain tau aggregates in non-AD tauopathies. Finally, we have found that YKL-40 inflammatory marker is associated with tau pathology in neurodegenerative diseases that accumulate tau.

We also demonstrate the potential role of super-resolution microscopy in the neuropathology field by combining two techniques, array tomography (AT) and stimulated emission depletion microscopy (STED), to examine the composition of human amyloid β plaques in the brain at a nanometer scale. We described that the distribution of non-fibrillar Aβ assemblies consists of a dense core of higher order Aβ species surrounded by a peripheral halo of small Aβ structures. Also, we provide preliminary evidence of higher levels of non-fibrillar Aβ structures in an ADAD case compared to a SAD case.

Finally, we report the neuropathological findings of a case that participated in a clinical trial with a BACE-1 inhibitor. We demonstrate that Verubecestat may be exerting some effect on the non-fibrillar forms of Aβ as we observed a reduction in the treated case. Moreover, we detected clearance of these species at synapses using super-resolution microscopy techniques.

Abbreviations

Aβ = amyloid β
AD = Alzheimer's disease
ADAD = autosomal dominant Alzheimer's disease
ADI = Alzheimer's disease International
AGD = argyrophilic grain disease
AICD = amyloid precursor protein intracellular domain
ALS = amyotrophic lateral sclerosis
APOE = apolipoprotein E
APP = amyloid precursor protein
APP-CTF = amyloid precursor protein C-terminal fragment
AT = array tomography microscopy
BACE-1 = β-site APP cleaving enzyme 1
BBB = blood-brain-barrier
bvFTD = behavioural variant of frontotemporal dementia
CAA = cerebral amyloid angiopathy
CBD = corticobasal degeneration
CBS = corticobasal syndrome
CERAD = Consortium to Establish a Registry for Alzheimer Disease
ChEIs = cholinesterase inhibitors
CHI3L1 = chitinase 3-like 1
CHL1 = Cell Adhesion Molecule L1 Like
CLEM = correlative light and electron microscopy
CNS = central nervous system
CSF = cerebrospinal fluid
EM = electron microscopy
FDA = Food and Drug Administration
FIB/SEM = Focused Ion Beam Scanning Electron Microscope
FTD = frontotemporal dementia
FTD-MND = frontotemporal dementia with motor neuron disease
FTLD = frontotemporal lobar degeneration
GFAP = glial fibrillary acidic protein
GGT = globular glial tauopathy
GM = grey matter
GSK3β = glycogen synthase kinase-3 β
H&E = haematoxylin and eosin
Iba1 = ionized calcium-binding adapter molecule 1
IL-6 = interleukin 6
IL-1β = interleukin 1β
LBD = Lewy body dementia
LM = light microscopy
MAPT = microtubule-associated protein tau
MCI = mild cognitive impairment
NDDs = **n**eurodegenerative diseases
NFT = neurofibrillary tangles
nfavPPA = nonfluent/agrammatic variant primary progressive aphasia
NIA-AA = National Institute on Aging and Alzheimer's Association
NMDA = N-methyl D-aspartate receptor
NT = neuropil thread
PALM = Photo-activated localization microscopy
PART = primary age-related tauopathy
PD = Parkinson's disease
PET = positron emission tomography
PiD = Pick's disease
PSD-95 = postsynaptic density protein 95
PSEN1 = Presenilin 1
PSEN2 = Presenilin 2
PSP = progressive supranuclear palsy
PSP-S = progressive supranuclear palsy syndrome

SAD = sporadic Alzheimer's disease
sAPP = soluble fragment of amyloid precursor protein
sCJD = sporadic Creutzfeldt–Jakob disease
SEM = scanning electron microscopy
SANP-25 = Synaptosomal-associated Protein 25
SR = super-resolution microscopy
SSEA-4 = stage-specific embryonic antigen-4
STED = stimulated emission depletion microscopy
STORM = stochastic optical reconstruction microscopy
svPPA = semantic variant PPA
SYPH = synaptophysin
TBI = traumatic brain injury
TEM = transmission electron microscopy
TNFα = tumor necrosis factor α
VAMP2 = Vesicle-associated membrane protein 2
WM = white matter
WHO = World Health Organization

List of publications included in this thesis

The main content of this thesis consist of a compilation of the following publications:

Study 1.

Querol-Vilaseca M, Colom-Cadena M, Pegueroles J, San Martín-Paniello C , Clarimon J, Belbin O, Fortea J & Lleó A. **YKL-40 (Chitinase 3-like I) is expressed in a subset of astrocytes in Alzheimer's disease and other tauopathies**. J Neuroinflammation. 2017;14(1):118

Study 2.

Querol-Vilaseca M, Colom-Cadena M, Pegueroles J, Nuñez-Llaves R, Luque-Cabecerans J, Muñoz-Llahuna L, Andilla J, Belbin O, Spire-Jones TL, Gelpi E, Clarimon J, Loza-Alvarez P, Fortea J & Lleó A. **Nanoscale structure of amyloid-β plaques in Alzheimer's disease**. Sci. Rep.2019; 9, 5181

Study 3.

Querol-Vilaseca M, Sirisi S, Molina-Porcel L, Molina B, Pegueroles J, Ferrrer-Raventós P, Nuñez-Llaves R, Blesa, R, Belbin O, Fortea J, Sánchez-Valle R, Lleó A. **Reduced non-fibrillar Aβ species in a patient treated with low doses of BACE1 inhibitor.** 2020. [In preparation]

Chapter 1: Introduction

NEURODEGENERATIVE DISEASES

Every 3 seconds someone in the world develops dementia. This fact highlights the worldwide medical, social and economic problem caused by neurodegenerative diseases (NDDs). In 2019 the Alzheimer's Disease International (ADI) group published that around 50 million people worldwide were living with dementia. They also predicted that this number will reach to 152 million by 2050[1]. On the other hand, the World Health Organization (WHO) predicts that, as populations get older, neurodegenerative diseases with Alzheimer's disease (AD), Parkinson's disease (PD) and frontotemporal dementia (FTD) as the most prevalent forms, will overtake cancer to become the second leading cause of death after cardiovascular disease in 2040.

NDDs are a group of disorders characterized by selective dysfunction and progressive loss of synapses and neurons associated with the deposition of pathologically altered proteins in the human brain and spinal cord. Importantly, glial cells also accumulate these pathological proteins [2]. Different aspects have to be taken into account for the classification of NDDs, such as the clinical presentation, anatomical regions and cell types affected, conformationally altered proteins involved in the pathogenic process and the aetiology if known [3,4] **[Fig 1.].**

The main risk factor of NDDs is aging. The majority of these diseases are late-onset and present a gradually neuronal loss of function associated with cognitive decline that progresses over time. There is a high degree of similarity in symptoms between NDDs, making differential diagnostics difficult. In clinical practise, diagnosis is performed following clinical guidelines and neuropsychological assessments, supported by cerebrospinal fluid (CSF) and neuroimaging biomarker tests to increase the diagnostic confidence and accuracy. However, no NDD is currently curable, and the treatments available are only effective in managing the symptoms or slowing the progression of the disease.

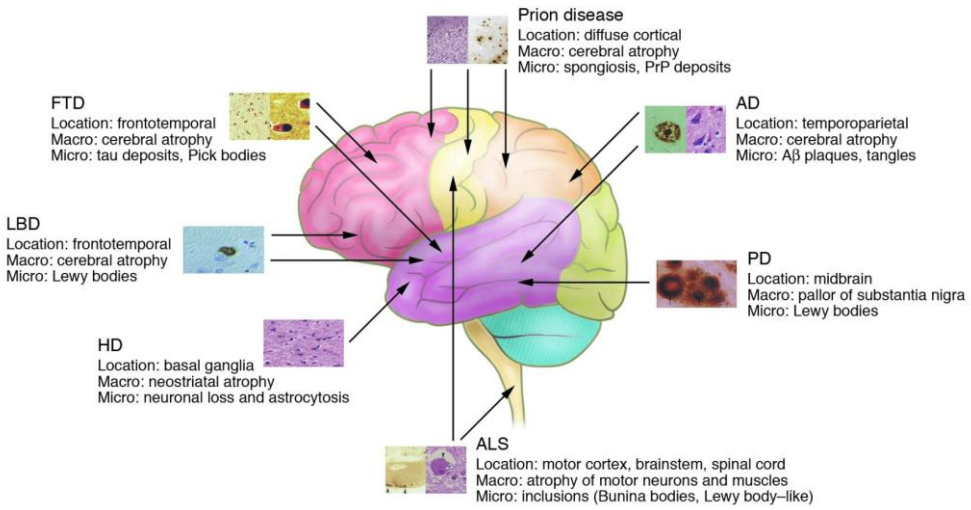

Figure 1. Overview of the anatomical location , macroscopic and microscopic changes characteristic of the main neurodegenerative disorders (from Bertram and Tanzi, 2005)[5]. Note that the full neuropathological spectrum of these disorders is much more complex than depicted here. When there is more than one characteristic histopathological feature, these are depicted from left to right, as indicated in the labels listing microscopic changes.

Research is fundamental to elucidate the biochemical and molecular events underlying degeneration. Mechanisms that are involved in the pathophysiology of NDDs are genetic mutations, deposition of misfolded proteins, impairment of degradation systems, membrane and DNA damage, and mitochondrial dysfunction, among others. Advances in research will help to identify potential novel therapeutic targets.

Inside the research field, neuropathology plays a key role in the understanding of the different diseases as it allows describing the lesions and the alterations of mechanisms underlying each condition. The frequent observation of more than one lesion in the brain, indicating that there are concomitant pathologies, is adding more complexity to the understanding of these disorders. Studies that may increase our knowledge of the alterations present in NDDs can be focused on the synaptic, intracellular and extracellular protein accumulations; the subcellular location of the intracellular deposits (nuclear, cytoplasmic or cell process); the alteration on the morphology of different cell types; quantification of neuronal, glial or synaptic loss; among other ones. However, neuropathology has a limitation, its descriptive and irreversible nature. Even though, investigating human brain samples of different NDDs can be the closest approach to the real pathology compared to other approaches, like cell culture and animal models.

ALZHEIMER'S DISEASE

Alzheimer's disease (AD) is the most common cause of dementia representing 60-80% of the cases[6]. AD is characterized by a gradually progressive cognitive and functional decline sufficient to impact on activities of daily living. The main risk factor of AD is aging. The vast majority of AD cases are sporadic with a late age of onset, typically between 70 and-90 years. Only less that 1% of AD cases are associated with an autosomal dominant mutation in three genes: amyloid precursor protein (*APP*), presenilin 1 (*PSEN1*) and presenilin 2 (*PSEN2*). *PSEN1* is the most frequently mutated gene, accounting for the majority of autosomal dominant AD (ADAD) cases with onset prior to age 50[5]. Family history is the second most important risk factor for the disease after age. In addition, presence of the *APOEε4* allele, female gender, cerebrovascular disease, hyperlipidemia, smoking, diabetes, obesity and traumatic brain injury are other risk factors associated with AD[7]. On the other hand, higher cognitive reserve, consumption of a Mediterranean diet and regular exercise are protective factors for AD[8].

Clinical symptoms

The majority of AD cases present the typical (amnestic) form, but up to 15% of cases are considered atypical, presenting early or prominent visual, frontal or parietal symptoms[9]. Typical AD is characterized by gradual progression of memory loss in association with other cognitive domains, often visuospatial and executive functions, that leads to a loss of functional independence[7].

It is well established that neuropathological changes occur about 20 years prior to the onset of the symptoms, supporting the idea of AD as a continuum[10]. In 2011, the National Institute on Aging and Alzheimer's Association (NIA-AA) published the diagnostic criteria including three different stages of the AD continuum: preclinical AD, mild cognitive impairment (MCI) and dementia due to AD. Moreover, they recognized the potential use of biomarkers such as CSF amyloid β (Aβ) and tau; and positron emission tomography (PET) measures to diagnose AD[11].
The preclinical AD stage is defined by biomarker changes of AD in the absence of cognitive deficits[12].

The stage of Mild Cognitive Impairment (MCI) due to AD is characterized by mild changes in memory and other cognitive abilities that are measurable by cognitive tests, but are not severe enough to disrupt a person's day-to-day life[13].

In Dementia due to AD cognitive deficits are significant enough to impair a person's ability to function independently. Neuropathological features describing AD are required for a definite diagnoses although AD related biomarkers can highly predict it and they are considered sufficient to make the diagnosis[14].

At this moment, medical management of AD consist on symptomatic treatment to improve the patient symptoms and patient's and caregiver's qualities of life. Currently there are no disease-modifying pharmacologic treatments for AD, although some trials with anti-amyloid therapies have shown promising preliminary results (https://www.biogen.com/en_us/alzheimers-disease.html).

Neuropathological hallmarks in AD

Macroscopically, AD presents a typical symmetric pattern of cortical atrophy of medial temporal lobes with little atrophy of primary motor, sensory and visual cortices. As a result, the lateral ventricles can appear prominently dilated. Cortical microinfarcts, lacunar infarcts in the basal ganglia and demyelination of the periventricular white matter are also relatively common.

Microscopically, AD is characterized by the presence of extracellular neuritic plaques, composed primarily of amyloid β-42 (Aβ-42), and accumulation of intracellular neurofibrillary tangles (NFTs), composed of hyperphosphorylated species of microtubule-associated protein tau. Astrogliosis, microglial activation, cerebral amyloid angiopathy (CAA), synaptic and neuronal loss are also key aspects of the AD pathology[15].

The aetiology of AD remains controversial. The cortical atrophy present in AD brains resulting from a massive neuronal and synaptic loss can be explained by the accumulation of neurotoxic forms of Aβ and the hyperphosphorylation of tau inducing inflammatory and microglial cascades, ionic and neurotransmitter abnormalities, mitochondrial dysfunction and oxidative stress[16]. In fact, the amyloid hypothesis of AD proposes that accumulation of Aβ in the brain triggers the spread of tau-related pathology, neuroinflammation and neuronal degeneration[17,18].

Amyloid plaques are the result of the abnormal extracellular accumulation and deposition of Aβ peptides. Aβ is produced after sequential cleavage of APP by three protease activities mainly in neurons. APP is a type I single-pass transmembrane protein with a large extracellular domain and a short cytoplasmic tail[19]. APP is firstly sorted in the Endoplasmic Reticulum and Golgi[20,21], and subsequently delivered to the synaptic terminal of the axon[22]. Its cleavage is guided by alternative splicing, ending up with two different pathways. In the non-amyloidogenic pathway APP is cleaved by α-secretase and consecutively by γ-secretase on the cell surface, a process that does not generate amyloidogenic peptides. Contrarily, the so-called amyloidogenic pathway initiates when APP is re-internalized into an endosomal compartment, where it is cleaved by β-secretase (also referred to as β-site APP–cleaving enzyme 1 (BACE-1)) and γ-secretase generating the amphipathic Aβ peptides of different lengths from 40 to 43 amino acids[21] **[Fig. 2a]**.

The Aβ-42 specie is the most abundant in plaques due to its higher rate of fibrillation and insolubility[23]. The process of a plaque formation begins with amyloid monomers (Aβ peptides) that assemble to form a variety of oligomeric species that aggregate to form protofibrils, then mature and elongate into insoluble fibrils ultimately forming the amyloid plaques. There is considerable controversy regarding the toxicity of fibrillar versus oligomeric amyloid, but the main hypothesis supports that small oligomeric forms of Aβ are the most toxic ones and can trigger synaptic dysfunction and neuronal loss[24] **[Fig. 2b].**

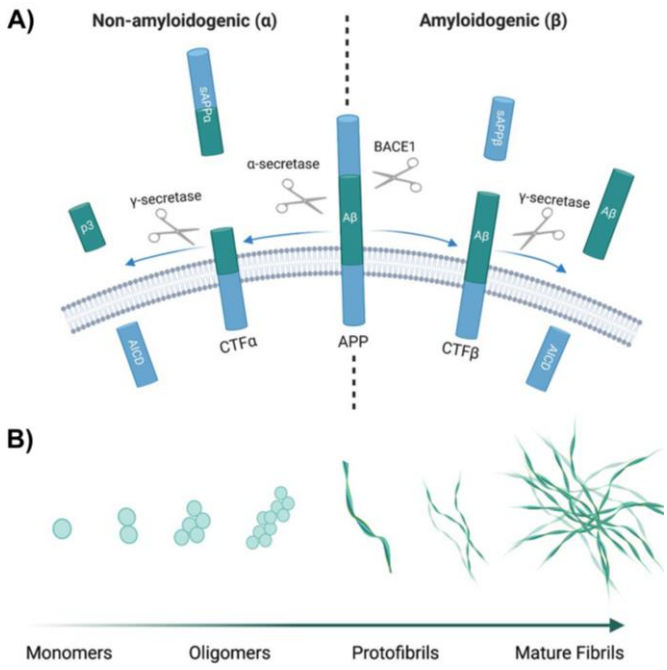

Figure 2: Overview of canonical APP-processing pathways. A) In the non-amyloidogenic pathway α-secretase generates different fragments: soluble α fragment of APP (sAPPα) and APP α C-terminal fragments (APP-CTFα) which in turn is proteolysed by γ-secretase generating the APP intracellular domain (AICD) and the nontoxic substrate p3. By contrast, in the amyloidogenic pathway BACE-1 liberates sAPPβ and APP-CTFβ which is later cleaved by γ-secretase generating AICD and Aβ peptides. **B)** Stages of aggregation of Aβ, from monomers to mature fibrils (adapted from Kent, Spires-Jones & Durrant 2020)[25]

At least, two main types of plaques can be distinguished: diffuse and dense-core plaques**.** The second ones, also known as neuritic plaques, are associated with impairment of the neuropil area including dystrophic neurites, synaptic loss, neuron loss and recruitment and activation of astrocytes and microglial cells. The topographic distribution of amyloid deposition is from the isocortex to the subcortical structures[15] **[Fig. 3]**. Besides common plaques there are other types such as cotton wool plaques reported in few sporadic cases and predominantly described in patients with specific *PSEN1* mutations[26,27]. Moreover, a very recent paper has described a new type of plaque called coarse-grained plaque with a multi-cored coarse-grainy appearance, Aβ-devoid pores and an ill-defined border. Increased presence of coarse-grained plaque was associated with early disease onset in AD, a homozygous APOE ε4 status, and the presence of CAA-Type 1[28].

Neurofibrillary tangles (NFTs) are the result of intracellular accumulation of paired helical filaments consisting of abnormal hyperphoshorylated tau[15]. Phosphorylation of tau can be induced by different protein kinases such as glycogen synthase kinase-3 β (GSK3β)[30]. In AD, GSK3β activity is increased leading to hyperphosphorylation of tau which causes its dissociation from microtubules and its accumulation to tangles[31,32]. In addition to NFTs, neuropil threads (NT) (tau positive processes from neurons and glial cells) are also characteristic in AD. Tau pathology begins in the allocortex of the medial temporal lobe (enthorhinal cortex and hippocampus) before spreading to the associative isocortex

sparing the primary sensory, motor, and visual areas[15] **[Fig. 3].** Severity of AD better correlates with NFT pathology occurring in parallel with neuronal and synaptic loss. Indeed, the loss of synapses in the neocortex and limbic system is the best correlate of the cognitive impairment in patients with AD[33,34,35].

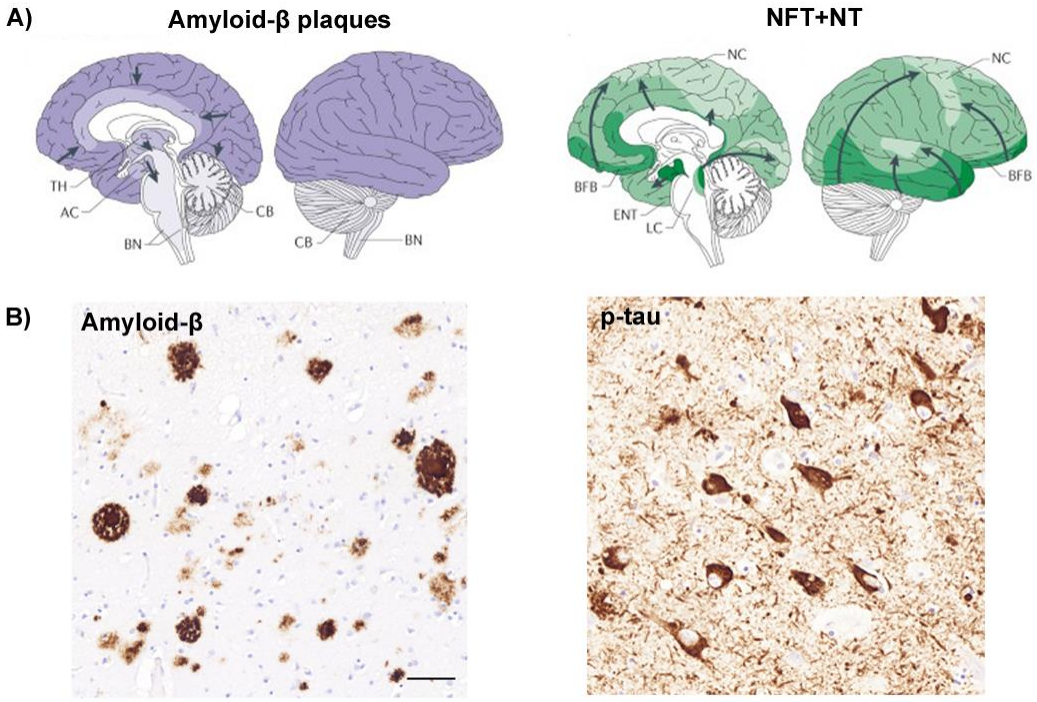

Figure 3. Topographic dissemination and immunoreactivity patterns of Aβ and tau in AD. A) Schematic representation of sequential topographic dissemination of Aβ and tau pathology (adapted from Brettschneider et al. 2015)[29]. **B)** Different types of amyloid beta plaques: dense core and diffuse plaques; and tau positive neurofibrillary tangles (NFT) and neuropil threads (NT). Source: Marta Querol-Vilaseca, Neurobiology of dementia Laboratory.

The current neuropathological criteria for AD is based on an "ABC" score that includes the Thal criteria for Aβ deposition (score A for "amyloid"), the Braak system for NFTs (score B for "Braak") and the Consortium to Establish a Registry for Alzheimer Disease (CERAD) for neuritic plaques (score C for "CERAD"). The range of ABC scores is from 0 to 3 representing four different levels of AD neuropathological change: not, low, intermediate or high[36]. The NIA-AA guidelines published by Montine et al. in 2012 report that a proper neuropathological assessment should consist in an evaluation of regional atrophy and blood vessels at a macroscopic level. Thus, a minimum of 14 brain regions are recommended to be sampled performing haematoxylin and eosin (H&E) staining together with immunohistochemistry assay of different antibodies against the most common NDDs-associated proteins. In summary, the state-of-the-art neuropathological examination should include several anatomical regions and immunostainings to be able to report stages or phases of proteinopathies and their combinations[37].

Therapeutic strategies in AD

No disease-modifying therapy for Alzheimer's disease has yet been approved. However, multitude targets have been identified as potentials therapeutic approaches for AD. Three main strategies can be highlighted towards identifying a drug that can halt the progression of AD: 1) Acting on the pathological proteins Aβ and tau by inhibiting their formation, aggregation or inducing their clearance. 2) Modulating the function of neurotransmitters or their receptors to stabilise neuron health and downstream cascades. 3) Restoring or protecting protein targets that are sensitive to Aβ-induced toxicity[30]. The main approaches tested for the three strategies are summarized in **table 1.**

Table 1. Summary of the targeted mechanisms of action in AD clinical trials.

	Mechanism of action
Clearance of pathogenic proteins Aβ and tau	Inhibition of Aβ protein aggregation
	Immunotherapy against Aβ using active immunization
	Immunotherapy using passive immunization
	Secretase modulators (α- β-, γ-secretase)
	Aβ transport
	Aβ degrading enzymes
	Inhibition of tau protein aggregation
	Inhibition of tau protein hyperphosphorylation
	Immunotherapy against tau
Stabilize neuron transmission	Cholinergic system
	GABAergic system
	N-methyl D-aspartate (NMDA) receptor
	Serotonin receptors
	Histamine receptors
Identify sensitive targets in AD	Membrane receptors targets
	Nuclear targets
	Intracellular cytoplasmic targets
	Mitochondrial targets
	Neuroinflammatory targets

On one hand, until date, there are five prescription drugs currently approved by the U.S. Food and Drug Administration (FDA) to treat AD symptoms. Donepezil, Galantamine and Rivastigmine are three cholinesterase inhibitors (ChEIs) commonly prescribed to treat symptoms related to memory, thinking, language, judgment and other thought processes. The mechanism of action consists in preventing the breakdown of the neurotransmitter acetylcholine by blocking the activity of the enzyme acetylcholinesterase. Increased levels of acetylcholine in the synaptic cleft may help strengthen neuron-

neuron communication. Memantine is a NMDA receptor antagonist prescribed to improve memory, attention, reason, language and ability to perform simple tasks. The mechanism of action is blocking the calcium channel and maintaining the open conformation, which leads to a decreased of intracellular calcium[38] preventing neuronal death. Finally, Namzaric is a combination of Donepezil and Memantine approved by the FDA for the treatment of moderate-to-severe AD in people who are taking donepezil hydrochloride 10 mg. The ability of these drugs to improve symptoms eventually declines as brain cell damage progresses.

On the other hand, the majority of drugs in clinical trials so far fall in the first category (**Table 1**) as they target the main pathogenic proteins of AD. However, despite that some trials have shown inhibition of the aggregation and reduction of Aβ deposits in the brain with some therapies, most of them have shown no cognitive benefit[30].

Several small molecules have been generated with the intent to target Aβ oligomers, the most toxic form of Aβ[39], as they cause synaptic dysfunction leading to neurodegeneration. For example, Tramiprosate acts by binding to Aβ monomers and maintaining them in a non-fibrillar form. This compound moved into a clinical study but did not demonstrate efficacy in improving cognitive function[40,41].

Furthermore, inhibition of BACE-1 was recently proposed as a potential therapeutic strategy for slowing the progression of AD by reducing the production of Aβ. This approach was improved from previous strategies that were unsuccessful using γ-secretase inhibitors or modulators[42,43], and active immunotherapy[44] to clear Aβ from the brain. Verubecestat (MK-8931) is an oral BACE-1 inhibitor that was tested in a randomized, placebo-controlled phase 3 trial. In this study Verubecestat at doses of 12 or 40 mg per day was tested in patients with mild-to-moderate AD and prodromal AD. The trail failed as Verubecestat did not have a beneficial effect on clinical outcomes. Moreover, some measures suggested possible worsening of cognition and daily function[45,46].

At this moment, immunotherapy using passive immunization is the strategy that has yielded more promising results. Two monoclonal antibodies, Aducanumab (BIIB037) and BAN2401 (human version of mAb158), are in active clinical trials. Aducanumab has high affinity against conformational epitope found in Aβ and BAN2401 selectively binds to large, soluble Aβ protofibrils. Both antibodies showed significant reduction in brain amyloid and cognitive decline in patients with early AD.

Other therapies have focused on tau pathology. Recent studies have shown that AD patients have elevated levels of kinases, such as GSK3β that lead to hyperphosphorylation of tau and inhibition of those kinases has become a therapeutic strategy for AD. A phase III clinical trial performed with a GSK3β inhibitor, Tideglusib, showed no clinical benefit in AD patients[47]. However, current trials are mainly focussed on monoclonal antibodies directed against aggregated tau.

The challenges observed in clinical trials directed to Aβ and tau as drug targets for AD have led to focus the attention in identifying alternative targets, signalling pathways or processes that may contribute to disease pathophysiology. Neuroinflammation[48,49] and microbiota[50]are two emerging mechanisms that may contribute to understand and treat AD.

TAUOPATHIES

Tauopathies are a group of neurodegenerative diseases clinically, biochemically and morphologically heterogeneous characterized by the deposition of abnormal tau in the brain. Different neuropathologic phenotypes are included under this term taking into account the anatomic areas and the cell types affected, and the presence of distinct isoforms of tau. The primary tauopathies, disorders in which tau protein accumulation is the main feature[51], include the frontotemporal lobar degeneration (FTLD). FTLD-tau accounts for 36–50% of all cases of FTLD[52]. Secondary tauopathies are diseases that accumulate tau but also other proteins as hallmark neuropathologic traits[51] **[Table 2].**

Table 2. Tauopathies classification.

Type	Tauopathy
Primary tauopathies	Frontotemporal dementia with MAPT mutation
	Pick's disease
	Progressive supranuclear palsy
	Corticobasal degeneration
	Argyrophilic grain disease
	Globular glial tauopathy
	Primary age-related tauopathy
	Myotonic dystrophy
Secondary tauopathies	Alzheimer's disease
	Down Syndrome
	Chronic traumatic encephalopathy
	Niemann-Pick disease type C

Tau is a microtubule-associated protein encoded by the gen *MAPT* that stabilizes and promotes microtubule assembly. Six tau isoforms are generated by alternative splicing: three isoforms contain three repeats of microtubule-binding regions (3R) and three isoforms have four repeats (4R)[53] **[Fig. 4a]**. Mutations in the *MAPT* gene can cause hereditary frontotemporal dementia (FTD) associated with FTLD[54,55,56,57]. Primary tauopathies can also be classified based on the predominating isoform of tau (3R or 4R) that accumulates in the brain. Pick's Disease (PiD) is a 3R tauopathy and progressive supranuclear palsy (PSP), corticobasal degeneration (CBD), argyrophilic grain disease (AGD) and globular glial tauopathy (GGT) are 4R tauopathies[58]. Mixed 3R and 4R tauopathies are observed in the neurofibrillary tangle predominant senile dementia (NFT dementia or "tangle-only" dementia; now included also in the category of primary age-related tauopathy (PART) and AD[59] **[Fig 4b].** It is well known that the major post-transcriptional modification of neuronal or glial aggregated 3R or 4R tau is hyperphosphorylation, although other biochemical modifications of the protein can be detected such as N- or C- terminal truncation, glycosylation, glycation, nitration of residues, acetylation, etc[51].

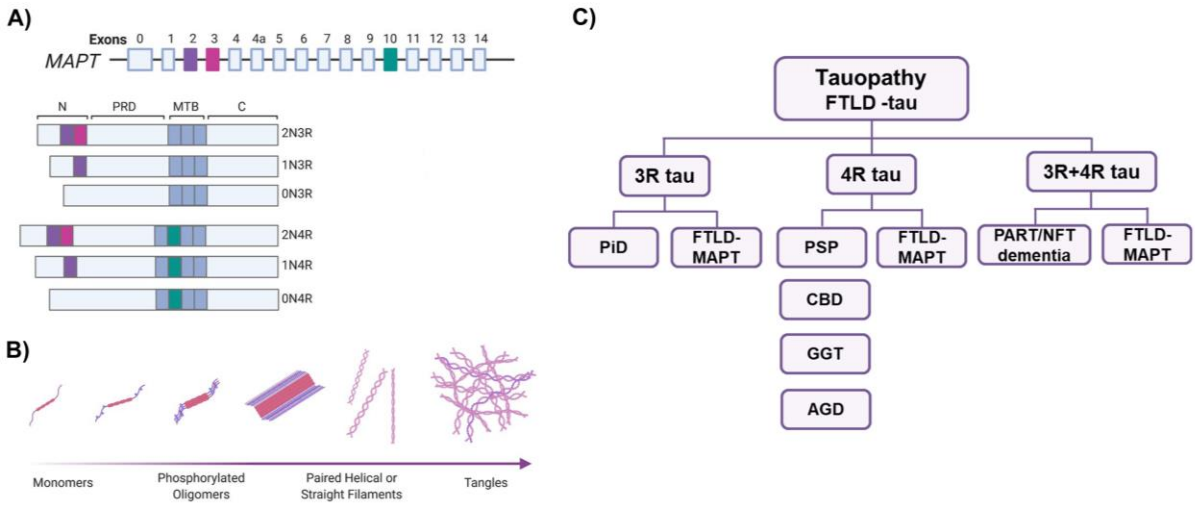

Figure 4. Human Tau isoforms and FTLD-tau classification. **A)** Representation of *MAPT* and the six Tau isoforms expressed in adult human brain. *MAPT* consists of 14 exons (E). Alternative mRNA splicing of E2 (purple), E3 (pink), and E10 (green) generates the six Tau isoforms. **B)** Stages of aggregation of Tau, from monomers to tangles (adapted from Kent, Spires-Jones & Durrant 2020)[25]. **C)** Molecular classification of FTLD-tau based on the predominant Tau isoform present. AGD, argyrophilic grain disease; CBD, corticobasal degeneration; FTLD-MAPT, FTLD with MAPT gene mutations; GGT, globular glial tauopathy; NFT, neurofibrillary tangle; PART, primary age-related tauopathy; PiD, Pick disease; PSP, progressive supranuclear palsy (adapted from Kovacs 2017)[51].

Clinical spectrum of tauopathies

FTLD is a highly heterogeneous disorder with different histopathologies that cause different clinical syndromes. FTLD is usually clinically presented as FTD, the second most common cause of early-onset dementia in patients below 65 years old[60,61]. FTD clinical spectrum covers several syndromes characterized by the degeneration of the frontal and temporal lobes that includes changes in behaviour, language, executive control and often motor symptoms[62]. The core of FTD spectrum disorders includes the following syndromes: behavioural variant FTD (bvFTD), nonfluent/agrammatic variant primary progressive aphasia (nfavPPA), and semantic variant PPA (svPPA). Other related FTD disorders are FTD with motor neuron disease (FTD-MND), the progressive supranuclear palsy syndrome (PSP-S) and corticobasal syndrome (CBS)[62,63] **[Fig 5].**

The behavioural variant FTD (bvFTD) is the most common phenotype of FTLD. The main symptoms are marked behavioral and personality changes such as apathy, disinhibition, perserveration and executive dysfunction. In about 50% of patients, the underlying pathology consists of tau inclusions (FTLD-tau: PSP, CBD, PiD and AGD)[63].

The clinical features of nfavPPA include effortful speech with motor speech apraxia or agrammatism[64]. The tauopathies underlying nfavPPA include PSP, CBD and PiD.

The svPPA include impaired confrontational naming, single word comprehension and object knowledge, surface dyslexia, spared repetition, and spared speech production[64]. svPPA is typically caused by inclusions of transactive response DNA binding protein 43 (TDP-43), also named FTLD-TDP[63].

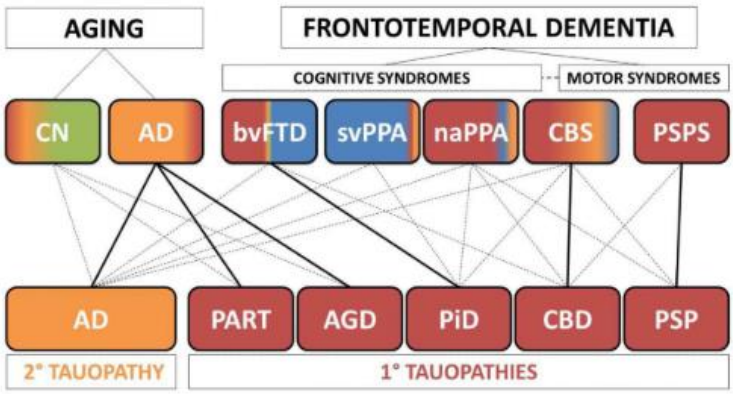

Figure 5. Clinicopathological correlations in tauopathies. The scheme portrays (top) the relative frequencies of neuropathological subtypes of FTLD- Tau (red), AD (yellow) and TDP-43 proteinopathies (blue) seen at autopsy in clinical phenotypes in FTD-spectrum disorders and aging. Unremarkable neuropathological findings are shaded in green. Solid lines represent the predominant clinicopathological association for each specific tauopathy (bottom) while dashed lines represent less common clinical manifestations of each tauopathy. AD neuropathology is most commonly associated with the amnestic AD clinical phenotype but may also present as bvFTD, PPA variants and CBS. PART and AGD are largely associated with late onset (>80 years) amnestic syndrome similar to clinical AD and less commonly in CN individuals. PiD is most commonly found in association with bvFTD but can present with PPA variants or CBS. CBD tauopathy is primarily associated with CBS but also can manifest as bvFTD, nfavPPA or PSPS, while PSP is predominantly associated with PSPS and less commonly associated with naPPA or CBS (adapted from Irwin 2016)[63]

The two motor syndromes related to FTLD are 1) PSP-S characterized by different syndromes that include postural instability, vertical supranuclear palsy and speech deficits[65]. The most common underlying pathology of the PSP syndrome is PSP although some cases are associated with CBD at autopsy. 2) CBS is characterized by asymmetric combination of cortical symptoms (apraxia, cortical sensory disturbance or alien limb phenomenon) and basal ganglionic symptoms (akinesia, rigidity, myoclonus, or dystonia). CBS clinical phenotype is typically caused by CBD, but also by PSP and PiD[66].

Neuropathological hallmarks in FTLD

Pick's disease

PiD was first described by Arnold Pick in 1892 and the main neuropathological hallmarks were reported by Alois Alzheimer in 1911. Pick's disease presents clinically mainly as bvFTD, less frequent as PPAs, or even CBS depending on the distribution of the neurodegeneration[63,67].

Macroscopically, the brain in PiD shows severe gyral atrophy of the frontal and temporal lobes, anterior cingulate gyrus and insula, with ventricular enlargement and variable atrophy of the neostriatum[63,68]. Limbic structures (hippocampus and amygdala) are often severely affected[69].

Microscopically, PiD is characterized by the presence of ballooned neurons known as Pick cells, as well as large neuronal spherical cytoplasmic tau-positive inclusions known as Pick bodies, affecting both pyramidal and granular neurons. The predominantly isoform that compose Pick bodies is 3R tau, although 4R can be rarely present[70]. Two other relevant neuropathological traits are the presence of ramified astrocytes and less frequently small oligodendroglial globular inclusions[58,68,69] **[Fig. 6]**.

Progressive supranuclear palsy

PSP was originally described as a distinct disorder by neurologists John Steele, John Richardson and Jerzy Olszewski in 1964. PSP is classified as a 4R tauopathy[71,72]. The most common clinical presentation is PSP-S, although patients with clinical features of the nfavPPA, CBS or bvFTD with neuropathological PSP have been also recognized.

Macroscopically, the brain in PSP includes atrophy in mild frontal cortex and subthalamic nucleus, atrophy of the midbrain with neuromelanin pigment loss in the substantia nigra, and atrophy of the cerebellar dentate nucleus and the superior cerebellar peduncle[69].

Microscopically, PSP is characterized by globose neurofibrillary tangles in subcortical nuclei, oligodendroglial coiled bodies in the white matter of the neocortex and tufted astrocytes in the motor cortex and neostriatum[73,74,75,76]. In addition, flame-shaped neurofibrillary tangles, diffuse granular pre-tangles and threads (p-tau accumulation in neuronal and glial processes) can be detected in the grey matter (GM) of affected brain regions[77] **[Fig. 6]**.

Corticobasal degeneration

CBD is a 4R tauopathy that was first described by Rebeiz in 1968 as a degeneration of the frontoparietal association cortices and the basal ganglia. In 1989 Gibb et al. applied the term CBD to describe this entity. The clinical presentation is mainly a CBS, but it can also present as PPA, bvFTD or a PSP-S[63].

Macroscopically, the brain in CBD typically presents focal and asymmetrical cortical atrophy affecting parasagittal, perisylvian, and perirolandic regions. Other features include superior frontal gyrus atrophy, cerebral white matter (WM) volume loss, thinning of the corpus callosum, enlargement of ventricular system and depigmentation of substantia nigra. Regions of the basal ganglia, including globus pallidus, striatum, thalamic and subthalamic nuclei, and the brainstem can be variably affected[78].

Microscopically, CBD is characterized by 4R-tau spherical neuronal inclusions, threads in the white and grey matter, coiled bodies and astrocytic plaques predominating in cortical and subcortical areas. The

presence of poorly formed cytoplasmic inclusions in neurons (pretangles) and ballooned neurons are also common[73,78] **[Fig. 6]**.

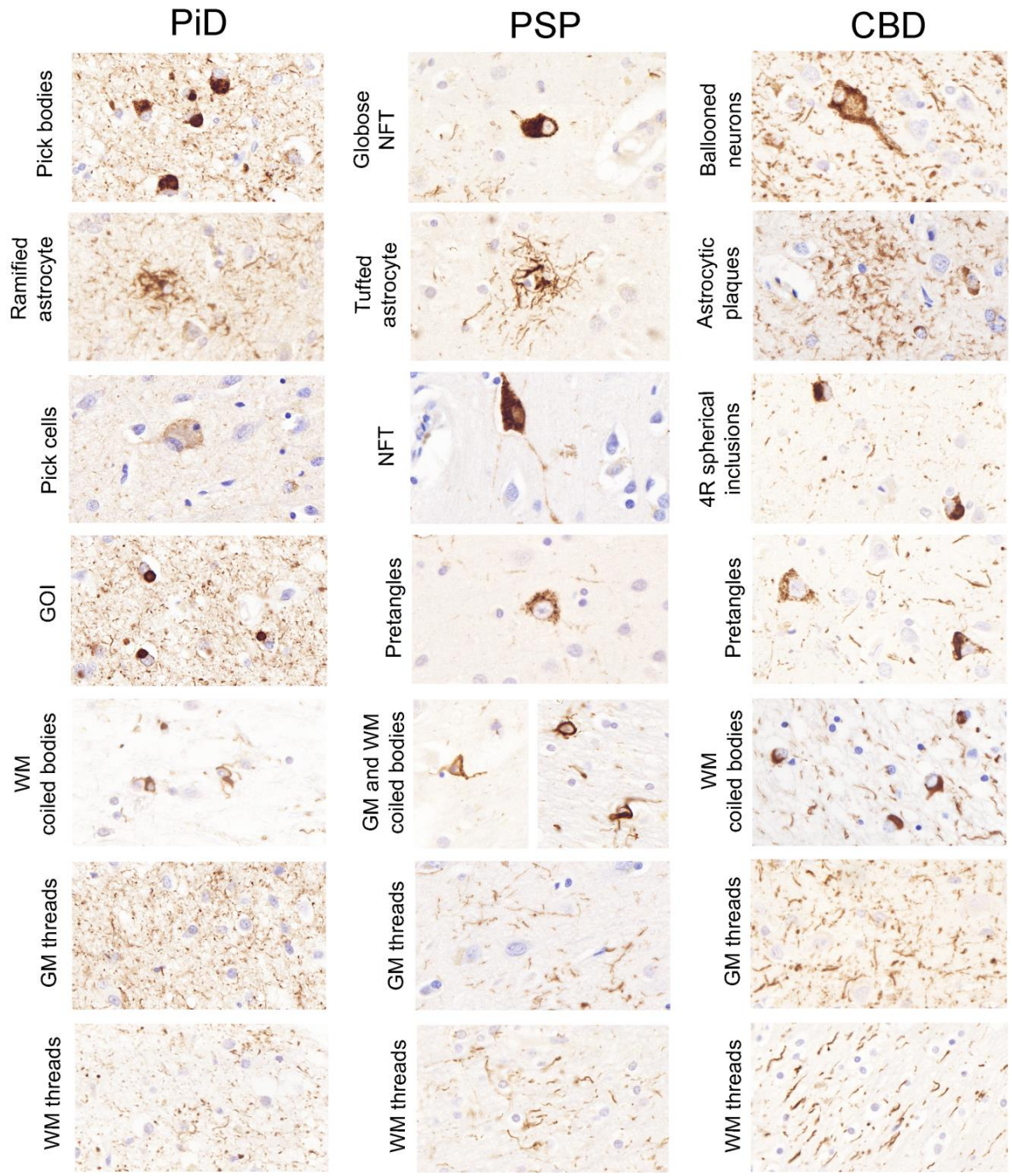

Figure 6. Overview of pTau positive inclusions in PiD, PSP and CBD. Different p-tau inclusions present in PiD, PSP and CBD using an antibody against phosphorylated tau (AT8). PiD: Pick's disease; PSP: progressive supranuclear palsy; CBD: corticobasal degeneration; NFT: neurofibrillary tangles; GOI: globular olidendroglial inclusions; GM: grey matter; WM: white matter. Source: Marta Querol-Vilaseca, Neurobiology of dementia Laboratory.

NEUROINFLAMATION IN NEURODEGENERATIVE DISEASES

Growing evidence suggest that neuronal damage present in NDDs is frequently associated with chronic activation of innate immune response[79,80]. Microglia and astrocytes are the main cell types in the brain involved in neuroinflammatory processes. Whether neuroinflammation is the consequence or the trigger of pathological aggregates still remains unclear, but there is a wide agreement that it is an early stage phenomenon. Although neuroinflammation arises innately as a protective mechanism of the central nervous system (CNS), alteration in any of the components of this response may become chronic, non-resolving and toxic to the brain[48].

In the normal CNS, resting microglia has multi-branched long processes and participates in monitoring local synapses and surveying for injury or infection[79]. Astrocytes in a non-reactive state also have large number of long processes and are involved in regulation of neurotransmission, calcium homeostasis, modulation of synapse formation, maturation and elimination, stabilization of blood-brain barrier, and provide nutritional and trophic support to the brain[81,82,83]. When homeostasis is disrupted, microglia and astrocytes change their morphology becoming rounded and with shorter and thicker processes. Their function also changes, microglia increases its phagocytic capacity and production of proinflammatory cytokinies[84] and astrocytes release cytokines and other potential cytotoxic molecules, loss their synaptic functions, such as glutamate up-take to avoid excitotoxicity or gliotransmission, leading to impaired clearance and degradation systems[83,85].

Many NDDs have been associated with the presence of abnormal neuroinflammation triggered by the deposition of Aβ and tau in the case of AD, and tau in the case of other tauopathies[86]. During this last decade numerous studies have been focused on measuring different inflammatory mediators in biofluids, like CSF and plasma. One of the inflammatory proteins that has been frequently measured in CSF in NDDs is YKL-40. YKL-40, also known as chitinase 3-like 1 (CHI3L1), is a member of the glycoside hydrolase 18 chitinase family that targets chitin but lacks enzymatic activity[87]. It is produced by a wide range of cells such as macrophages, chondrocytes, synovial cells, osteoblasts, neutrophils, and vascular smooth muscle cells[88,89,90]. In the CNS, some studies have reported that YKL-40 is expressed in astrocytes, microglia or in rare occasions neurons[91,92] but its biological and physiological functions still remain unclear. CSF studies of YKL-40 shows increased levels in different NDDs such as AD, FTD, multiple sclerosis (MS) and amyotrophic lateral sclerosis (ALS) [93,94,95,96,97,98]. Interestingly, increased levels of YKL-40 in CSF were found in the preclinical stages of AD indicating that the immune system activation occurs early in the disease. In AD and FTD, there is a strong correlation between YKL-40 and tau pathology suggesting that inflammation and neurodegeneration associated with tau are strongly related processes[93].

As neuroinflammation has been established as an early event in NDDs, it is crucial to find molecular changes that can be translated to potential targets, like YKL-40, for a promising treatment of the diseases.

IMPLEMENTATION OF SUPER-RESOLUTION TECHNIQUES TO DIGITAL NEUROPATHOLOGY

Over the last 100 years technology has radically changed the way we understand neuropathology. Microscopy and staining techniques together with computational sciences have advanced dramatically making these techniques powerful quantitative tools.

In the field of NDDs, standard diagnostic neuropathology is still based on conventional H&E staining and immunohistochemical assays with specific antibodies. The assessment of lesions is usually carried out by qualified neuropathologists following the respective diagnostic criteria. This evaluation is still mostly based on semi-quantitative ratings of the disease burden on an ordinal scale (i.e. 0 = none/rare, 1 = mild, 2 = moderate, 3 = severe)[36].

In the research field, neuropathology is evolving to digitalized imaging assessments and the incorporation of super-resolution microscopy techniques. Stereology and manual quantification[99,100,101] can provide a measure of pathological burden but these methods are time-consuming and viable only in small sample studies. Emerging methods for automated digital image analysis of histology sections may provide a high-throughput means of quantification. Studies using this new methodology have already been published to quantify AD[102,101,103,104] and FTLD[105] pathology. This new approach allows not only the quantification of typical hallmark lesions of NDDs, but also the assessment of a wide-range of novel markers that can be found in these disorders. In addition, immunofluorescense assays and confocal microscopy can add great value to the neuropathological studies allowing the accurate description of possible alterations in the location of proteins, abnormal colocalization or aggregation in different cell types for example. All these techniques are adequate for studies of aggregates or cellular abnormalities, but leaving synapses and other potential interesting small structures such as oligomers out of the picture due to lack of resolution.

Electron microscopy (EM), invented in 1931, was the first technique that confirmed that synapses where part of the neuronal processes. EM also allowed the description of synapses formed by a pre- and post-synaptic terminal, usually surrounded by astrocytic terminals[106,107]. More recent studies using EM have already revealed morphological alterations and synaptic degeneration in NDDs[108,109,110]. However, EM has some limitations and cannot give information of molecular composition of synapses and possible abnormal protein accumulation.

To overcome these limitations during the last decade novel strategies have been developed. Super-resolution microscopy (SR) techniques take advantage of immunofluorescence-labelling methods to resolve structures below the diffraction limit of light. In a conventional microscopy the limit of resolution at the lateral plane (x-y axis) is around 200 nm and 600 nm at the axial plane (z axis)[111]. SR techniques, such as stimulated emission depletion microscopy (STED), stochastic optical reconstruction microscopy (STORM) or photo-activation localization microscopy (PALM) allow resolving structures

below the diffraction limit like synapses. The approach of each of these methods is different so their application must be decided depending on the scientific question. While these techniques can achieve very low resolutions on the lateral plane (20-60 nm), they are very time-consuming in the acquisition and less efficient resolving structures in the axial plane, limiting the study of large tissue volumes[112]. In 2007, Micheva and Smith group proposed a new methodology to overcome these limitations: the array tomography[113].

Array tomography microscopy

Array tomography microscopy (AT) offers the advantage of better axial resolution by special processing and cutting of the tissue sample into consecutive 70nm-thick sections **[Fig 7]**. Tissue needs to be collected in fresh state, sectioned in small fragments, fixed for a short period of time and embedded into an acrylic resin (LR white). After polymerization, tissue blocks can be stored for a long term at room temperature. Ultrathin serial sectioning of the tissue is performed with an ultramicrotome, where ribbons of around 30 consecutive sections are collected on coverslips. Next steps consist of an immunofluorescence reaction to label different proteins of interest achieving a high penetration of the antibodies due to the reduced thickness of the sections. Then, visualization and image acquisition can be performed with a conventional epifluorescence microscope as the resolution of the z plane has been determined by the physical sectioning. The final step includes the image processing and analysis that consist of a 3D-reconstruction of all the consecutive sections and quantification of the previously labelled proteins. The majority of studies using AT has been focused on the study of synapses in NDDs and their pathological features. In particular, AT has been used to study the presence of p-tau and Aβ in synapses in AD and control cases[109,114,115] and p-α-synuclein in Lewy body dementia (LBD) cases[116].

Stimulated emission depletion microscopy

The Stimulated emission depletion (STED) phenomenon was first described by Hell and Wichmann in 1994 as a method to break the diffraction limit of light[117]. The maturation and implementation of this unprecedented idea lead to the recognition of Hell's work with a Nobel Prize in chemistry in 2014.

STED microscopy is a super-resolution technique that provides real-time enhanced resolution imaging capabilities. It combines a high resolution confocal microscope with a high power donut-shaped depletion laser. The STED configuration uses the excitation and depletion lasers simultaneously increasing the lateral resolution (~80 nm) by reducing the emission area selectively depleting the fluorescent molecules under the donut-shaped beam[118,119]. The scanning of the sample is immediate allowing the direct acquisition of super-resolved images with minimal computational post-processing[120] **[Fig. 7]**.

STED has been shown to be very useful for studying subcellular structures on the nanometer range. STED has been used to visualize individual vesicles in the synapses of primary cultures[121], to study the structure of complex organelles like mitochondria[122], live-cell applications to investigate cellular adhesion

and migration processes[123], dynamic and morphology of dendritic spines and their inner protein distributions[124], among others. The majority of these studies have been performed in cell cultures or rodent brain slices, since these experiments in human brain samples are more challenging. However, there are few reports, like Benda *et al.* were they investigated tau filaments in post-mortem human brain sections using STED[125].

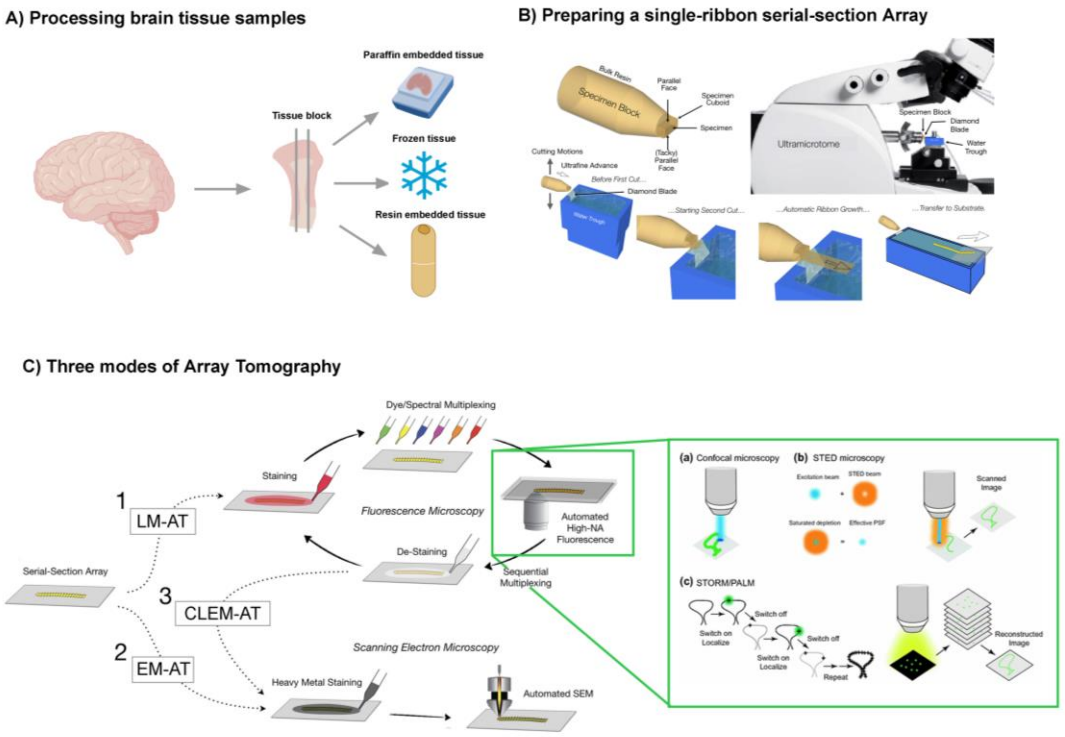

Figure 7. Array tomography workflow. A) Brain tissue blocks are divided in three sections for different protocols: paraffin-embedded samples, frozen samples and AT resin-embedded samples. B) Cutting a single-ribbon serial-section Array using an ultramicrotome with a diamond knife. C) Combination of LM, EM or CLEM with AT. 1) LM-AT: single-ribbon coverslip is stained with fluorescence dyes and imaged for multiplex light microscopy including confocal, STED or STORM microscopy. 2) EM-AT: single-ribbon coverslip is stained with heavy metals for EM acquisition (SEM or TEM). 3) CLEM-AT: single-ribbon coverslip is stained with fluorescence dyes and imaged using LM. Then, glass slide is removed and sample is washed. Single-ribbon coverslip is stained with heavy metals for EM acquisition.

Stochastic optical reconstruction microscopy

Stochastic optical reconstruction microscopy (STORM) was first described by Hess et al. in 2006 as a powerful new tool for immunofluorescence imaging of biological structures with sub-diffraction limit resolution[126]. The principal relies on the sequential activation and time-resolved localization of photoswitchable fluorophores to generate high-resolution images. During imaging, only an optically resolvable subset of fluorophores is randomly activated from a dark state to an emission state, followed by a quick switch back to the dark state or photobleaching. Iteration of this process allows numerous

fluorophores to be localized obtaining super-resolution images reconstructed from the images of the individual molecules. In 2008, Heilemann et al. introduced a most efficient version, the direct STORM (dSTORM) that shares the same principal as STORM but can be performed with regular, bright and photostable organic fluorophores[127,128] **[Fig. 7]**.

STORM is able to achieve the highest resolutions to date (~10-30nm) on an optical imaging system and the lower light levels needed makes this technique more suitable for *in vivo* applications. However, the acquisition is very time consuming depending on the desired resolutions and requires an extensive post-acquisition image processing to reconstruct the final image[120].

STORM imaging has been usually used in neuroscience in cell culture or animal models to measure molecular distributions at a nanoscale level in selected cells or subcellular compartments[129,130] to study synapses and the nanodomains present at both pre and postsynaptic terminals[131,132,133,134,135,136] or to investigate oligomeric Aβ aggregation in synapses[115]. Published studies using human brain tissue samples are difficult to find due to the limitation imposed by sample preparation. However, resolved subcellular structures, such as neurofilaments or myelin sheaths within intact white matter of human brain samples, have been reported[137].

Correlative light and electron microscopy

Correlative light and electron microscopy (CLEM) consists of the combination of light microscopy (LM) with high-resolution EM. LM offers an immense variety of labelling strategies such as dyes, immuno-labelling or labels using genetically encoded fluorescent proteins. Also, several types of microscopes can be used, like epifluorescense microscope, but studies frequently rely on confocal, two-photon and recently super-resolution microscopy, such as STED or STORM. EM is used to obtain structural information at a nanometer scale. Electron micrographs rely to a large extent on transmission electron microscopy (TEM) or scanning electron microscopy (SEM). While TEM uses electron shadows to create an image, SEM uses the interaction of electrons with molecules in the sample to recreate the image[138]. CLEM has been applied to reveal fine structures in mitochondria, mitotic chromosomes, neuronal synapses and glial cells in the nervous system of a wide range of organisms[138,139,140, 141,142,143,144].

In general, the correlation of LM with EM data has shown to be challenging, since the z-resolution of the LM is much worse than the required thickness for EM[145]. A way to overcome this problem is to combine AT, SR techniques and EM to deliver a volumetric super-resolved and multicoloured image with three-dimensional ultrastructure. The workflow of this approach consist of the combination of the AT protocol followed by removal of the coverslip with the sample from the glass slide, heavy metal staining and a new image acquisition with electron microscopy[146] **[Fig. 7]**. Some studies have already been published using this approach. Collman et al. used AT-SEM to image different types of synapses labelled with multiple synaptic markers[147]. Another example is provided by Bloss et al., who used AT-TEM to demonstrate that the connectivity between interneurons and pyramidal cell dendrites is more precise and spatially segregated than previously appreciated, which may be a critical determinant of how

inhibition shapes dendritic computation[148]. As previously mentioned, these studies have been performed using cell cultures or animal models and there are no studies in human samples.

There is still much more work to be done on the combination of AT, SR and/or EM using human brain samples. This is a powerful tool that can help to understand possible alterations in synaptic mechanisms or the composition of hallmark lesions of NDDs at a nanometer scale.

To summarise, the field of neuropathology is changing and adapting to the new technological era, but still has a long way ahead to fully take advantage of all the tools available. A lot of research, whenever possible using human samples, is still needed to elucidate the underlying altered mechanisms of NDDs.

Chapter 2: Hypotheses and objectives

This thesis is based on the following hypothesis:

1. YKL-40, a marker of inflammation, is close associated with core neuropathological markers in AD and other tauopathies.

2. The combination of super-resolution techniques can be applied for the study of non-fibrillar Aβ species conforming human amyloid β plaques. Higher levels of non-fibrillar Aβ forms may be expected in ADAD compared to SAD.

3. Administration of Verubecestat, a BACE-1 inhibitor, in a patient that participated in the phase 3 clinical trial may have reduced brain Aβ burden. Severe synaptic loss could underlie the cognitive declined experienced by the patient.

The specific objectives of this thesis are:

1. To determine the cellular pattern of YKL-40 expression in the human brain tissue in AD and other tauopathies and to investigate the relationship between YKL-40 expression and tau aggregates in these disorders.

2. To study the nanoscale architecture of non-fibrillar Aβ structures in human amyloid plaques combining ultrathin sections used in AT with super-resolution STED microscopy. Also, to investigate the load and size of these non-fibrillar Aβ entities in post-mortem human brain tissue of ADAD and SAD cases.

3. To evaluate postmortem the effect of the BACE-1 inhibitor Verubecestat on different Aβ species and synaptic markers in brain tissue samples in a treated patient compared to a group of untreated AD patients.

Chapter 3: Publications

YKL-40 (Chitinase 3-like I) is expressed in a subset of astrocytes in Alzheimer's disease and other tauopathies

Marta Querol-Vilaseca[1,2], Martí Colom-Cadena[1,2], Jordi Pegueroles[1,2,] Carla San Martín-Paniello[1], Jordi Clarimon[1,2], Olivia Belbin[1,2], Juan Fortea[1,2], Alberto Lleó[1,2*]

[1]Memory Unit, Department of Neurology, Institut d'Investigacions Biomèdiques Sant Pau - Hospital de la Santa Creu i Sant Pau, Universitat Autònoma de Barcelona, Barcelona, Spain. [2]Centro de Investigación Biomédica en Red en Enfermedades Neurodegenerativas (CIBERNED), Madrid, Spain

Background: The innate immune system is known to be involved early in the pathogenesis of Alzheimer's disease (AD) and other neurodegenerative disorders. The inflammatory response in the central nervous system can be measured *postmortem* or through a series of inflammatory mediators surrogates. YKL-40 (also named Chitinase-3-like I) has been frequently investigated in body fluids as a surrogate marker of neuroinflammation in AD and other neurological disorders. However, the expression pattern of YKL-40 in human brain with neurodegenerative pathology remains poorly investigated. Our aim was to study the cellular expression pattern of YKL-40 in the brain of patients with clinical and neuropathological criteria for AD (n=11), three non-AD tauopathies: Pick's disease (PiD; n=8), corticobasal degeneration (CBD; n=8) and progressive supranuclear palsy (PSP; n=9), and a group of neurologically healthy controls (n=6).

Methods: Semiquantitative neuropathological evaluation and quantitative confocal triple immunofluorescence studies were performed. An in-house algorithm was used to detect and quantify pathology burden of random regions of interest on a full tissue section scan. Kruskal-Wallis and Dunn's multiple comparison tests were performed for colocalization and quantification analyses.

Results: We found that brain YKL-40 immunoreactivity was observed in a subset of astrocytes in all four diseases and in controls. There was a strong colocalization between YKL-40 and the astroglial marker GFAP but not with neuronal nor microglial markers. Intriguingly, YKL-40-positive astrocytes were tau-negative in PSP, CBD and PiD. The number of YKL-40-positive astrocytes was increased in tauopathies compared with that in controls. A positive correlation was found between YKL-40 and tau immunoreactivities.

Conclusions: This study confirms that YKL-40 is expressed by a subset of astrocytes in AD and other tauopathies. YKL-40 expression is elevated in several neurodegenerative conditions and correlates with tau pathology.

JOURNAL OF NEUROINFLAMMATION (2017) 14:118. **DOI:** 10.1186/s12974-017-0893-7

Background

There is growing evidence that the immune system is involved early in the pathogenesis of Alzheimer's disease (AD) and in other neurodegenerative diseases [1, 2]. The activation of the immune system in AD (often referred to as "neuroinflammation") is known to be present at all stages of AD and is believed to play an active role in the disease process. The activation of microglia and astrocytes as a reaction to ongoing deposition of Aβ triggers the production of several proinflammatory signal molecules including cytokines, chemokines, complement molecules, growth factors and cell adhesion molecules [3]. The recent association of gene encoding inflammatory proteins, such as TREM2 and CD33 with AD [4–6], has further supported the role of the innate immune response in the aetiology and progression of AD. In addition, the increased feasibility of measuring a wide range of inflammatory molecules in biofluids from patients at different AD stages has expanded our understanding about the type of immune responses observed in neurodegenerative diseases. A variety of cytokines, chemokines and other inflammatory mediators are increased in cerebrospinal fluid (CSF) or in plasma in AD [1]. One of the proteins that has been frequently measured in body fluids as a surrogate marker of neuroinflammation in AD and other neurological disorders is YKL-40 (also named Chitinase 3-like I) [7, 8]. It has been described that YKL-40 participates in connective tissue cell growth, endothelial cell migration and inhibition of mammary epithelial cell differentiation and promotes tumour angiogenesis [9]. However, its biological and physiological functions in the central nervous system remain unclear. YKL-40 is increased in the CSF of multiple sclerosis (MS) patients, and YKL-40 levels correlate well with disease progression [10]. In previous studies, we and others [11, 12] found elevated YKL-40 levels in the CSF of AD patients. Interestingly, increased levels of YKL-40 were found in the preclinical stages of AD [13, 14] indicating that the immune system activation occurs early in the disease. These studies have also shown that CSF levels of YKL-40 and tau strongly correlate [11, 12]. Additional studies have indicated that YKL-40 is also elevated in the CSF of patients with other tauopathies, such as frontotemporal dementia (FTD), corticobasal degeneration (CBD) and progressive supranuclear palsy (PSP) [11, 13, 15, 16]. Despite the wide use of YKL-40 as a biochemical marker in neurodegenerative diseases, its distribution and pattern of expression in the human brain remains unclear. A recent study found that expression levels of chitinase genes in the brain regions of late onset AD (LOAD) patients are increased compared with healthy controls [17], but the cellular source of expression of these proteins remains uncertain. Some studies have suggested that YKL-40 is expressed in astrocytes in a variety of acute neuroinflammatory conditions, such as traumatic brain injury or multiple sclerosis [18, 19]. Other studies, however, support the idea that YKL-40 is also expressed in macrophage/microglia cell types in these conditions [19, 20]. In AD, studies show a variable pattern of YKL-40 expression that includes astrocytes, microglia or, on rare occasions, neurons [12, 21, 22]. The aim of the present work was to determine the cellular pattern of YKL-40 expression in the human brain tissue in AD and other tauopathies. We also investigated the relationship between YKL-40 expression and tau aggregates in these disorders.

Methods

Standard protocol approval and patient consent

A written informed consent was given by all donors and/or next of kin for the use of brain tissue for research. This study was approved by the local ethics committee at Hospital de Sant Pau, Barcelona, Spain.

Human brain samples

Human brain samples were provided by the Neurological Tissue Bank (NTB) of the Biobanc-Hospital Clínic-IDIBAPS and processed as previously described [23] and as internationally recommended [24]. The initial study group consisted of 40 patients who met clinical and neuropathological criteria for AD (n = 11), PSP (n = 10), CBD (n = 9), Pick's disease (PiD; n = 10) and a group of healthy controls (n = 7).

Neuropathologic assessment

We assessed formalin-fixed and paraffin-embedded tissue blocks from frontal cortex Brodmann areas 8/9. Immunohistochemistry was performed on 5-μm-thick sections on an automated stainer (DAKO Autostainer Plus; DAKO, Glostrup, Denmark) using the following primary antibodies: anti-amyloid β (clone 6F/3D, dilution 1:400; DAKO) and anti-phosphorylated tau (clone AT8, dilution 1:2000; Thermo Scientific, Waltham, MA). Reaction was visualized by the EnVision+ system peroxidase procedure (DAKO).

Immunoreactive structures of AT8 (NFTs, NTs, pretangles, dystrophic neurites, balloon cells, Pick bodies, ramified astrocytes, astrocytic plaques, tufted astrocyte and coiled bodies) and β-amyloid (mature, primitive and diffuse plaques) were systematically assessed in all cases. Neurofibrillary pathology was staged according to Braak criteria [25, 26]. β-amyloid phases were evaluated according to Thal criteria [27]. The National Institute on Aging-Alzheimer's Association Guidelines for neuropathologic assessment of AD was also applied [24]. Healthy controls without tau or amyloid pathology were included. Neuropathologic evaluation was carried out by three investigators on a multiheaded microscope.

Immunohistochemistry (IHC) and immunofluorescence (IF)

Formalin-fixed and paraffin-embedded brain sections of frontal cortex were dewaxed and pretreated with Tris/ EDTA buffer pH 9 at high temperature. The following primary antibodies were incubated overnight at 4 °C: polyclonal goat anti-YKL-40 (R&D Systems, AF2599, dilution 1:200), rabbit anti-GFAP (Sigma, G9269, dilution 1:500), phosphorylated tau clone AT8 (Thermo Scientific, MN1020, dilution 1:1000), monoclonal mouse anti-MAP2 (Sigma, M4403, dilution 1:500) and rabbit anti-Iba-1 (Wako Chemicals, 019-19741, 1:500). For IHC, the endogenous peroxidase activity was blocked, sections were HRP-labelled (Dako, Glostrup, Denmark, dilution 1:200) and the reaction was visualized by the EnVision+ system peroxidase procedure (DAKO, Glostrup, Denmark). For IF, sections were incubated for 1 h with Alexa Fluor 488, 555or 647 (Invitrogen, Carlsbad,CA, USA, dilution 1:1000) secondary antibodies and stained with Sudan black B (Merck, Whitehouse Station, NJ, USA) to mask tissue autofluorescence. Nuclei were stained with Hoechst 33258 (Life

Technologies, Carlsbad, CA, USA, dilution 1:1000), and coverslips were added with Immu-Mount (Fisher Scientific, Rockford, USA) mounting medium.

Image acquisition and analysis

Fluorescence images were acquired with a Leica inverted fluorescent confocal microscope (Leica TCD SP5-AOBS, Wetzlar, Germany) with a ×40 1.4 NA oil objective. Alexa Fluor 488, 555 and 647 were sequentially excited with 488-, 561- and 633-nm laser lines and captured with a spectral window of 498 to 530, 571 to 620 and 645 to 720 nm, respectively. A pulsed 405-nm laser was used for Hoechst visualization capturing images in a spectral range of 415 to 475 nm. Sections without antibodies or with secondary antibodies only were imaged to ensure specific and independent fluorophore visualization. For each case, at least 10 images per area were acquired. Pictures were taken in 4–5 z planes with a 0.7-µm pinhole. Maximal intensity projection of each type of aggregate was used for figure visualization.

For colocalization analyses, images were acquired avoiding saturated pixels. Saturation was only minimally applied for presentation purposes in the figure. Protein colocalization was evaluated using FIJI imaging software [28]. All images were analyzed following the same semiautomated in-house algorithm. Briefly, for each channel, the lowest intensity signals within a z-stack were removed to minimize background. An automated threshold was then estimated to create binary images. To quantify the overlap between proteins, Manders' colocalization coefficient was calculated for each channel [29, 30].

For quantification analysis of IHC stains, full-section scans were obtained with Pannoramic MIDI II (3DHistech, Budapest, Hungary). Cortical grey matter of each case was delimited blinded to clinical phenotypes. An in-house computer-based algorithm was developed to quantify tau pathology burden and GFAP immunoreactivity with MATLAB R2015b software (The MathWorks, Inc., Natick, MA, USA) **(Additional file 1: Figure S1)**. Briefly, the algorithm allows defining random regions of interest (ROIs) on a full-section scan, to compute densities of protein expression and to quantify the number of immunoreactive objects. This procedure was adapted from a published digital image analysis [31]. An outlier test was performed, and cases reported as statistical outliers were removed from the analysis. Five cases were excluded such that the final sample included the following cases: 11 AD, 9 PSP, 8 CBD, 8 PiD and 6 healthy controls. All quantitative analyses performed with the developed semi-automated method were manually validated in a subset of images. YKL-40-positive objects were manually validated by two investigators in order to ensure the correct identification of immunoreactivity patterns by the automated algorithm. Both investigators were blinded to clinical phenotypes.

Statistical analysis

Kruskal-Wallis and Dunn's multiple comparison tests were performed for colocalization and quantification analyses. Correlation between proteins was measured by the Spearman coefficient. Statistical significance was set at 5% ($\alpha = 0.05$). All data were analyzed using the GraphPad Prism 6.0 software (GraphPad Software, Inc., CA, USA).

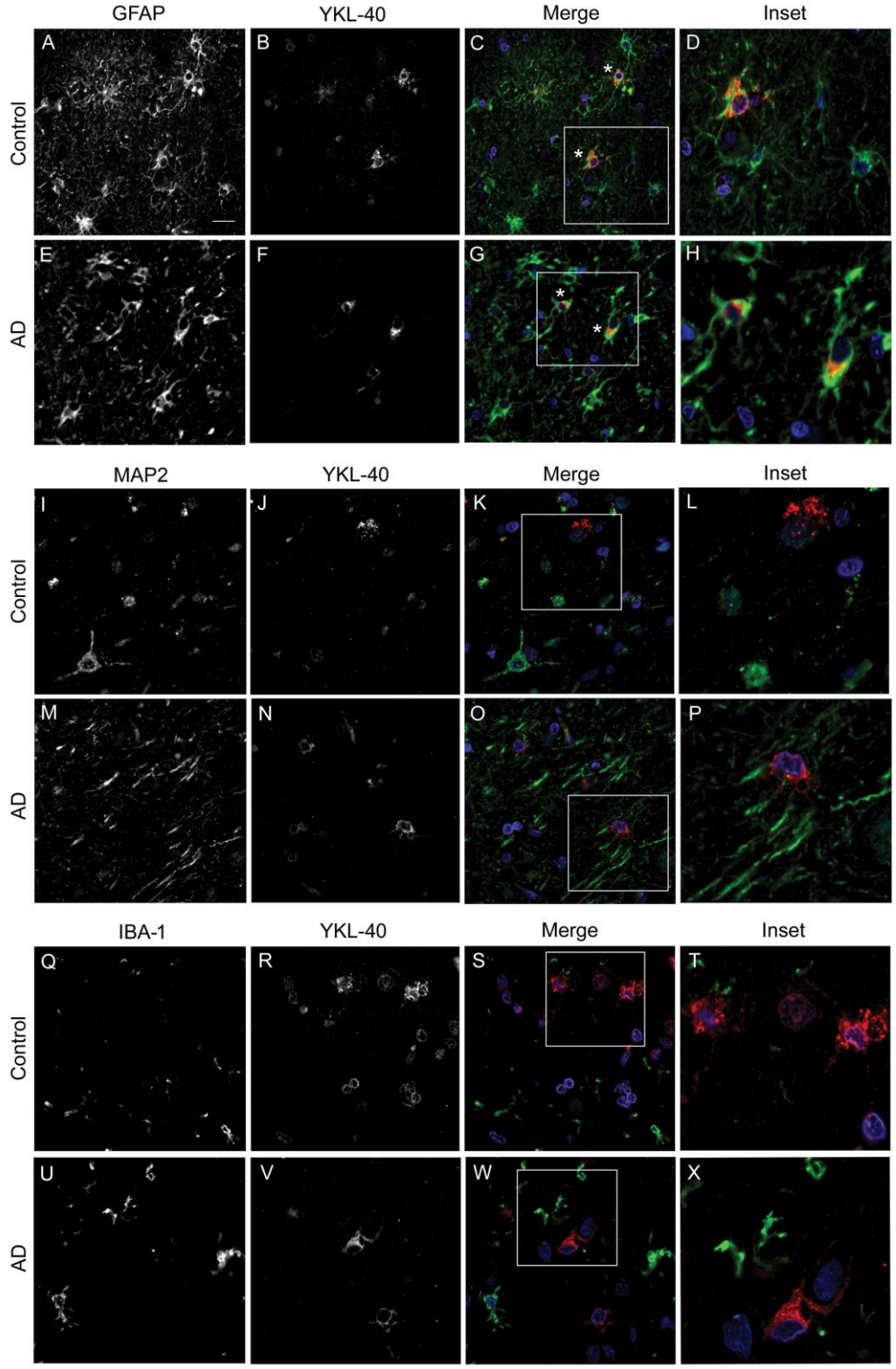

Figure 1. YKL-40 expression pattern in human brain tissue from an AD patient and a healthy control. Representative images of double immunofluorescence performed with YKL-40 (red) and three different cellular markers, GFAP (astroglial, green), MAP2 (neuronal, green) and IBA-1 (microglial, green). Nuclei are marked in blue. **a–h** YKL-40 immunoreactivity was detected in the cytoplasm of GFAP+ cells (asterisk), indicating anastroglial origin. **i–p** No colocalization was observed between YKL-40 and the neuronal marker, MAP2 or **(q–x)** with the microglial marker, IBA-1. Scale bar = 20 µm

Results

YKL-40 is expressed by astrocytes in human brain tissue

We first examined the cellular expression of YKL-40 in human brain tissue from an AD patient and a healthy control. Using a double immunofluorescence technique, we investigated the colocalization between YKL-40 and three different markers: MAP2 as a neuronal marker, GFAP as an astroglial marker and IBA-1 as a microglial marker **(Fig. 1)**. In both the AD and control brains, we found that YKL-40 colocalized in some cells labeled with the astrocytic marker GFAP, with a perinuclear cytoplasmic pattern extending to some proximal astroglial processes **(Fig. 1a–h)**. Conversely, there was no colocalization between YKL-40 and the neuronal marker, MAP2, or with the microglia marker, IBA-1 **(Fig. 1i–x)**. These findings indicate that YKL-40 is expressed by astrocytes in the frontal cortex of healthy and diseased human brain tissue.

YKL-40 is expressed in a subset of astrocytes in AD and other non-AD tauopathies

We next investigated whether the pattern of YKL-40 was similar between AD and other neurodegenerative diseases. YKL-40 expression pattern was examined in the frontal cortex from patients with different forms of frontotemporal lobar degeneration (FTLD) such as PiD, CBD and PSP. Since tau is known to aggregate in astrocytes in these subtypes of FTLD [32], we explored the relationship between YKL-40 expression and the different forms of tau aggregates in these conditions.

We performed triple immunofluorescence studies with antibodies against YKL-40, GFAP and tau in different cases of AD and non-AD tauopathies (n = 40) **(Fig. 2)**. We confirmed that 75–85% of YKL-40 immunoreactivity colocalized with GFAP indicating an astroglial origin in cases with AD, PiD, CBD and PSP **(Fig. 2u)**. The immunoreactivity of YKL-40 was mainly cytoplasmic while GFAP immunoreactivity extended distally to astrocytic processes and plasma membrane, which explains the lack of complete overlap. No differences in the expression pattern of YKL-40 between the AD and FTLD cases were found (all $p > 0.05$). Interestingly, in PSP, CBD and PiD, where tau-positive astrocytes are commonly found, most YKL-40-positive astrocytes were tau negative and vice versa. Accordingly, colocalization between YKL-40 and tau was negligible (<7%). On the other hand, as previously described [32], substantial overlap between tau and GFAP immunoreactivity was found in PiD (~37%), CBD (~37%) and PSP (~51%), whereas no overlap was found in AD. The distribution of YKL-40-positive astrocytes was mainly isolated but occasionally found surrounding blood vessels. These data support the idea that the immunoreactivity patterns of astroglial YKL-40 and tau are spatially distinct in non-AD tauopathies.

Relationship between YKL-40 expression, tau pathology and astrogliosis

We next investigated the differences in total YKL-40 immunoreactivity between the neurodegenerative conditions and healthy control brains. Immunohistochemistry for YKL-40, GFAP and tau was performed on three consecutive sections from the frontal cortex from each case, respectively.

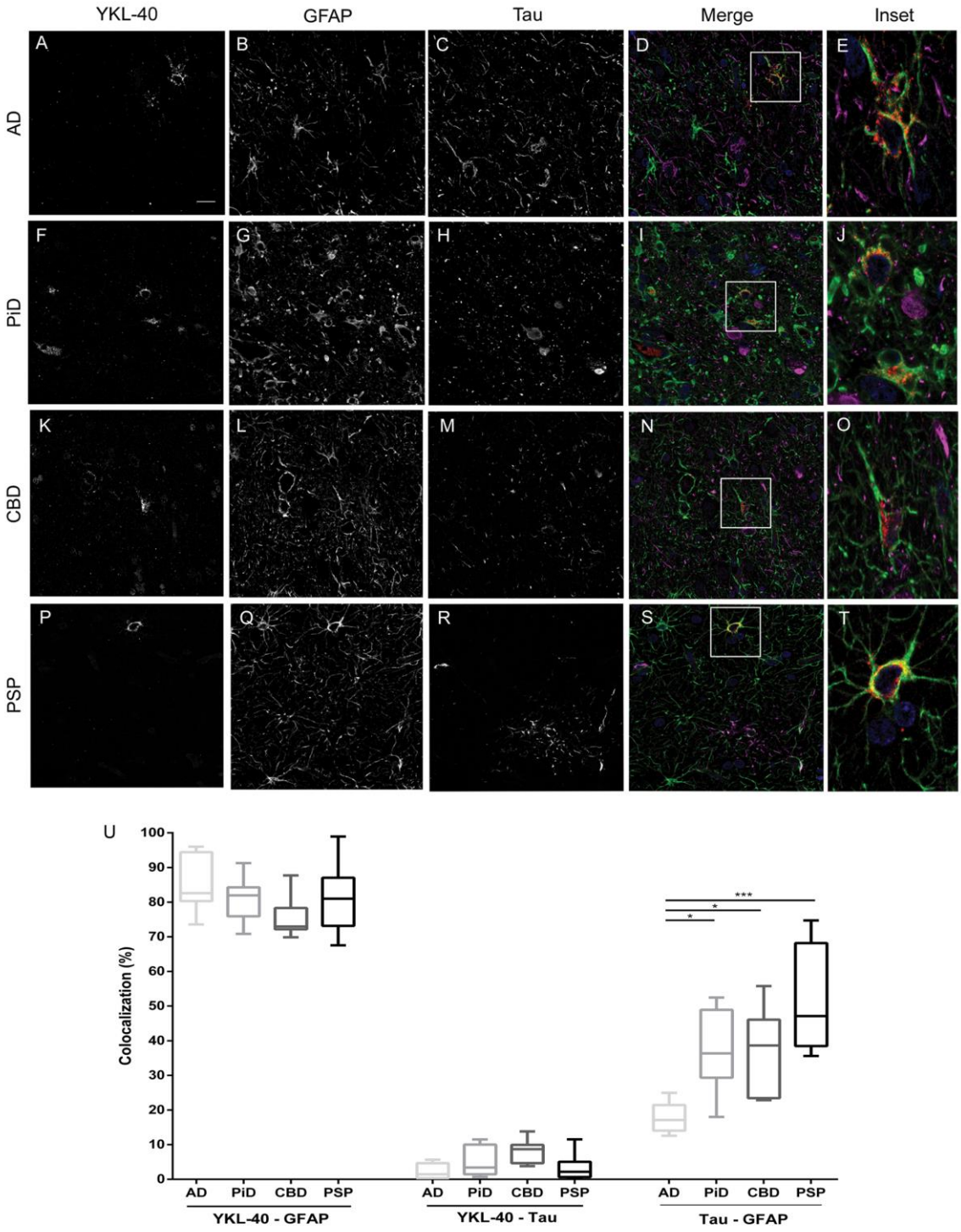

Figure 2. YKL-40 immunoreactivity pattern and colocalization analyses in different tauopathies. Representative images of the triple immunofluorescence studies performed with YKL-40 (red), GFAP (green) and tau (magenta) antibodies. Nuclei are marked in blue. All four tauopathies investigated, **a–e** AD, **f–j** PiD, **k–o** CBD and **p–t** PSP, showed a cytoplasmic astroglial expression pattern of YKL-40. Scale bar = 20 µm. **u** Colocalization analysis confirmed that approximately 80% of YKL-40 colocalized with GFAP in all tauopathies. No colocalization was detected between YKL-40 and tau in any condition. As expected, non-AD tauopathies showed an overlap between tau and GFAP. ***$p < 0.001$; *$p < 0.05$

Full-section scans of all samples were obtained, and quantification of tau, YKL-40 and GFAP was performed. Representative images of YKL-40, tau and GFAP immunoreactivity are shown in **Fig. 3(a–o)**. A similar YKL-40 expression pattern was observed across all neurodegenerative conditions although expected differences in tau deposits were detected between conditions. We next applied our in-house semi-automated algorithm to quantify total immunoreactivity (density/μm2) and number of objects of Tau and GFAP markers **(Additional file 1: Figure S1)**. YKL-40 levels were increased in all neurodegenerative diseases (except PiD) compared with controls ($p < 0.05$). No differences were observed between the different tauopathies (Fig. 3p). Less than 10% of GFAP-positive astrocytes expressed YKL-40 (10% in PSP, 7% in CBD, 5% in AD, 4% in PiD and 1% in healthy controls). We next examined the correlation between YKL-40, tau and GFAP markers. We found a positive correlation between tau pathology burden scores and YKL- 40 ($n = 36$; $r = 0.447$; $p = 0.006$) (Fig. 3q) and between GFAP and tau pathology ($n = 36$; $r = 0.651$; $p < 0.0001$) (Fig. 3s). However, we did not detect a correlation between YKL-40 and GFAP ($n = 36$; $p = 0.776$) scores **(Fig. 3r)**.

Discussion

In the present study, we found that YKL-40 is expressed by astrocytes in human brain tissue in healthy controls and in different neurodegenerative diseases. The immunoreactivity pattern of YKL-40 was mainly cytoplasmic extending to proximal astrocytic processes. We also observed that this protein is expressed in a subset of astrocytes (<10%) that do not contain tau aggregates in non-AD tauopathies.

To date, the pattern of expression of YKL-40 in the central nervous system has remained controversial and has not been fully elucidated. Some studies have described that YKL-40 is expressed in microglia [33, 34] while others have found it in astrocytes [12, 35]. These discrepancies may be because YKL-40 expression seems to vary depending on the disease and the severity of the neuroinflammatory response [19, 35]. It has been shown that in multiple sclerosis, YKL-40 is expressed by macrophages/microglial cells (CD68+) in low and high inflammatory activity lesions [19]. However, YKL-40 expression was also expressed in the cytoplasm of astrocytes (GFAP+) in high inflammatory activity lesions [19]. Another study reported that in human brain infarction, YKL-40 astrocytic expression depends on the stage of underlying inflammation, increasing during the acute inflammation phase and diminishing as the inflammation resolves [35]. Moreover, it has been shown by others that YKL-40 is also expressed by peripheral cells including chondrocytes [36], synoviocytes [37], vascular smooth muscle cells [38], macrophages [39] and neutrophils [40]. For example, it has been reported that expression of YKL-40 in breast cancer tissue correlates with tumour grade [41] and that YKL-40 macrophage expressionis upregulated in patients with chronic obstructive pulmonary disease and correlates with its severity [42]. *In vitro* studies have shown a dramatically increase of YKL-40 expression during astrocyte differentiation [43]. Other studies based on immunohistochemical techniques suggested that YKL-40 together with SSEA-4 marker expression represent an unexplored astrogenic lineage [44]. Here, we have confirmed that YKL-40 shows an astroglial cytoplasmic immunoreactivity pattern in postmortem human frontal cortex from healthy controls and AD patients.

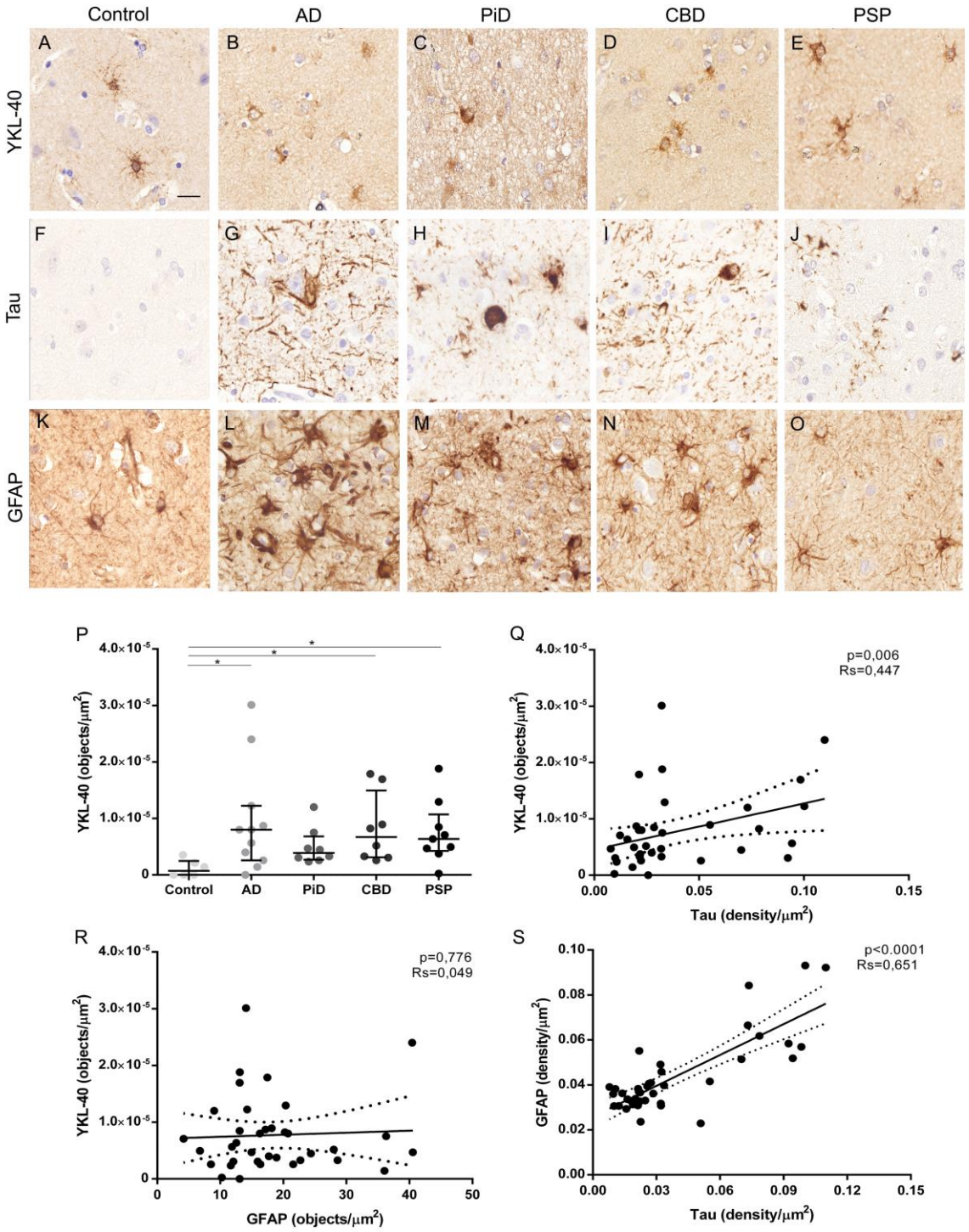

Figure 3. Quantification of YKL-40, tau pathology burden and astrogliosis in different tauopathies. Representative images of YKL-40, tau and GFAP immunoreactivity of controls and the four tauopathies under study**. a–e** YKL-40 expression pattern. **f–j** Main tau deposits and aggregates of each condition. **k–o** Astrogliosis among the tauopathies and controls. Scale bar = 20 µm. **p** YKL-40 immunoreactivity (objects/µm2) measured in all conditions. **q–s** Correlation between different markers. Levels of YKL-40 and GFAP correlated positively with tau aggregation. Solid lines indicate the linear regression, and dotted lines indicate 95% CI. RS, Spearman rho coefficient.

We did not detect YKL-40 expression in microglia or in neurons. We also found YKL-40 in the cytoplasm of astrocytes in non-AD tauopathies, including PiD, CBD and PSP. Although YKL-40 was typically found in isolated astrocytes, we occasionally observed focal astrocytic YKL-40 immunoreactivity around blood vessels. Previous studies have suggested that YKL-40 transcription is induced in astrocytes by proinflammatory factors released from macrophages [21]. One possible explanation for this observation is that perivascular macrophages may induce YKL-40 expression in astrocytes that are in close proximity. The colocalization between YKL-40 and GFAP was around 80% indicating that GFAP immunoreactivity, typically extending towards the astrocyte membrane and processes, surrounds that of YKL-40. Interestingly, YKL-40 immmunoreactivity was independent of tau, indicating that in non-AD tauopathies, YKL-40 is expressed in a taunegative subset of astrocytes. Whether YKL-40 could be a compensatory response to inhibit tau aggregation or, on the contrary, represents an initial event that facilities tau deposition requires further investigation. As expected, colocalization between tau and GFAP was found in non-AD tauopathies reflecting the distinctive glial tau aggregation in these disorders [32]. The 15% overlap observed in AD may be explained by neuropil threads crossing astrocyte processes in close proximity that are measured as colocalization due to the resolution limits.

Recent studies have demonstrated that YKL-40 levels are increased in the CSF of patients with AD and FTD compared with those in the healthy controls [11–16, 45, 46]. In addition, a positive correlation between YKL-40, total tau and p-tau has been reported in CSF, suggesting that inflammation and tau-associated neurodegeneration are related pathophysiological processes. In agreement, animal models and co-culture studies have shown that activated gliainduced neuronal tau phosphorylation and aggregation [47]. In postmortem brains, our semi-automated method revealed that total YKL-40 levels were statistically increased in all tauopathies (except PiD) compared with healthy controls. These results are in agreement with studies that investigated YKL-40 levels in CSF of AD and FTD patients [11–16, 45, 46]. It is important to note that only a limited proportion of astrocytes (always less than 10%) expressed YKL-40 in human frontal cortex. Interestingly, we found a positive correlation between YKL-40 and tau pathology burden ($r = 0.447$) suggesting that inflammation and neurodegeneration may be closely related processes in humans. The lack of correlation between YKL-40 and GFAP together with the positive correlation between tau and GFAP ($r = 0.651$) in our study also may indicate that YKL-40 expression is independent of astrocyte activation in neurodegenerative disease.

Conclusions

In conclusion, this is, to our knowledge, the first detailed neuropathologic characterization of YKL-40 expression in human brain tissue. Moreover, the study includes tissue samples from healthy controls and four neurodegenerative diseases. Combining confocal microscopy and the application of a semi-automated method to quantify pathology burden, we have shown that the immunoreactivity pattern of YKL-40 in AD and other tauopathies is astroglial. YKL-40 is expressed by a subset of astrocytes that do not contain tau aggregates in non-AD tauopathies. Finally, we have found that YKL-40 inflammatory marker is associated with tau pathology in neurodegenerative diseases that accumulate tau.

Acknowledgements

The authors thank Ellen Gelpi for the neuropathological review of the cases and Eva Companys for the confocal microscopy assistance.

References

1. Heppner FL, Ransohoff RM, Becher B. Immune attack: the role of inflammation in Alzheimer disease. Nat Rev Neurosci. 2015;16:358-72.

2. Heneka MT, Carson MJ, El Khoury J, Landreth GE, Brosseron F, Feinstein DL,Jacobs AH, Wyss-Coray T, Vitorica J, Ransohoff RM, et al. Neuroinflammation in Alzheimer's disease. Lancet Neurol. 2015;14:388-405.

3. Rubio-Perez JM, Morillas-Ruiz JM. A review: inflammatory process in Alzheimer's disease, role of cytokines. Sci World J. 2012;2012:756357.

4. Guerreiro R, Wojtas A, Bras J, Carrasquillo M, Rogaeva E, Majounie E, et al. TREM2 variants in Alzheimer's disease. N Engl J Med. 2013;368:117–27.

5. Jonsson T, Stefansson H, Steinberg S, Jonsdottir I, Jonsson PV, Snaedal J, et al. Variant of TREM2 associated with the risk of Alzheimer's disease. N Engl J Med. 2013;368:107–16.

6. Bradshaw EM, Chibnik LB, Keenan BT, et al. CD33 Alzheimer's disease locus: altered monocyte function and amyloid biology. Nat Neurosci. 2013;16:848–50.

7. Perrin RJ, Craig-Schapiro R, Malone JP, et al. Identification and validation of novel cerebrospinal fluid biomarkers for staging early Alzheimer's disease. PLoS One. 2011;6, e16032.

8. Fagan AM, Perrin RJ. Upcoming candidate cerebrospinal fluid biomarkers of Alzheimer's disease. Biomark Med. 2012;6:455–76.

9. Shao R. YKL-40 acts as an angiogenic factor to promote tumor angiogenesis. Front Physiol. 2013;4:122.

10. Comabella M, Fernandez M, Martin R, et al. Cerebrospinal fluid chitinase 3-like 1 levels are associated with conversion to multiple sclerosis. Brain. 2010; 133:1082–93.

11. Alcolea D, Carmona-Iragui M, Suarez-Calvet M, Sanchez-Saudinos MB, Sala I, Anton-Aguirre S. Relationship between ß-secretase, inflammation and core cerebrospinal fluid biomarkers for Alzheimer's disease. J Alzheimers Dis. 2014;42:157–67.

12. Craig-Schapiro R, Perrin RJ, Roe CM, Xiong C, Carter D, Cairns NJ, Mintun MA, Peskind ER, Li G, Galasko DR, et al. YKL-40: a novel prognostic fluid biomarker for preclinical Alzheimer's disease. Biol Psychiatry. 2010;68(10): 903–12.

13. Alcolea D, Martínez-Lage P, Sánchez-Juan P, Olazarán J, Antúnez C, Izagirre A, Ecay-Torres M, Estanga A, Clerigué M, Guisasola MC, Sánchez Ruiz D, Marín Muñoz J, Calero M, et al. Amyloid precursor protein metabolism and inflammation markers in preclinical Alzheimer disease. Neurology. 2015;85:626–33.

14. Antonell A, Mansilla A, Rami L, Lladó A, Iranzo A, Olives J, Balasa M, Sánchez-Valle R, Molinuevo JL. Cerebrospinal fluid Level of YKL-40 protein in preclinical and prodromal Alzheimer's disease. J Alzheimer's Dis. 2014;42:901–8.

15. Teunissen CE, Elias N, Koel-Simmelink MJA, et al. Novel diagnostic cerebrospinal fluid biomarkers for pathologic subtypes of frontotemporal dementia identified by proteomics. Alzheimers Dement (Amst). 2016;2:86– 94.

16. Alcolea D, Vilaplana E, Suarez-Calvet M, Illán-Gala I, Blesa R, Clarimón J, et al. Cerebrospinal fluid sAPPβ, YKL-40 and neurofilament light in frontotemporal lobar degeneration. Neurology. 2017 (in press).

17. Sanfilippo C, Malaguarnera L, Di Rosa M. Chitinase expression in Alzheimer's disease and non-demented brains regions. J Neurol Sci. 2016;369:242–9.

18. Bonneh-Barkay D, Zagadailov P, Zou H, et al. YKL-40 expression in traumatic brain injury: an initial analysis. J Neurotrauma. 2010;27:1215–23.

19. Cantó E, Tintoré M, Villar LM, Costa C, Nurtdinov R, Álvarez-Cermeño JC, Arrambide G, Reverter F, Deisenhammer F, Hegen H, Khademi M, Olsson T, Tumani H, Rodríguez-Martín E, et al. Chitinase 3-like 1: prognostic biomarker in clinically isolated syndromes. Brain. 2015;138:918–31.

20. Hinsinger G, Galéotti N, Nabholz N, Urbach S, Rigau V, Demattei C, Lehmann S, Camu W, Labauge P, Castelnovo G, et al. Chitinase 3-like proteins as

diagnostic and prognostic biomarkers of multiple sclerosis. Mult Scler. 2015; 21:1251–61.

21. Bonneh-Barkay D, Bissel SJ, Kofler J, Starkey A, Wang G, Wiley CA. Astrocyte and macrophage regulation of YKL-40 expression and cellular response in neuroinflammation. Brain Pathol. 2012;22:530–46.

22. Mattsson N, Tabatabaei S, Johansson P, Hansson O, Andreasson U, Mansson JE, Johansson JO, Olsson B, Wallin A, Svensson J, et al. Cerebrospinal fluid microglial markers in Alzheimer's disease: elevated chitotriosidase activity but lack of diagnostic utility. Neuromolecular Med. 2011;13(2):151–9.

23. Colom-Cadena M, Gelpi E, Charif S, Belbin O, Blesa R, Martí MJ, Clarimón J, Lleó A. Confluence of α-synuclein, tau, and β-amyloid pathologies in dementia with Lewy bodies. J Neuropathol Exp Neurol. 2013;72:1203–12.

24. Montine TJ, Phelps CH, Beach TG, Bigio EH, Cairns NJ, Dickson DW, Duyckaerts C, Frosch MP, Masliah E, Mirra SS, et al. National Institute on Aging-Alzheimer's Association guidelines for the neuropathologic assessment of Alzheimer's disease: a practical approach. Acta Neuropathol. 2012;123(1):1–11.

25. Braak H, Alafuzoff I, Arzberger T, Kretzschmar H, Del Tredici K. Staging of Alzheimer disease-associated neurofibrillary pathology using paraffin sections and immunocytochemistry. Acta Neuropathol. 2006;112(4):389–404.

26. Alafuzoff I, Pikkarainen M, Al-Sarraj S, et al. Interlaboratory comparison of assessments of Alzheimer disease-related lesions: a study of the BrainNet Europe Consortium. J Neuropathol Exp Neurol. 2006;65:740–57.

27. Thal DR, Rub U, Orantes M, Braak H. Phases of A beta-deposition in the human brain and its relevance for the development of AD. Neurology. 2002; 58:1791–800.

28. Schindelin J, Arganda-Carreras I, Frise E, Kaynig V, Longair M, Pietzsch T, et al. Fiji: an open-source platform for biological-image analysis. Nat Methods. 2012;9:676–82.

29. Manders EMM, Verbeek FJ, Aten JA. Measurement of colocalization of objects in dual-colour confocal images. J Microscopy. 1993;169:375–82.

30. Dunn KW, Kamocka MM, McDonald JH. A practical guide to evaluating colocalization in biological microscopy. Am J Physiol Cell Physiol. 2011;300: C723–42.

31. Irwin DJ, Byrne MD, McMillan CT, Cooper F, Arnold SE, Lee EB, Van Deerlin VM, Xie SX, Lee VM, Grossman M, Trojanowski JQ. Semi-automated digital image analysis of Pick's disease and TDP-43 proteinopathy. J Histochem Cytochem. 2016;64(1):54–66.

32. Kovacs GG. Invited review: neuropathology of tauopathies: principles and practice. Neuropathol Appl Neurobiol. 2015;41:3–23.

33. Hellwig K, Kvartsberg H, Portelius E, Andreasson U, Oberstein TJ, Lewczuk P, Blennow K, Kornhuber J, Maler JM, Zetterberg H, Spitzer P. Neurogranin and YKL-40: independent markers of synaptic degeneration and neuroinflammation in Alzheimer's disease. Alzheimers Res Ther. 2015;7(1):74

34. Lautner R, Mattsson N, Schöll M, Augutis K, Blennow K, Olsson B, Zetterberg H. Biomarkers for microglial activation in Alzheimer's disease. Int J Alzheimers Dis. 2011;2011:939426.

35. Bonneh-Barkay D, Wang G, Starkey A, Hamilton RL, Wiley CA. In vivo CHI3L1 (YKL-40) expression in astrocytes in acute and chronic neurological diseases. J Neuroinflammation. 2010;7:34.

36. Hu B, Trinh K, Figueira WF, Price PA. Isolation and sequence of a novel human chondrocyte protein related to mammalian members of the chitinase protein family. J Biol Chem. 1996;271:19415–20.

37. Nyirkos P, Golds EE. Human synovial-cells secrete a 39-kDa protein similar to a bovine mammary protein expressed during the nonlactating period. Biochem J. 1990;269:265–8.

38. Shackelton LM, Mann DM, Millis AJ. Identification of a 38-kDa heparinbinding glycoprotein (gp38k) in differentiating vascular smooth muscle cells as a member of a group of proteins associated with tissue remodeling. J Biol Chem. 1995;270:13076–83.

39. Rehli M, Krause SW, Andreesen R. Molecular characterization of the gene for human cartilage gp-39 (CHI3L1), a member of the chitinase protein family and marker for late stages of macrophage differentiation. Genomics. 1997; 43:221–5.

40. Kzhyshkowska J, Gratchev A, Goerdt S. Human chitinases and chitinase-like proteins as indicators for inflammation and cancer. Biomark Insights. 2007;2:128–46.

41. Shao R, Cao QJ, Arenas RB, Bigelow C, Bentley B, Yan W. Breast cancer expression of YKL-40 correlates with tumour grade, poor differentiation, and other cancer markers. Br J Cancer. 2011;105(8):1203–9.

42. Lai T, Wu D, Chen M, Cao C, Jing Z, Huang L, Lv Y, Zhao X, Lv Q, Wang Y, Li D, Wu B, Shen H. YKL-40 expression in chronic obstructive pulmonary disease: relation to acute exacerbations and airway remodeling. Respir Res. 2016;17:31.

43. Singh SK, Bhardwaj R, Wilczynska KM, Dumur CI, Kordula T. A complex of nuclear factor I-X3 and STAT3 regulates astrocyte and glioma migration through the secreted glycoprotein YKL-40. J Biol Chem. 2011;286:39893–903.

44. Brøchner CB, Møllgård K. SSEA-4 and YKL-40 positive progenitor subtypes in the subventricular zone of developing human neocortex. Glia. 2016;64(1): 90–104.

45. Janelidze S, Hertze J, Zetterberg H, Landqvist Waldö M, Santillo A, Blennow K, Hansson O. Cerebrospinal fluid neurogranin and YKL-40 as biomarkers of Alzheimer's disease. Ann Clin Transl Neurol. 2015;3(1):12–20.

46. Irwin DJ, Trojanowski JQ, Grossman M. Cerebrospinal fluid biomarkers for differentiation of frontotemporal lobar degeneration from Alzheimer's disease. Front Aging Neurosci. 2013;5:6.

47. Arnaud L, Robakis NK, Figueiredo E, Pereira ME. It may take inflammation, phosphorylation and ubiquitination to "tangle" in Alzheimer's disease. Neurodegener Dis. 2006;3(6):313–9.

Supplementary data

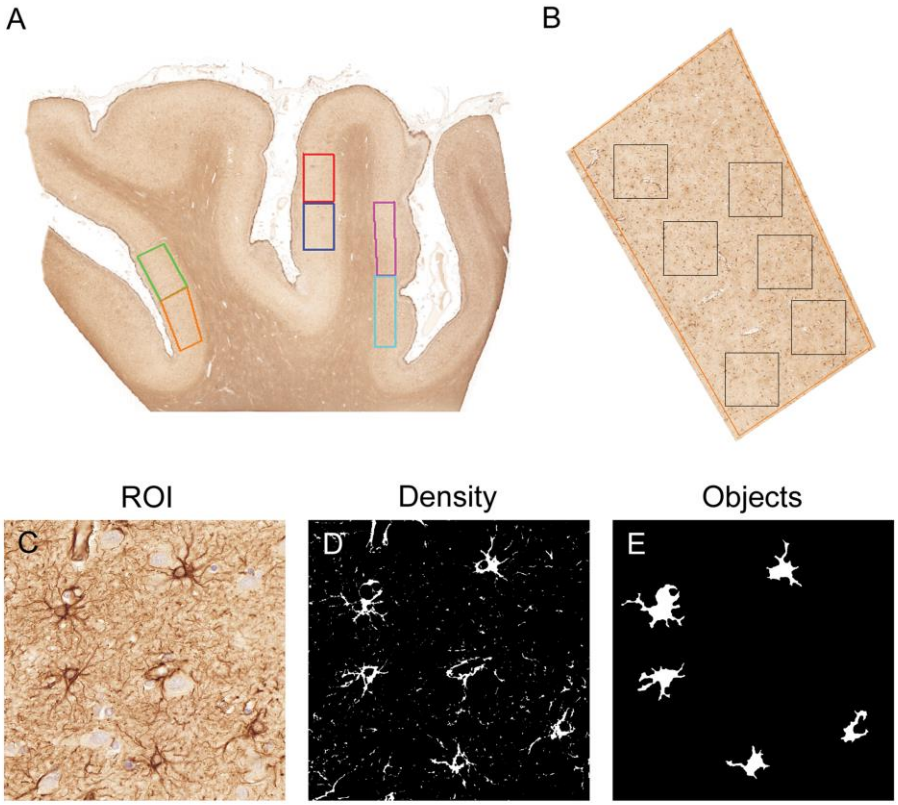

Additional file 1: Figure S1. Semi-automated method for pathological burden quantification. For all conditions tau and GFAP were assessed using a randomized computer-based quantification of patterns and severity in immunohistochemical stains. Cortical grey matter of each case was delimited blinded to clinical phenotypes **(A)**. We developed an in-house algorithm that allows defining randomized regions of interest (ROIs) on a full-section scan **(B–C)**, to compute density of protein expression **(D)** and to quantify the number of pathological objects **(E)**.

Nanoscale structure of amyloid-β plaques in Alzheimer's disease

Marta Querol-Vilaseca[1,2], Martí Colom-Cadena[1,2], Jordi Pegueroles[1,2,] Raúl Nuñez-Llaves[1,2], Joan Luque-Cabecerans[1,2], Laia Muñoz-Llahuna[1,2], Jordi Andilla[3], Olivia Belbin[1,2], Tara L. Spires-Jones[5], Ellen Gelpi[4,6], Jordi Clarimon[1,2], Pablo Loza-Alvarez[3], Juan Fortea[1,2], Alberto Lleó[1,2*]

[1]Memory Unit, Department of Neurology, Institut d'Investigacions Biomèdiques Sant Pau - Hospital de la Santa Creu i Sant Pau, Universitat Autònoma de Barcelona, Barcelona, Spain. [2]Centro de Investigación Biomédica en Red en Enfermedades Neurodegenerativas (CIBERNED), Madrid, Spain. [3]ICFO-Institut de Ciències Fotòniques, The Barcelona Institute of Science and Technology, Castelldefels, Barcelona, Spain. [4]Neurological Tissue Bank of the Biobanc-Hospital Clinic-IDIBAPS, Barcelona, Spain. [5]The University of Edinburgh, UK Dementia Research Institute, Centre for Discovery Brain Sciences, Edinburgh, EH8 9JZ, UK. [6]Institute of Neurology, Medical University of Vienna, Vienna, Austria.

Soluble amyloid-β (Aβ) is considered to be a critical component in the pathogenesis of Alzheimer's disease (AD). Evidence suggests that these non-fibrillar Aβ assemblies are implicated in synaptic dysfunction, neurodegeneration and cell death. However, characterization of these species comes mainly from studies in cellular or animal models, and there is little data in intact human samples due to the lack of adequate optical microscopic resolution to study these small structures. Here, to achieve super-resolution in all three dimensions, we applied Array Tomography (AT) and Stimulated Emission Depletion microscopy (STED), to characterize in postmortem human brain tissue non-fibrillar Aβ structures in amyloid plaques of cases with autosomal dominant and sporadic AD. Ultrathin sections scanned with super-resolution STED microscopy allowed the detection of small Aβ structures of the order of 100 nm. We reconstructed a whole human amyloid plaque and established that plaques are formed by a dense core of higher order Aβ species (~0.022 µm3) and a peripheral halo of smaller Aβ structures (~0.003 µm3). This work highlights the potential of AT-STED for human neuropathological studies.

SCIENTIFIC REPORTS (2019) 9:5181 **DOI:** 10.1038/s41598-019-41443-3

Introduction

Amyloid-β (Aβ) aggregation is believed to be a key initial pathophysiological event in Alzheimer's disease (AD). Several *in vitro* and *in vivo* studies have shown that, under certain conditions, Aβ peptides are able to form small soluble oligomers that grow into protofibrils and finally into dense insoluble structures that accumulate in the brain in form of extracellular β-amyloid plaques[1–3]. There is growing evidence that soluble Aβ species are more toxic than fibrillar Aβ in causing neuronal loss and synaptic dysfunction[4–7]. Aβ oligomers can induce neuronal and synaptic damage through different mechanisms, such as inhibition of hippocampal long-term potentiation[8], inhibition of exocytosis by impairing SNARE complex formation[9], deregulation of NMDA-mediated calcium influx triggering synaptic collapse[10] or the formation of membrane pores causing permeabilization and inducing neuronal death[11,12].

The majority of cases of AD are sporadic (SAD) but in ~1% of cases the disease segregates with an autosomal dominant pattern (ADAD) and an early age of onset[13,14]. ADAD is caused by mutations in the amyloid precursor protein (APP) or in the two presenilin (*PSEN1* and *PSEN2*) genes[15,16]. Different studies have demonstrated that these mutations cause a chronic increase in the relative or absolute production of the 42-aa form of Aβ peptide (Aβ42) leading to the formation of oligomeric Aβ, fibrillar Aβ deposition and neurodegeneration[15,17]. In contrast, the mechanisms underlying Aβ accumulation in SAD patients are far more complex. The main hypothesis to explain Aβ deposition in SAD is the existence of a chronic imbalance between Aβ production and clearance as a result of aging and other risk factors[17–22].

Although it is often assumed that the soluble Aβ species are the most toxic, the main properties such as size, morphology, structure and stability in human brain remain under study[23–26]. The majority of available data is based on experiments that used synthetic Aβ42 oligomers on cell cultures or animal models that overexpress mutant APP[5,6,27–30] and few studies have investigated the role of non-fibrillar Aβ in intact human brain samples[31–39].

The study of small structures such as non-fibrillar Aβ species in human brain samples has been challenging due to the limited resolution of immunohistochemistry using conventional microscopy. The lowest resolution obtained with optical microscopy is 200 nm, thus precluding any detailed characterization of those species. A recent study showed that the combination of new technologies such as focused ion beam milling and scanning electron microscopy (FIB/SEM) plus computational tools can be applied for the study of human amyloid plaques or synapses in the AD brain[40]. The use of hyperspectral Raman imaging has been also applied for the study of the biochemical components and β-sheet content of amyloid plaques and their surroundings[41]. In light microscopy, other techniques are also emerging for the study of small structures in brain tissue. One example is array tomography (AT), a technique that combines ultrathin sectioning of the tissue to increase the axial resolution with immunofluorescence, allowing quantitative analysis of high-resolution and large-field volumetric imaging of different specimens, such as synapses or pathological aggregates[42]. AT has demonstrated the ability to resolve Aβ synaptic deposits in AD brains[6]. Additionally, in the super-resolution (SR) fluorescence microscopy domain, Stimulated Emission Depletion (STED) microscopy is a technique that combines a high

resolution confocal microscope with a high power donut-shaped depletion laser. The STED configuration uses the excitation and depletion lasers simultaneously increasing the lateral resolution by reducing the emission area selectively depleting the fluorescent molecules under the donut-shaped beam[43,44].

In the present work, we propose a new tool to study the nanometric neuropathology of neurodegenerative diseases by combining ultrathin sections used in AT scanned with super-resolution STED microscopy. Applying AT-STED, we investigate the nanoscale architecture of non-fibrillar Aβ structures in human amyloid plaques. We also investigated the load and size of these non-fibrillar Aβ entities in post-mortem human brain tissue in ADAD (*PSEN1* mutation carriers) and early-onset sporadic AD (eoSAD) patients.

Materials and Methods

Standard protocol approval and patient consent

We obtained written informed consent from all brain donors and/or next of kin for the use of brain tissue for research. The study was approved by the local ethics committee of Hospital de Sant Pau, Barcelona, Spain. All research was performed in accordance with relevant guidelines and regulations.

Postmortem human brain samples

Brain samples for immunohistochemical assays were provided by the Neurological Tissue Bank (NTB) of the Biobanc-Hospital Clínic-IDIBAPS and processed as previously described[61] and as internationally recommended[62]. The study group consisted of 34 subjects: 10 patients with *PSEN1* mutations, 14 eoSAD patients with an age of onset <65 years and a group of 9 healthy controls. Fresh brain tissue from one ADAD (*PSEN1* G206D, age 63) and one SAD case (age 90) was processed for AT as previously described[57,63] and included in our collection.

Immunohistochemistry, image acquisition and analysis

Immunohistochemistry was performed on 5-µm-thick consecutive sections of occipital cortex on an automated stainer (DAKO Autostainer Plus; DAKO, Denmark) using the following primary antibodies: mouse monoclonal anti-amyloid beta clone 6F/3D (dilution 1:400, DAKO, Denmark) and mouse anti-NAB61 (dilution 1:250, a kind gift from Virginia Lee, University of Pennsylvania, Philadelphia, USA). Reaction was visualized by the EnVision + system peroxidase procedure (DAKO, Denmark). Full-section scans were obtained with Pannoramic MIDI II (3DHistech, Budapest, Hungary) using a 40x objective. Cortical grey matter of each case was manually delimitated with Pannoramic viewer software (3DHistech, Budapest, Hungary). An adaptation of the algorithm previously described[64] was developed to quantify total Aβ and NAB61 immunoreactivity with MATLAB software (The Math Works, Inc., MA, USA). Specifically, a colour deconvolution was used to split the channels and a mean local filter was then applied to segment the structures **(Supplementary Fig. S1)**.

Array Tomography

Brain samples for AT were processed using previously described methods[57,63]. Briefly, 70 nm-thick sections were obtained using an ultramicrotome (Leica Microsystems) equipped with an Ultra Jumbo Diamond Knife 35° Diatome) from LR white embedded tissue blocks.

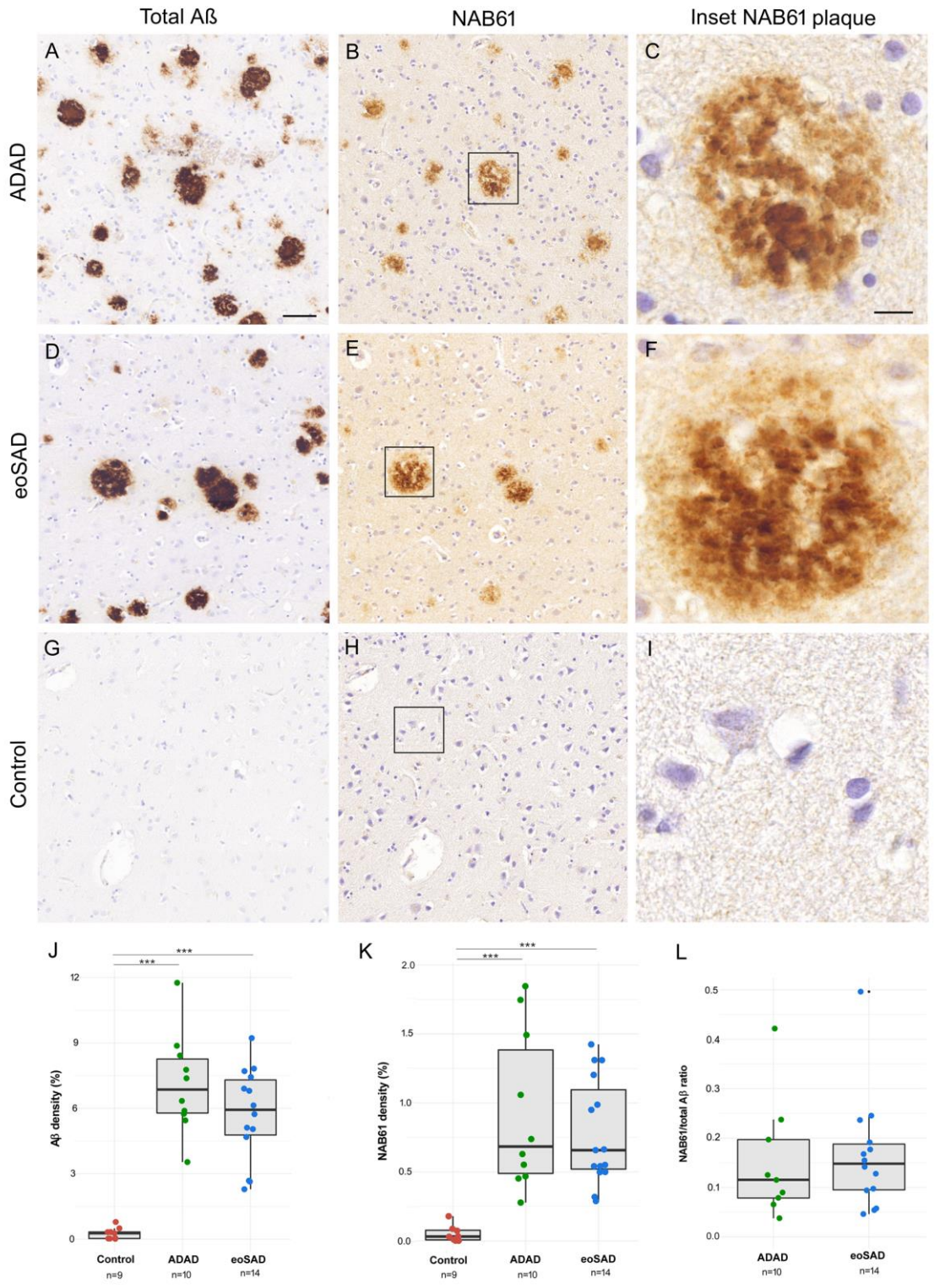

Figure 1. Quantification of total and non-fibrillar Aβ in ADAD and eoSAD cases. (A–I) Representative images of total Aβ and NAB61 immunoreactivity of ADAD, eoSAD and control cases. Strong immunoreactivity for both markers in consecutive sections from ADAD and eoSAD cases was found. Scale bar = 50 µm and 10 µm for inset. **(J,K)** Total Aβ and NAB61 densities were increased in both AD groups compared with controls. **(L)** No differences were found in the ratio NAB61/total Aβ between ADAD and eoSAD. ***p < 0.001.

The ribbons were stained as previouslydescribed[63] and incubated with Tris-Glycine solution 5' at RT followed by a blocking of unspecific antigens with a cold water fish blocking buffer (Sigma-Aldrich) for 30 min. Sections were then incubated for 2 hours with the following primary antibodies: mouse anti-NAB61 (dilution 1:50, kindly provided by Virginia Lee, University of Pennsylvania, Philadelphia, USA) and rabbit anti-Neurofilament Light (dilution 1:50, #2837, Cell Signaling). After TBS washings, secondary fluorescent antibodies Alexa 488 and Alexa 555 (dilution 1:50, Invitrogen) were applied for 30'. Sections were washed with TBS and samples were stained with Hoechst 33258 (dilution 1:100, Life Technologies) for 5 min for nuclei visualization. Finally, coverslips were mounted on microscope slides with Immu-Mount (Fisher Scientific) mounting medium.

STED and confocal image acquisition

The acquisition of confocal and STED images has been performed using a Leica STED CW microscope (Leica Microsystems). The excitation wavelength was 488 nm and the spectral detector window has been set from 495 nm to 588 nm. The objective used was a Leica HCX PL APO CS 100.0x STED with 1.4 NA. The 592 nm STED laser was set to 85% and the detectors used were Hybrid detectors in photon counting mode. The scanning speed was 1000 Hz per line and each acquisition has been obtained accumulating six times per line and averaging two acquisitions per image. Finally, these settings provided a set of images of 2048 × 2048 with effective pixel dwell time of 5.9 µs.

Image processing and analysis

For the analysis of AT images, MATLAB software (The Math Works, Inc., Natick, MA, USA) was used. Image stacks of each channel comprising all 70 nm consecutive sections were first registered using a rigid registration followed by an affine registration of a reference channel. Aligned sections were segmented using an automated mean local thresholding. Additionally, objects that were not in at least two consecutive sections or that were less than 3px were considered background and removed. After identification of three-dimensional structures, the density and size of individual entities were quantified. In order to perform the 3D visualization of the human amyloid plaque, the 2D images were stacked in a whole 3D reconstruction.

Statistical analysis

R software (version 3.2.5, www.r-project.org) was used to assess the statistical analysis. Due to the non-normal distribution of the data, non-parametric tests were applied. For immunohistochemical assays, Kruskal-Wallis with Dunn's post testing were used to detect differences in NAB61 and total Aβ levels between groups and a Mann-Whitney test was used for the ratio. To assess the differences between the ADAD case and the SAD case, an unpaired Mann-Whitney test was used.

Results

Conventional immunohistochemistry reveals no differences between ADAD and eoSAD cases in total or non-fibrillar Aβ.

We included a group of 14 patients with eoSAD, 10 patients with ADAD carrying a PSEN1 mutation and 9 healthy controls. Demographic, clinical and genetic data are shown in **Supplementary Table S1**. Detailed neuropathological data of the cases is shown in **Supplementary Table S2**.

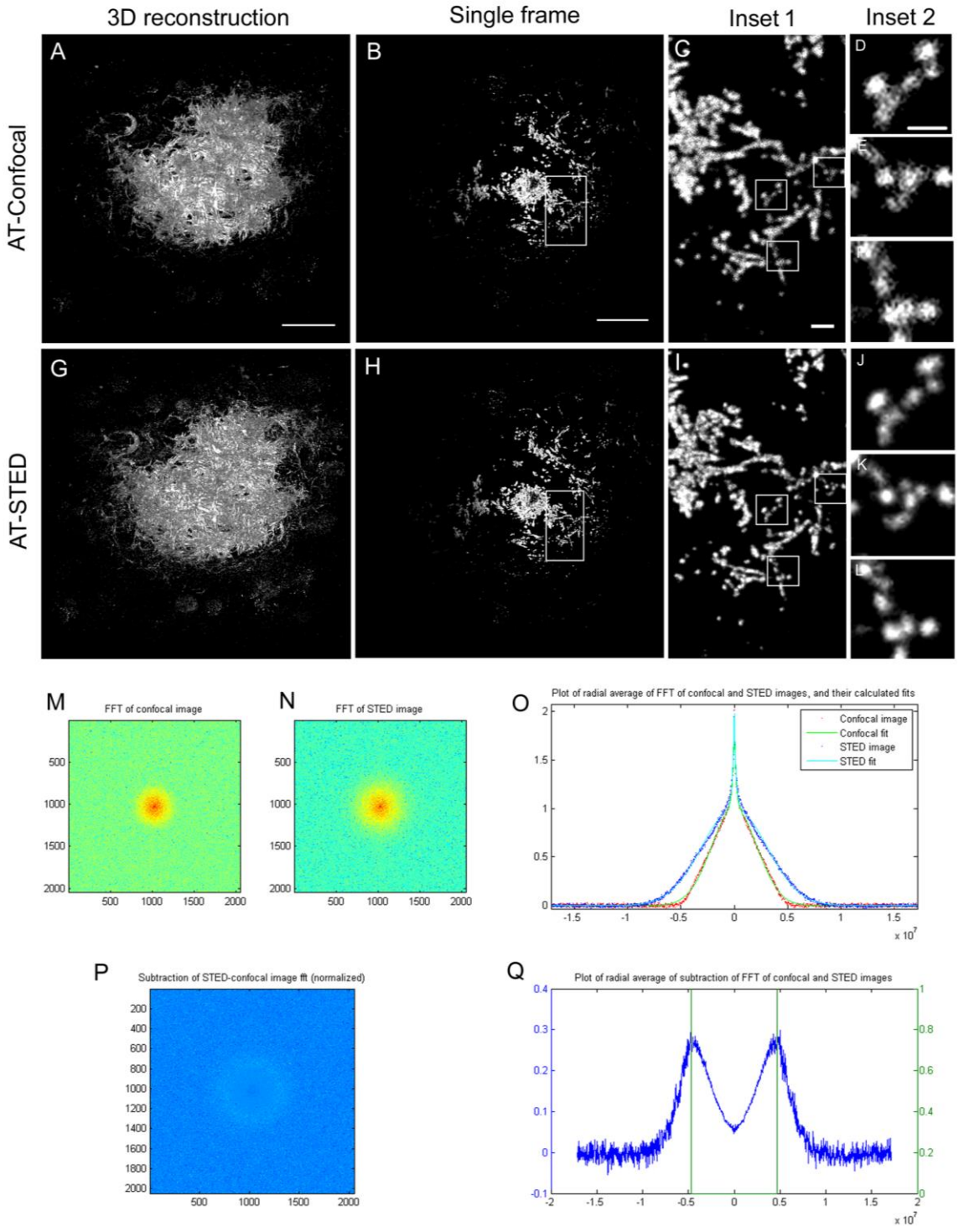

Figure 2. Comparison of the resolution between AT-Confocal and AT-STED modalities. **(A,G)** Maximal projection of a 3D reconstruction of an amyloid beta plaque in AT-Confocal and AT-STED respectively. **(B,H)** Image of a single slice of the amyloid-β plaque. **(C–F; I–L)** insets. **(M,N)** Scale bar = 10 µm, 1 µm for inset 1 and 0,5 µm for inset 2. Frequency domain representation of B and H. **(O)** Radial average of the frequency information for the AT-Confocal and AT-STED cases. **(P,Q)** Difference between of the radial frequency information between modalities. Green lines show the theoretical diffraction limit for 1.4NA objective.

As expected, eoSAD cases had a later age of onset and death and higher frequency of the APOEε4 allele compared to ADAD cases. We employed conventional immunohistochemistry of consecutive sections to examine the differences in total and non-fibrillar Aβ immunoreactivity (using the NAB61 antibody) between ADAD, eoSAD and control cases. We found higher amyloid load in ADAD and eoSAD cases ($p < 0.001$) compared to controls but without differences between the AD groups (**Fig. 1**).

Improving spatial and axial resolution with AT and STED.

We next investigated the potential of combining two microscopy techniques to investigate non-fibrillar Aβ structures in human AD brains. AT provides improved resolution in the axial plane by obtaining 70 nm thick tissue sections. Due to the special fixation and tissue processing requirements for this method, the availability of samples for this type of studies is limited.

In order to obtain nanometric resolution in the lateral directions here we combined AT with STED. STED microscopy combines a high resolution confocal microscope with a high power depletion laser. This laser has been engineered to obtain a donut-shaped focal-spot and it is scanned simultaneously with the excitation laser. This configuration enables stimulated depletion emission on the molecules under the donut-shaped beam. Thus, the emitted light in this outer region of the excitation beam is forced to emit at the wavelength of the STED laser. Using adequate spectral filtering, the light generated in the center of the donut is then collected for analysis which is determined by the power of the STED laser. We acquired images of amyloid-β plaques with an STED microscope using both confocal and STED configurations. The combination of AT and the settings of STED used in this experiment yielded a minimum effective voxel size of 70 × 100 × 100 nm.

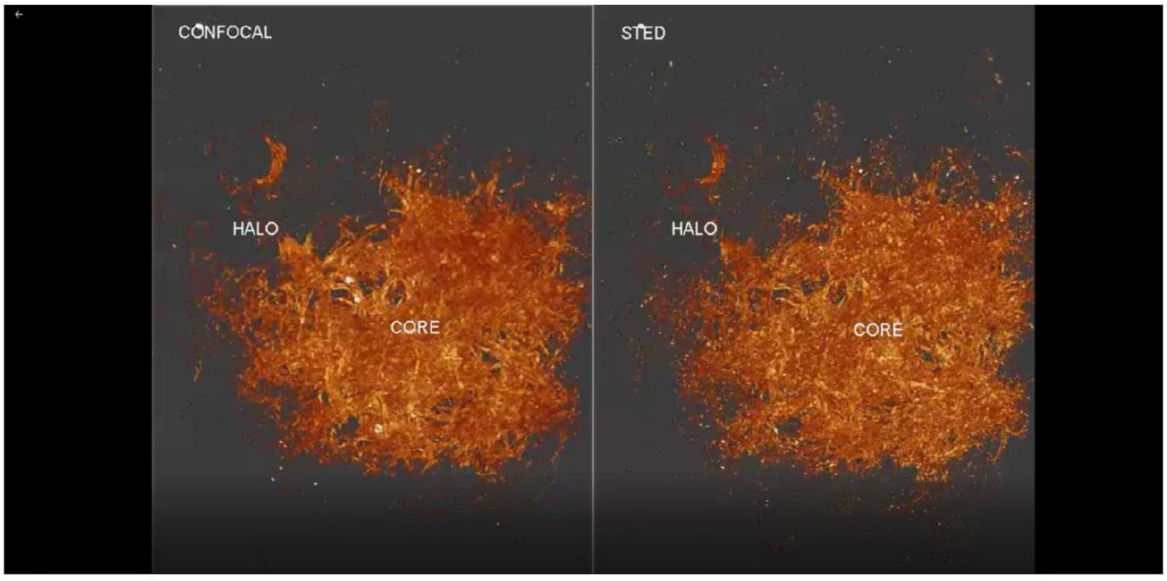

Figure 3. Nanoscale architecture of an entire human amyloid plaque using AT-STED. Reconstruction of 368 consecutive sections of an amyloid plaque from a SAD case. Zoom during the video shows the non-fibrilar Aβ structures better resolved in STED compared to confocal microscopy.

This voxel size allowed us to resolve smaller non-fibrillar Aβ structures in comparison with using AT alone (**Fig. 2**). A 3D reconstruction of a full amyloid β plaque of ~50 µm of diameter is shown in **Fig. 2**. The use of AT-STED microscopy provided increased resolution of the amyloid-β aggregates compared with high resolution confocal microscopy. A tool published by Merino et al.[44], enables to obtain an objective parameter, in which the sample is also considered, that can be used to determine the optimal settings for the STED image acquisition. Using this tool, we demonstrated an extension in the frequencies that allowed identifying objects down to 110 nm; in contrast, with AT alone the size of the smallest structure detected in the lateral plane was 220 nm.

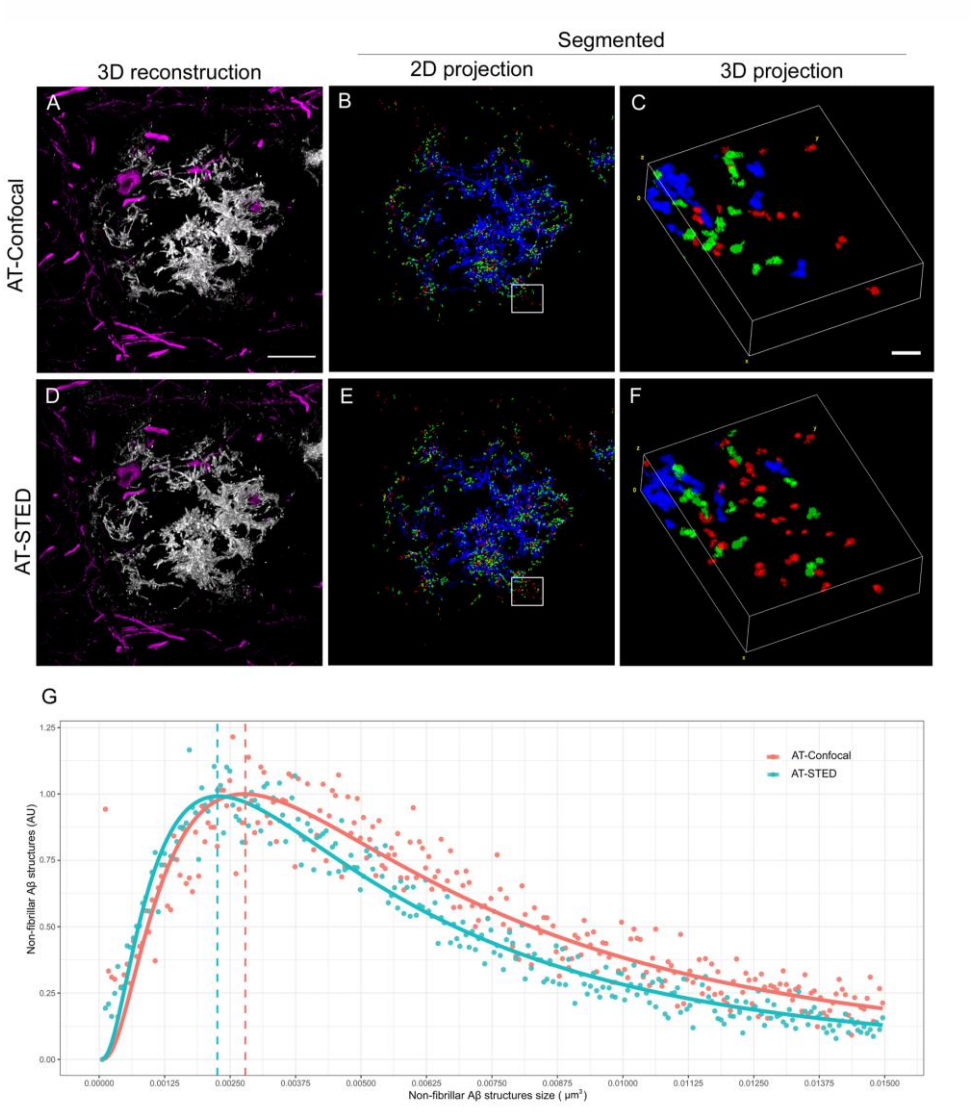

Figure 4. Distribution and quantification of non-fibrillar Aβ structures using AT-Confocal vs AT-STED. (A,D) Representative images of a human amyloid beta plaque and the surrounding neuronal structures (neurofilament light magenta) using **(A)** AT alone or **(D)** AT-STED. **(B,E)** Images of a segmented 2D projection of the Aβ plaque and **(C,F)** the respective 3D insets. Each color indicates a different Aβ structure's size: large (>0,015 µm3; blue), medium (>0,006 < 0,015 µm3; green) and small (<0,006 µm3; red). Detection of a dense core formed by large Aβ structures and a halo around the plaque formed by medium and small Aβ entities. Scale bar = 10 µm and 1 µm for the inset. **(G)** AT-Confocal and AT-STED distribution of NAB61 structures.

The combination of AT and STED allows the identification of smaller non-fibrillar Aβ structures.

We applied AT-STED to 368 consecutive sections to obtain a detailed architecture of a whole human amyloid β plaque at a nanoscale resolution (**Fig. 3**). We next selected randomly amyloid β plaques (n = 13) from two AD cases (one ADAD and one SAD) and captured images using both confocal and STED configurations to examine the size and distribution of NAB61-immunoreactive Aβ structures (a total of 18.000 objects).

We also immunostained for neurofilaments to visualize the neuronal structures around the plaque (**Fig. 4A,D**). We divided the objects into three categories: small (<0,006 μm3; red), medium (>0,006 <0,015 μm3; green) and large (>0,015 μm3; blue). We obtained a distinguished dense core formed by higher order Aβ structures (blue) and a halo of medium and small non-fibrillar Aβ entities (green and red) surrounding the plaque (**Fig. 4**). Using the combination of AT-STED compared to AT alone, we observed an increase of all Aβ structures (**Fig. 4**). Quantitative analyses of the distributions confirmed that the combination of AT-STED allows detecting smaller Aβ structures compared with AT alone (**Fig. 4**).

Higher levels of non-fibrillar Aβ structures in ADAD than in SAD.

Taking advantage of the enhanced resolution, we applied AT-STED to investigate potential differences in non-fibrillar Aβ structures between an ADAD and a SAD case. We stratified the objects depending on the presence of PSEN1 mutation and analyzed the distribution, size, proportion and quantity of non-fibrillar Aβ structures (total of ~18.000 objects). We observed an increase in the number of Aβ structures for all sizes (small, medium and large) in the ADAD case compared with the SAD case ($p < 0.001$) (**Fig. 5**).

Discussion

This study combines two microscopy techniques to examine non-fibrillar Aβ structures in human amyloid plaques in the brain. Using this enhanced resolution we demonstrate that the distribution of Aβ assemblies consists of a dense core of higher order Aβ species surrounded by a peripheral halo of small Aβ structures. The combination of AT and STED allowed detecting non-fibrillar Aβ forms of at least 100 nm. Finally, we provide preliminary evidence of higher levels of Aβ structures in an ADAD case compared to a SAD case.

Several studies have focused on the characterization of Aβ oligomers in AD[6,45–47]. Electrophysiological and biochemical experiments have suggested that soluble Aβ oligomers correlate with disease severity[48,49] and that there is an inverse correlation between the size of Aβ assemblies and their toxicity in multiple *in vitro* and *in vivo* models[3,6,7]. The potential structure, size, conformation, aggregation and induction of neurotoxicity of Aβ oligomers in AD pathogenesis has been thoroughly investigated through the application of several advanced technologies such as ion mobility-based mass spectrometry[25], atomic force microscopy[50,51], solid-state nuclear magnetic resonance[52] and X-ray microdiffraction[53]. Other studies have used FIB/SEM to investigate the relationship between amyloid plaques and the synaptic organization in human AD brains[40].

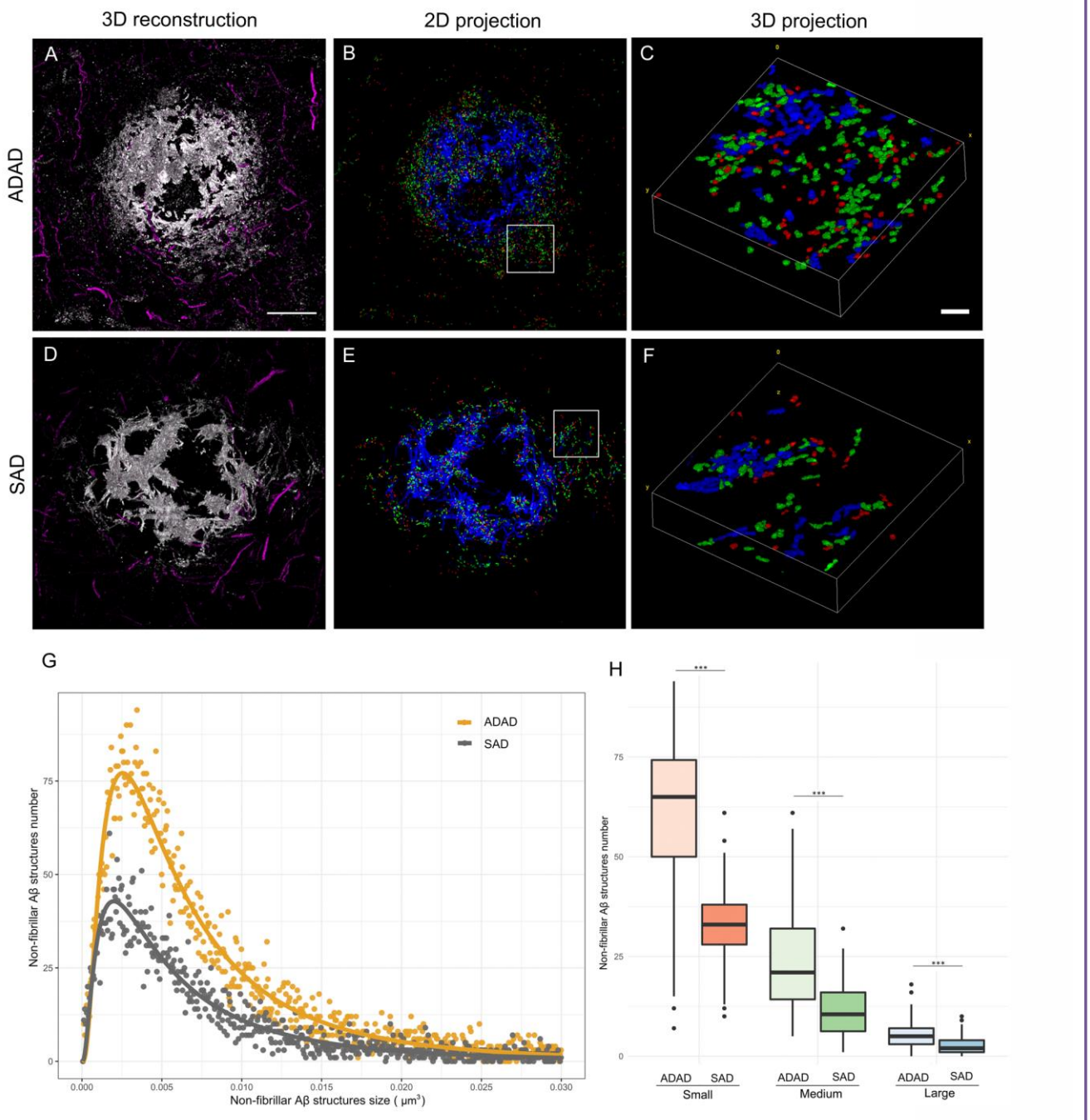

Figure 5. Non-fibrillar Aβ structures are increased in an ADAD case. (A–F) Representative images of non-fibrillar Aβ structures distribution and size identified in plaques of an ADAD (n = 8) and a SAD (n = 5) case using AT-STED. Neurofilament light protein (magenta) was stained to visualize the neuronal distribution around the plaques. Scale bar = 10 µm and 1 µm for the inset. **(G)** ADAD and SAD distribution of NAB61 structures number by size. Differences were found between both distributions ($p < 0.001$). **(H)** All Aβ entities were significantly increased in ADAD compared to SAD case ($p < 0.001$).

Here, we combined AT and STED to improve the resolution obtained with conventional confocal microscopy (x, y: 250 nm and z: 700 nm) and the detection of non-fibrillar Aβ structures in human amyloid plaques. AT achieves a resolution of 70 nm on the axial plane, while STED microscopy can increase the lateral resolution. In our case the addition of STED increased the lateral resolution up to 100 nm. This technique has been applied to investigate in detail the cellular mechanisms underlying dendritic spine plasticity[54,55], glial processes[56] or α-synuclein synaptic aggregation[57] among others. Using the enhanced resolution of AT-STED we were able to reconstruct a whole human amyloid plaque and examined in detail the nanoscale distribution and size of the non-fibrillar Aβ species. AT-STED allows detection of Aβ structures of at least 100 nm, an undetectable size range for immunohistochemical assays due to the resolution limit of light and confocal microscopes (~250 nm)[43,58]. The study revealed that human amyloid plaques consist of a dense core of NAB61 large immunoreactive structures (~0.022 μm3) and a peripheral halo of medium and small non-fibrillar Aβ entities (~0.01 μm3 and ~0.003 μm3 respectively). These results are in agreement with a study that used the AT technique to study NAB61 immunoreactivity in an animal model of AD[5]. However, we were able to detect non-fibrillar Aβ structures 2 times smaller using AT-STED in human tissue.

In addition, we show preliminary evidence that non-fibrillar Aβ structures were increased in an ADAD case compared to a SAD case in human brain tissue. It is known that oligomeric Aβ accumulation induces neuronal cell loss[27], astrocytic dysfunction[59] and synaptic toxicity[6,33], and it is possible that higher levels of non-fibrillar Aβ are a characteristic of ADAD and may be the reflection of abnormal APP processing[17]. Interestingly, this result was not detectable in conventional immunoassays pointing out the importance of implementing super-resolution techniques for detailed neuropathological studies.

The strengths of this work are the inclusion of two microscopy techniques for the study of human brain samples; and the implementation of computational tools for image processing and analysis. The main limitations are the small sample size for AT-STED due to fact that the requirement of fresh tissue makes these samples extremely scarce. Second, we only used one antibody to detect non-fibrillar Aβ. However, in our hands specific antibodies for oligomeric Aβ suitable for human tissue are exceedingly rare and NAB61 has been extensively characterized[5,33,60].

In conclusion, as a proof of concept our study shows that the combination of AT and STED can be successfully applied to investigate non-fibrillar Aβ structures in AD human brain. The obtained nanoscale architecture of human amyloid plaques reveals a dense core with a peripheral halo and we provide evidence of higher levels of non-fibrillar Aβ species in ADAD compared to SAD. Additional studies are needed to further investigate the potential relevance of these assemblies in the pathogenesis of the disease. This new tool proposed opens an important door for the neuropathology field allowing the characterization of aggregates or structures at a nanometric scale as potential therapeutic targets.

Acknowledgements

The authors would like to thank all brain donors and their relatives for generous brain donation

for research and the Neurological Tissue Bank of the IDIBAPS-Hospital Clinic-Biobank for data and sample procurement. This work was supported by FISPI14/1561, FISPI17/1896 Fondo Europeo de Desarrollo Regional (FEDER), Unión Europea, "Una manera de hacer Europa", PERIS SLT002/16/00408-01 and Marató TV3 to Alberto Lleó and CIBERNED. Tara Spires-Jones is supported by an ERC consolidator award and the UK Dementia Research Institute and gratefully acknowledges affiliations with Edinburhg Neuroscience and the FENS-Kavli Network of Excellence. Pablo Loza-Alvarez and Jordi Andilla acknowledge financial support from the Spanish Ministry of Economy and competitiveness through the "Severo Ochoa" program for Centres of Excellence in R&D (SEV-2015-0522), from Fundació Privada Cellex, Fundación Mig-Puig, from Generalitat de Catalunya through the CERCA program and form Laser lab europe (Grant agreement No. 654148).

References

1. Walsh, D. M. & Selkoe, D. J. A beta oligomers - a decade of discovery. J Neurochem. 101(5), 1172–84 (2007).

2. Kayed, R. & Lasagna-Reeves, C. A. Molecular mechanisms of amyloid oligomers toxicity. J Alzheimers Dis. 33(Suppl 1), S67–78 (2013).

3. Viola, K. L. & Klein, W. L. Amyloid β oligomers in Alzheimer's disease pathogenesis, treatment, and diagnosis. Acta Neuropathol. 129(2), 183–206 (2015).

4. Lacor, P. N. et al. Abeta oligomer-induced aberrations in synapse composition, shape, and density provide a molecular basis for loss of connectivity in Alzheimer's disease. J Neurosci. 27(4), 796–807 (2007).

5. Koffie, R. M. et al. Oligomeric amyloid beta associates with postsynaptic densities and correlates with excitatory synapse loss near senile plaques. Proc Natl Acad Sci USA 106(10), 4012–7 (2009).

6. Pickett, E. K. et al. Non-Fibrillar Oligomeric Amyloid-β within Synapses. J Alzheimers Dis. 53(3), 787–800 (2016).

7. Sengupta, U., Nilson, A. N. & Kayed, R. The Role of Amyloid-β Oligomers in Toxicity, Propagation, and Immunotherapy. EBioMedicine. 6, 42–49 (2016).

8. Walsh, D. M. et al. Naturally secreted oligomers of amyloid beta protein potently inhibit hippocampal long-term potentiation in vivo. Nature. 416(6880), 535–9 (2002).

9. Yang, Y. et al. Amyloid-β Oligomers may mpair SNARE-mediated exocytosis by direct binding to syntaxin 1a. 2015. Cell Rep. 12(8), 1244–51 (2015).

10. Arbel-Ornath, M. et al. Soluble oligomeric amyloid-β induces calcium dyshomeostasis that precedes synapse loss in the living mouse brain. Mol Neurodegener. 12(1), 27 (2017).

11. Zhao, L. N., Long, H., Mu, Y. & Chew, L. Y. The toxicity of amyloid β oligomers. Int J Mol Sci. 13(6), 7303–27 (2012).

12. Serra-Batiste, M. et al. Aβ42 assembles into specific β-barrel pore-forming oligomers in membrane-mimicking environments. Proc Natl Acad Sci USA 113(39), 10866–71 (2016).

13. Lleó, A., Castellví, M., Blesa, R. & Oliva, R. Uncommon polymorphism in the presenilin genes in human familial Alzheimer's disease: not to be mistaken with a pathogenic mutation. Neurosci Lett. 318(3), 166–8 (2002).

14. Lleó, A., Berezovska, O., Growdon, J. H. & Hyman, B. T. Clinical, pathological, and biochemical spectrum of Alzheimer disease associated with PS-1 mutations. Am J Geriatr Psychiatry. 12(2), 146–56 (2004).

15. Bateman, R. J. et al. Autosomal-dominant Alzheimer's disease: a review and proposal for the prevention of Alzheimer's disease. Alzheimers Res Ther. 3(1), 1 (2011).

16. Lleó, A. et al. Frequency of mutations in the presenilin and amyloid precursor protein genes in early-onset Alzheimer disease in Spain. Arch Neurol. 59(11), 1759–63 (2002).

17. Pera, M. et al. Distinct patterns of APP processing in the CNS in autosomal-dominant and sporadic

Alzheimer disease. Acta Neuropathol. 125(2), 201–13 (2013).

18. Hebert, S. S. et al. Loss of microRNA cluster miR-29a/b-1 in sporadic Alzheimer's disease correlates with increased BACE1/betasecretase expression. Proc Natl Acad Sci USA 105(17), 6415–20 (2008).

19. Li, R. et al. Amyloid beta peptide load is correlated with increased beta-secretase activity in sporadic Alzheimer's disease patients. Proc Natl Acad Sci USA 101(10), 3632–3637 (2004).

20. Yang, L. B. et al. Elevated beta-secretase expression and enzymatic activity detected in sporadic Alzheimer disease. Nat Med. 9(1), 3–4 (2003).

21. Hata, S. et al. Alternative processing of gamma-secretase substrates in common forms of mild cognitive impairment and Alzheimer's disease: evidence for gammasecretase dysfunction. Ann Neurol 69(6), 1026–1031 (2011).

22. Mawuenyega, K. G. et al. Decreased clearance of CNS beta-amyloid in Alzheimer's disease. Science. 330(6012), 1774 (2010).

23. Yang, T., Li, S., Xu, H., Walsh, D. M. & Selkoe, D. J. Large Soluble Oligomers of Amyloid β-Protein from Alzheimer Brain Are Far Less Neuroactive than the smaller oligomers to which they dissociate. J Neurosci. 37(1), 152–163 (2017).

24. Breydo, L. & Uversky, V. N. Structural, morphological, and functional diversity of amyloid oligomers. FEBS Lett. 589(19 Pt A), 2640–8 (2015).

25. Gessel, M. M., Bernstein, S., Kemper, M., Teplow, D. B. & Bowers, M. T. Familial Alzheimer's disease mutations differentially alter amyloid β-protein oligomerization. ACS Chem Neurosci. 3(11), 909–18 (2012).

26. Nag, S. et al. Nature of the amyloid-beta monomer and the monomer-oligomer equilibrium. J Biol Chem. 286(16), 13827–33 (2011).

27. DaRocha-Souto, B. et al. Brain oligomeric β-amyloid but not total amyloid plaque burden correlates with neuronal loss and astrocyte inflammatory response in amyloid precursor protein/tau transgenic mice. J Neuropathol Exp Neurol. 70(5), 360–76 (2011).

28. DiChiara, T. Alzheimer's Toxic Amyloid Beta Oligomers: Unwelcome Visitors to the Na/K ATPase alpha3 Docking Station. Yale J Biol Med. 90(1), 45–61 (2017).

29. Shafrir, Y., Durell, S. R. & Guy, H. R. Beta-barrel models of soluble amyloid beta oligomers and annular protofibrils. Proteins. 78(16), 3458–72 (2010).

30. Marsh, J., Bagol, S. H., Williams, R. S. B., Dickson, G. & Alifragis, O. Synapsin I phosphorylation is dysregulated by beta-amyloid oligomers and restored by valproic acid. Neurobiol Dis. 106, 63–75 (2017).

31. Walsh, D. M., Tseng, B. P., Rydel, R. E., Podlisny, M. P. & Selkoe, D. J. The oligomerization of amyloid beta-protein begins intracellularly in cells derived from human brain. Biochemistry. 39(35), 10831–9 (2000).

32. Gouras, G. K., Tampellini, D., Takahashi, R. H. & Capetillo-Zarate, E. Intraneuronal beta-amyloid accumulation and synapse pathology in Alzheimer's disease. Acta Neuropathol. 119(5), 523–41 (2010).

33. Koffie, R. M. et al. Apolipoprotein E4 effects in Alzheimer's disease are mediated by synaptotoxic oligomeric amyloid-beta. Brain. 135(Pt 7), 2155–68 (2012).

34. Perez-Nievas, B. G. et al. Dissecting phenotypic traits linked to human resilience to Alzheimer's pathology. Brain. 136(Pt 8), 2510–26 (2013).

35. Bodani, R. U. et al. Antibody against Small Aggregated Peptide Specifically Recognizes Toxic Aβ-42 Oligomers in Alzheimer's Disease. ACS Chem. Neurosci. 6(12), 1981–9 (2015).

36. Bilousova, T. et al. Synaptic Amyloid-β oligomers precede p-Tau and differentiate high pathology control cases. Am. J. Pathol. 186(1), 185–98 (2016).

37. Kumar, S. et al. Phosphorylation of the amyloid beta-peptide at ser26 stabilizes oligomeric assembly and increases neurotoxicity. Acta Neuropathol. 131(4), 525–37 (2016).

38. Savioz, A. et al. A Study of Abeta Oligomers in the Temporal Cortex and Cerebellum of Patients with Neuropathologically Confirmed Alzheimer's Disease Compared to Aged Controls. Neurodegener-Dis. 16(5–6), 398–406 (2016).

39. Li, S. et al. Decoding the synaptic dysfunction of bioactive human AD brain soluble Aβ to inspire novel therapeutic avenues for Alzheimer's disease. Acta Neuropathol Commun. 6(1), 121 (2018).

40. Blazquez-Llorca, L., Merchán-Pérez, Á., Rodríguez, J. R., Gascón, J. & DeFelipe, J. FIB/SEM technology and Alzheimer's disease: three-dimensional analysis of human cortical synapses. J Alzheimers Dis. 34(4), 995–1013 (2013).

41. Michael, R. et al. Hyperspectral Raman imaging of neuritic plaques and neurofibrillary tangles in brain tissue from Alzheimer's disease patients. Sci Rep. 7(1), 15603 (2017).

42. Micheva, K. D. & Smith, S. J. Array tomography: a new tool for imaging the molecular architecture and ultrastructure of neural circuits. Neuron. 55(1), 25–36 (2007).

43. Schermelleh, L., Heintzmann, R. & Leonhardt, H. A guide to super-resolution fluorescence microscopy. J Cell Biol. 190(2), 165–75 (2010).

44. Merino, D. et al. STED imaging performance estimation by means of Fourier transform analysis. Biomed. Opt. Express. 8(5), 2472–2482 (2017).

45. Kayed, R. et al. Common structure of soluble amyloid oligomers implies common mechanism of pathogenesis. Science. 300(5618), 486–9 (2003).

46. Stroud, J. C., Liu, C., Teng, P. K. & Eisenberg, D. Toxic fibrillar oligomers of amyloid-β have cross-β structure. Proc. Natl. Acad. Sci. USA 109(20), 7717–7722 (2012).

47. Kotler, S. A. et al. High-resolution NMR characterization of low abundance oligomers of amyloid-β without purification. Sci Rep. 5, 11811 (2015).

48. McLean, C. A. et al. Soluble pool of Abeta amyloid as a determinant of severity of neurodegeneration in Alzheimer's disease. Ann Neurol 46(6), 860–866 (1999).

49. Tomic, J. L., Pensalfini, A., Head, E. & Glabe, C. G. Soluble fibrillar oligomer levels are elevated in Alzheimer's disease brain and correlate with cognitive dysfunction. Neurobiol Dis 35(3), 352–358 (2009).

50. Economou, N. J. et al. Amyloid β-Protein Assembly and Alzheimer's Disease: Dodecamers of Aβ42, but Not of Aβ40, Seed Fibril Formation. J Am Chem Soc. 138(6), 1772–5 (2016).

51. Ungureanu, A. A. et al. Amyloid beta oligomers induce neuronal elasticity changes in age-dependent manner: a force spectroscopy study on living hippocampal neurons. Sci Rep. 6, 25841 (2016).

52. Qiang, W., Yau, W. M., Lu, J. X., Collinge, J. & Tycko, R. Structural variation in amyloid-β fibrils from Alzheimer's disease clinical subtypes. Nature. 541(7636), 217–221 (2017).

53. Liu, J. et al. Amyloid structure exhibits polymorphism on multiple length scales in human brain tissue. Sci Rep. 6, 33079 (2016).

54. Wegner, W. et al. In vivo mouse and live cell STED microscopy of neuronal actin plasticity using far-red emitting fluorescent proteins. Sci Rep. 7(1), 11781 (2017).

55. Berning, S., Willig, K. I., Steffens, H., Dibaj, P. & Hell, S. W. Nanoscopy in a living mouse brain. Science. 335(6068), 551 (2012).

56. Bethge, P., Chéreau, R., Avignone, E., Marsicano, G. & Nägerl, U. V. Two-photon excitation STED microscopy in two colors in acute brain slices. Biophys J. 104(4), 778–85 (2013).

57. Colom-Cadena, M. et al. Synaptic phosphorylated α-synuclein in dementia with Lewy bodies. Brain. 140(12), 3204–3214 (2017).

58. Pawley, J.B. Handbook of Biological Confocal Microscopy. (Springer Science + Business Media, 2006).

59. Diniz, L. P. et al. Astrocyte Transforming Growth Factor Beta 1 Protects Synapses against Aβ Oligomers in Alzheimer's Disease Model. J Neurosci. 37(28), 6797–6809 (2017).

60. Lee, E. B. et al. Targeting amyloid-beta peptide (Abeta) oligomers by passive immunization with a conformation-selective monoclonal antibody improves learning and memory in Abeta precursor protein (APP) transgenic mice. J Biol Chem. 281(7), 4292–9 (2006).

61. Colom-Cadena, M. et al. Confluence of α-synuclein, tau, and β-amyloid pathologies in dementia with Lewy bodies. J Neuropathol Exp Neurol. 72(12), 1203–1212 (2013).

62. Montine, T. J. et al. National Institute on Aging-Alzheimer's Association guidelines for the neuropathologic assessment of Alzheimer's disease: a practical approach. Acta Neuropathol. 123(1), 1–11 (2012).

63. Kay, K. R. et al. Studying synapses in human brain with array tomography and electron microscopy. Nat Protoc. 8(7), 1366–80 (2013).

64. Querol-Vilaseca, M. et al. YKL-40 (Chitinase 3-like I) is expressed in a subset of astrocytes in Alzheimer's disease and other tauopathies. J Neuroinflammation. 14(1), 118 (2017).

Supplementary data

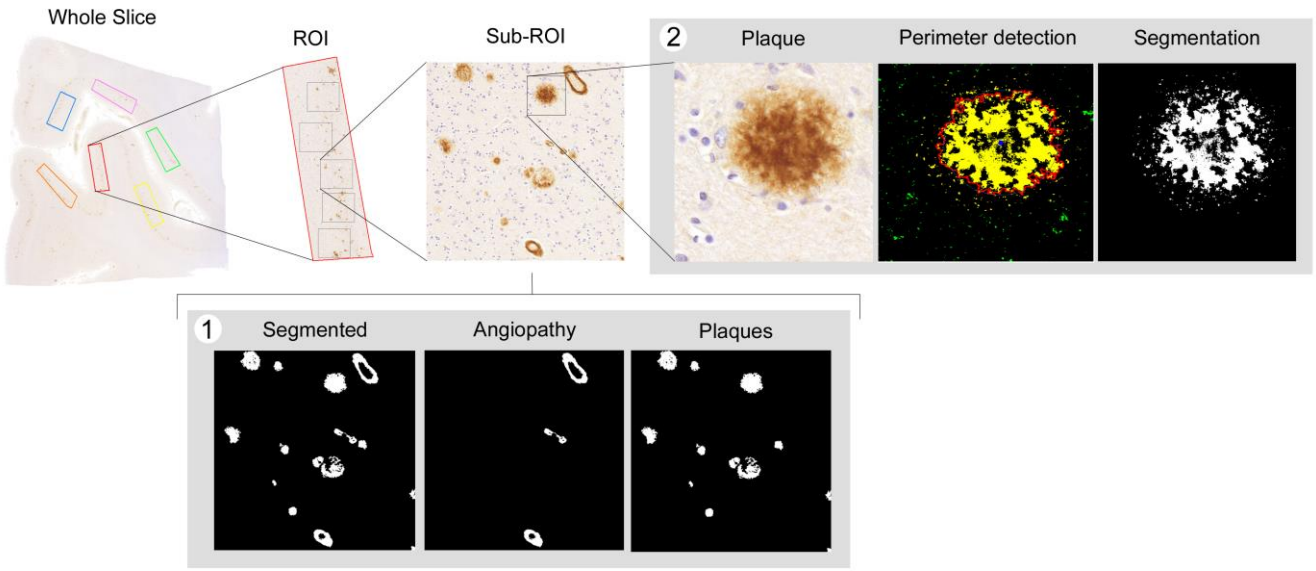

Supplementary Figure S1. **Image processing pipeline.** Whole slice scans are obtained and random regions of interest are manually delimitated. The application of an in-house algorithm allows two different analyses. **1)** Quantification of total Aβ or NAB61 immunoreactivity excluding amyloid angiopathy. **2)** Quantification of soluble NAB61+ structures around plaques.

Supplementary Table S1. Demographic, clinical and genetic data of eoSAD and ADAD patients.

	ADAD (N =10)	eoSAD (N =14)	p value
Gender = M (%)	7 (70.0)	6 (42.9)	0.368
Mean age at onset (mean (SD))	43.80 (6.16)	51.36 (3.52)	**0.001**
Mean age at death (mean (SD))	54.90 (5.69)	60.79 (4.10)	**0.007**
Mean disease duration (mean (SD))	11.10 (4.41)	9.43 (3.25)	0.296
***APOE ε4* allele carriers = n (%)**	2 (25.0)*	8 (66.7)*	0.171

*Calculated without missing data (ADAD n=8 and eoSAD n=12). M: male; SD: standard deviation.

Supplementary Table S2. Neuropathologic data of eoSAD and ADAD cases.

Case #	Mutation	Gender	Thal Aβ phase	Braak NF stage	CERAD	Age onset	Age death	APOE genotype	PMI (h)
PSEN1 mutation carriers									
1	V89L	M	5	V	freq	45	54	23	7,5
2	V89L	M	5	VI	freq	48	57	23	9.5
3	E120G	M	5	VI	freq	34	44	33	5.5
4	M139T	M	5	V	freq	47	64	33	14.7
5	M139T	M	5	VI	freq	48	57	33	15.2
6	M139T	M	5	VI	freq	45	53	33	5.3
7	M139T	F	5	VI	freq	38	48	23	5,25
8	P264L	F	5	VI	freq	45	56	44	6
9	P264L	M	5	VI	freq	53	60	34	7.2
10	G206D	M	5	VI	freq	37	44	34	19.2
Sporadic Early-onset AD									
11	-	M	4	V	freq	51	65	44	18
12	-	M	4	VI	freq	52	65	33	8
13	-	M	4	VI	freq	52	60	44	10,25
14	-	F	5	VI	freq	51	60	33	5
15	-	M	5	VI	freq	46	55	33	4,5
16	-	F	4	VI	freq	50	63	33	6,5
17	-	F	5	VI	freq	56	67	44	4
18	-	F	5	VI	freq	54	62	44	6
19	-	F	5	VI	freq	58	66	43	12,5
20	-	F	5	VI	freq	52	57	43	4,5
21	-	F	5	VI	freq	46	56	43	16,25
22	-	M	5	VI	freq	47	57	43	10
23	-	F	5	VI	freq	50	62	33	12,6
24	-	M	5	VI	freq	54	56	-	14,16

CERAD: Consortium to Establish a Registry for Alzheimer's Disease; F: female; M: male; NF: neurofibrillary; PMI: post-mortem interval.

Reduced non-fibrillar Aβ species in a patient treated with low doses of BACE-1 inhibitor

Marta Querol-Vilaseca[1,2], Sònia Sirisi[1,2], Laura Molina-Porcel[3,4], Beatriu Molina[1,2], Jordi Pegueroles[1,2], Paula Ferrer-Raventós[1,2], Raúl Nuñez-Llaves[1,2], Rafael Blesa[1,2], Olivia Belbin[1,2], Juan Fortea[1,2], Ellen Gelpi[3,4,5], Raquel Sanchez-Valle[3,4], Alberto Lleó[1,2*]

[1]Memory Unit, Department of Neurology, Institut d'Investigacions Biomèdiques Sant Pau - Hospital de la Santa Creu i Sant Pau, Universitat Autònoma de Barcelona, Barcelona, Spain. [2]Centro de Investigación Biomédica en Red en Enfermedades Neurodegenerativas (CIBERNED), Madrid, Spain. [3]Neurological Tissue Bank of the Biobanc-Hospital Clínic-IDIBAPS, Barcelona Spain. [4]Alzheimer's disease and other cognitive disorders unit. Neurology Service, Hospital Clínic de Barcelona-IDIBAPS, Barcelona Spain. [5]Institute of Neurology, Medical University of Vienna, Vienna, Austria.

We report the neuropathological examination of a patient with Alzheimer's disease (AD) treated for 38 months with low doses of the BACE-1 inhibitor Verubecestat. Brain examination showed unusually low levels of non-fibrillar Aβ despite high total Aβ load compared to 9 non-treated AD cases. In addition, examination showed reduced dystrophic neurites around plaques and less Aβ-associated with synapses. Our findings suggest that inhibition of Aβ production has an impact on soluble Aβ deposition and neuritic derangement in AD.

[BRIEF COMMUNICATION: IN PREPARATION]

Anti-amyloid therapies have been investigated in the last two decades in Alzheimer disease (AD) to slow disease progression. The two main approaches to anti-amyloid therapy have been to reduce the production or to increase the clearance of Aβ42. One approach for Aβ reduction has been the search for molecules that inhibit β-secretase[1]. Clinical data support this line of drug development, as β-secretase activity in human brain increases with age[2,3]. BACE-1 is the main enzyme responsible for brain β-secretase activity and several BACE-1 inhibitors have been developed[4]. Some of these drugs have reached clinical testing, but all have failed to show clinical benefit[4]. The knowledge about the specific effects of these compounds on brain histopathology can help to refine this drug target.

Here, we report the first neuropathological examination of a 63-year old man with AD who received active treatment with a BACE-1 inhibitor (Verubecestat, MK-8931)[5]. The patient presented at 54 years with gradually progressive memory impairment with worsening confusion and disorientation. His past medical history was relevant for diabetes mellitus, high blood pressure, celiac disease, and a partial factor VII deficiency (prothrombin time ≈ 80%). He was diagnosed of AD by means of CSF analyses with a characteristic AD signature. He had no family history of dementia and the *APOE* genotype was 33. At the initial evaluation his Mini Mental State Examination score was 28 out of 30 and formal neuropsychological testing showed impairment in verbal and visual memory and in executive functions. He was treated with rivastigmine patch (9.5 mg/daily). The patient had previously participated in a clinical trial with a GSK3 inhibitor (Tideglusib) from October 2011 until July 2012 receiving the active treatment[6]. In May 2013, the patient was enrolled in a randomized, placebo-controlled phase 3 trial of a BACE-1 inhibitor (Verubecestat, MK-8931)[7]. He received oral doses (12 mg of MK-8931/day) since June 2013 and continued to take the investigational product for 24 months during the double-blind phase, with no relevant adverse effects and no interruption in drug intake. In June 2015 he entered the extension phase of the study until the early termination of the study (last dose administered Aug 22, 2016, total treatment period 38 months). During the study period he showed relentless clinical progression in all cognitive domains. The patient's cognitive impairment continued to worsen until his death in November 2017 from aspirative pneumonia 53 months after the first dose and 15 months after the last dose.

Post-mortem examination of the patient's brain showed mild global brain atrophy. Frontal, temporal and parietal cortices were the most affected areas whereas occipital cortices appeared more preserved. There was moderate dilatation of the ventricular system with no alterations in white matter. He also showed mild atrophy of the amygdala, mild-moderate atrophy in the hippocampus and adequate pigmentation of the substantia nigra. Formal microscopic evaluation revealed numerous neuritic plaques, neurofibrillary tangles and neuropil threads. According to current diagnostic criteria (Consortium to Establish a Registry for Alzheimer's Disease (CERAD) 'frequent'; Braak stage VI and Thal stage 5) the patient was classified as high AD neuropathologic change (A3B3C3). There was also very infrequent cerebral amyloid angiopathy, moderate TDP-43 aggregates in limbic regions and no α-synuclein aggregates.

We next analyzed quantitatively the neuropathology of the case treated with Verubecestat and compared with that of a group

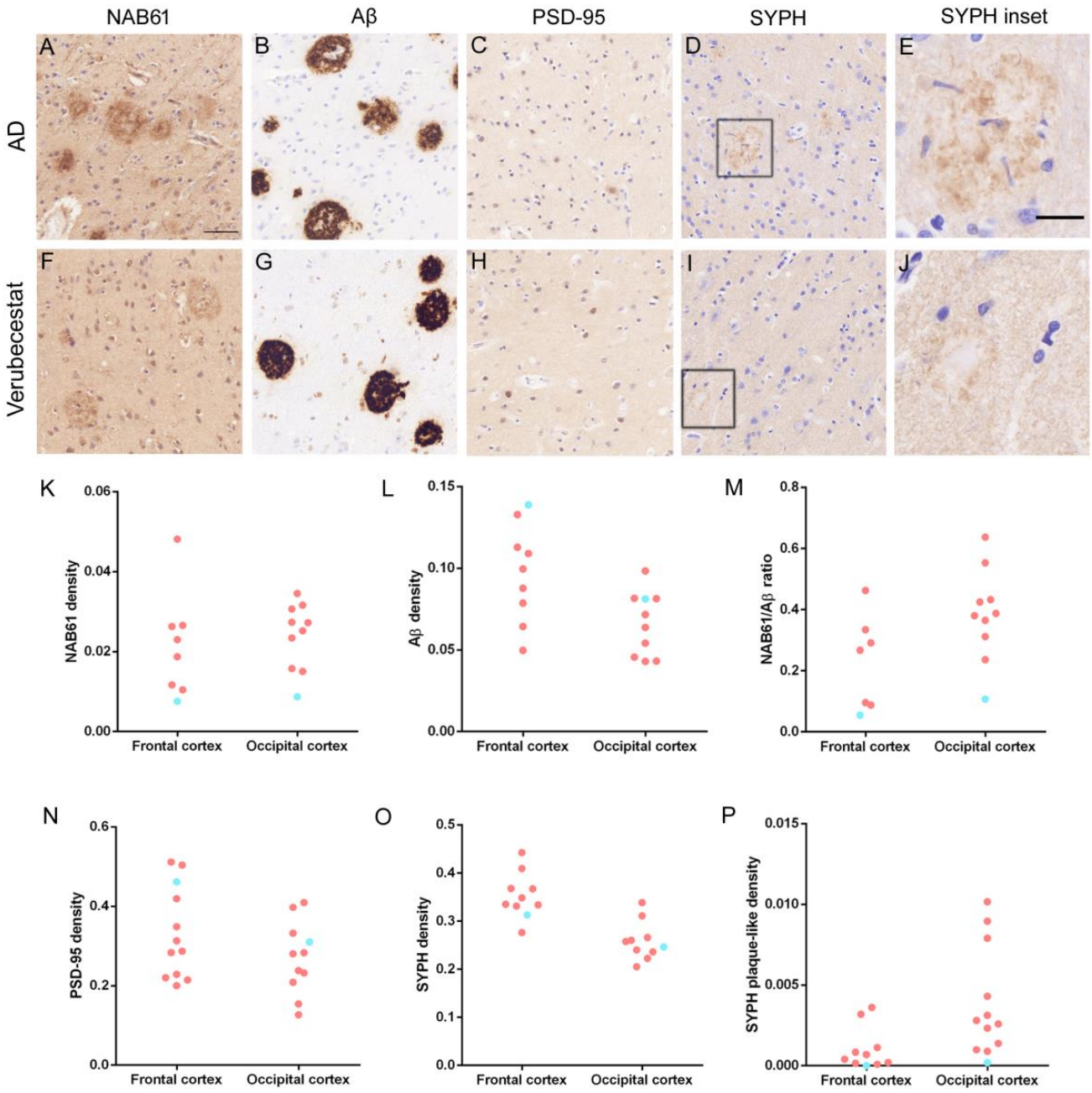

Figure 1. Quantification of total and non-fibrillar Aβ and synaptic markers in all cases of the study. Representative images of NAB61 (A, F), Aβ (B, G), postsynaptic marker PSD-95 (C,H) and presynaptic marker SYPH (D,I) immunoreactivity patterns of the occipital cortex of the case treated with Verubecestat and one AD case. Insets of SYPH positive plaque like staining (E,J). Quantification of NAB61 (K) total Aβ (L), NAB61/total Aβ ratio (M), PSD-95 (N), SYPH (O) and SYPH positive plaque-associated densities (Verubecestat = blue dot; untreated AD cases = red dots). The treated case showed low NAB61 immunoreactivity despite high total Aβ immunoreactivity. No differences were found in SYPH and PSD-95 densities. The case treated showed the lowest levels of SYPH-plaque-associated staining. Scale bar = 50µm and inset scale bar = 20µm.

of 9 EOSAD cases (detailed methods and neuropathological data of the cases is shown in **Supplementary Table S1**). We first quantified total and non-fibrillar Aβ burden. We found low NAB61 immunoreactivity in the patient treated with Verubecestat compared to the other AD cases in both frontal and occipital regions **(Fig. 1)**. In contrast, total Aβ immunoreactivity was similar in the treated case compared with the AD group in both regions. Thus, the patient showed the lowest ratio NAB61/total Aβ of all AD included cases.

Since Verubecestat was associated with early cognitive worsening during the trial[7], we next quantified synapse loss using conventional immunohistochemistry with pre and a postsynaptic markers (synaptophysin [SYPH] and postsynaptic density protein 95 [PSD-95], respectively). We found similar SYPH or PSD-95 immunoreactivity in the treated case compared to AD cases **(Fig 1)**.

However, besides the typical neuropil-like immunoreactivity pattern of SYPH, we observed SYPH-positive structures surrounding plaques[8,9,10,11]. Interestingly, the patient treated with Verubecestat showed the lowest SYPH-positive immunoreactivity around plaques SYPH-plaque-associated staining.

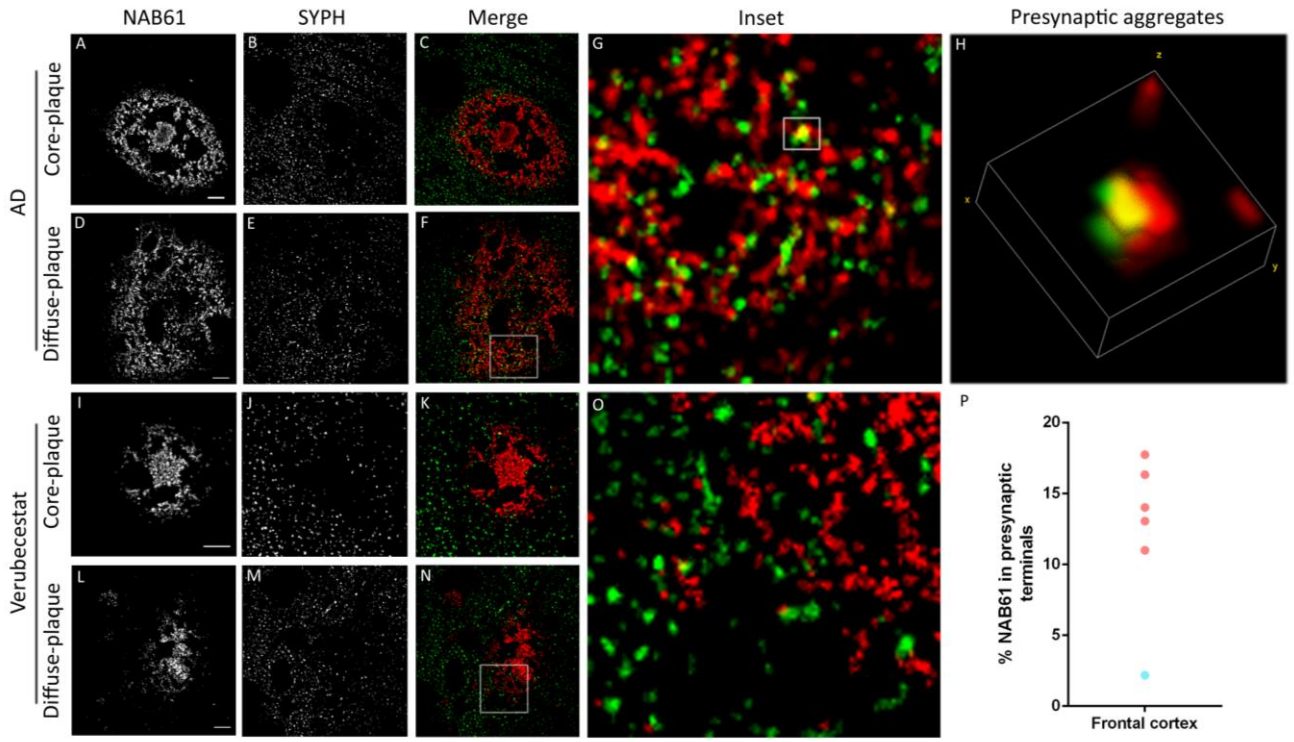

Figure 2. Non-fibrillar Aβ species at the presynaptic terminals. Representative images of amyloid plaques of the treated case and an untreated AD case stained with NAB61 antibody (red) and the presynaptic marker SYPH (green). Images are projections of 15-22 consecutive sections (A-N). Insets of AD and Verubecestat diffuse plaques (G,O). Inset of presynaptic NAB61 aggregate of the AD case (H). Colocalization analysis of NAB61 and SYPH shows a reduction of non-fibrillar Aβ at presynaptic terminals of the case treated with Verubecestat (P). Scale bar = 20 µm

Since conventional immunohistochemistry cannot resolve single synapses, we adapted our AT protocol to fixed samples to investigate the possible effect of Verubecestat on synaptic-associated Aβ. We applied AT using NAB61 and SYPH to the case treated with Verubecestat and to 5 untreated AD cases.

Despite the similar synaptic densities among cases, the treated case showed unusually low levels of non-fibrillar Aβ at synapses compared with AD cases (2% vs 14%) **(Fig 2)**.

We provide evidence of unusually low non-fibrillar Aβ in a patient treated with Verubecestat compared with other eoSAD cases. In this case we also found a reduction on the SYPH-positive dystrophic terminals around amyloid plaques and synaptic-associated Aβ.

BACE-1 inhibitors have been investigated as prime therapeutic strategies for AD[12]. Several BACE-1 inhibitors have reached advanced clinical testing, although all have been discontinued due to lack of clinical effect or safety concerns[4]. In particular, treatment with some BACE-1 inhibitors was associated with early worsening in cognitive function[7,13]. Both trials of Verubecestat in prodromal and mild-to-moderate AD have shown a 60-80% reduction of Aβ40 and Aβ42 levels in CSF and a modest reduction (~20%) in brain amyloid load measured by PET. However, this reduction was not effective in slowing the clinical progression[7,13]. Here we describe unusually low non-fibrillar Aβ ratio in a patient treated with low doses of Verubecestat. These data are in agreement with data from the trial, and studies in AD mouse models in which BACE-1 inhibition was less effective in removing existing plaques[14].

BACE-1 is expressed at synapses and has a key role in processing of substrates implicated in synaptic function[15]. Synapse dysfunction was hypothesized to underlie the deleterious cognitive effects of BACE-1 inhibition[16]. In spite of the lack of differences in SYPH and PSD-95 immunoreactivity between the case treated with Verubecestat and the other AD cases, the treated case showed less SYPH-plaque-associated immunoreactity. These results are in agreement with a study that showed that Verubecestat altered the formation but not the stability of dendritic spines in an AD animal model[17]. The SYPH-plaque-like staining has been associated with dystrophic presynaptic terminals in the surrounding environment of Aβ plaques[8,9,10,11]. The lowest SYPH-positive plaque-like immunoreactivity observed in the treated case could indicate that inhibition of BACE-1 may have reduced APP cleavage at synapses and Aβ accumulation, ameliorating the downstream effects of Aβ, such as presynaptic terminal dystrophies. To investigate this hypothesis in more detail we modified our AT protocol to specifically study Aβ species at synapses.

We describe that the patient treated with Verubecestat had the lowest levels of NAB61 in the presynaptic terminals compared to the untreated cases. These findings suggest that Verubecestat may have helped to clear soluble Aβ species from synaptic compartments. Since this is a single case study, we cannot exclude that these features as part of the inherent neuropathological variability of AD, and that they may be unrelated to the drug treatment.

In summary, our data indicate that low-dose Verubecestat may have exerted some effect on brain non-fibrillar forms of Aβ and synaptic derangement. This report may help to understand some aspects of BACE1 inhibition in humans and opens the possibility of revising its potential

therapeutic efficacy if administrated at early stages and at lower doses.

References

1. Morsy, A. & Trippier, P. C. Current and Emerging Pharmacological Targets for the Treatment of Alzheimer's Disease. *J. Alzheimer's Dis.* 72, S145–S176 (2019).

2. Fukumoto, H. et al. β-Secretase Activity Increases with Aging in Human, Monkey, and Mouse Brain. *Am. J. Pathol.* 164, 719–725 (2004).

3. Pera, M. et al. Distinct patterns of APP processing in the CNS in autosomal-dominant and sporadic Alzheimer disease. *Acta Neuropathol.* 125, 201–213 (2013).

4. Das, B. & Yan, R. A Close Look at BACE1 Inhibitors for Alzheimer's Disease Treatment. *CNS Drugs* 33, 251–263 (2019).

5. Scott, J. D. et al. Discovery of the 3-Imino-1,2,4-thiadiazinane 1,1-Dioxide Derivative Verubecestat (MK-8931)-A β-Site Amyloid Precursor Protein Cleaving Enzyme 1 Inhibitor for the Treatment of Alzheimer's Disease. *J. Med. Chem.* 59, 10435–10450 (2016).

6. Lovestone, S. et al. A phase II trial of tideglusib in alzheimer's disease. *J. Alzheimer's Dis.* 45, 75–88 (2015).

7. Egan, M. F. et al. Randomized trial of verubecestat for mild-to-moderate Alzheimer's disease. *N. Engl. J. Med.* 378, 1691–1703 (2018).

8. Kandalepas, P. C. et al. The Alzheimer's β-secretase BACE1 localizes to normal presynaptic terminals and to dystrophic presynaptic terminals surrounding amyloid plaques. *Acta Neuropathol.* 126, 329–352 (2013).

9. Sadleir, K. R. et al. Presynaptic dystrophic neurites surrounding amyloid plaques are sites of microtubule disruption, BACE1 elevation, and increased Aβ generation in Alzheimer's disease. *Acta Neuropathol.* 132, 235–256 (2016).

10. Gomez-Arboledas, A. et al. Phagocytic clearance of presynaptic dystrophies by reactive astrocytes in Alzheimer's disease. *Glia* 66, 637–653 (2018).

11. Hadley, K. C. et al. Determining composition of micron-scale protein deposits in neurodegenerative disease by spatially targeted optical microproteomics. *Elife* 4, 1–21 (2015).

12. Lleó, A., Greenberg, S. M. & Growdon, J. H. Current pharmacotherapy for Alzheimer's disease. *Annu. Rev. Med.* 57, 513–533 (2006).

13. Egan, M. F. et al. Randomized trial of verubecestat for prodromal Alzheimer's disease. *N. Engl. J. Med.* 380, 1408–1420 (2019).

14. Henley, D. et al. Preliminary Results of a Trial of Atabecestat in Preclinical Alzheimer's Disease. *N Engl J Med* 380, 1483–1485 (2019).

15. Peters, F. et al. BACE1 inhibition more effectively suppresses initiation than progression of β-amyloid pathology. *Acta Neuropathol.* 135, 695–710 (2018).

16. Das, B. & Yan, R. Role of BACE1 in Alzheimer's synaptic function. *Transl. Neurodegener.* 6, 4–11 (2017).

17. Dennis J. Selkoe. Alzheimer's Disease Is a Synaptic Failure. *Science* (80-.) 298, 789–791 (2002).

18. Blume, T. et al. BACE1 Inhibitor MK-8931 Alters Formation but Not Stability of Dendritic Spines. *Front. Aging Neurosci.* 10, 1–7 (2018).

19. Colom-Cadena, M. et al. Confluence of α-synuclein, tau, and β-amyloid pathologies in dementia with Lewy bodies. *J. Neuropathol. Exp. Neurol.* 72, 1203–1212 (2013).

20. Montine TJ, et al. National Institute on Aging-Alzheimer's Association guidelines for the neuropathologic assessment of Alzheimer's disease: a practical approach. *Acta Neuropathol.* 123, 1–11 (2012).

21. Kay, K. R. et al. Studying synapses in human brain with array tomography and electron microscopy. *Nat Protoc.* 8, 1366–1380 (2013).

22. Colom-Cadena, M. et al. Synaptic phosphorylated α-synuclein in dementia with Lewy bodies. *Brain* 140, 3204–3214 (2017).

23. Querol-Vilaseca, M. et al. Nanoscale structure of amyloid-β plaques in Alzheimer's disease. *Sci. Rep.* 9, 1–10 (2019).

Methods

Standard protocol approval and patient consent

We obtained written informed consent from all brain donors and/or next of kin for the use of brain tissue for research. The study was approved by the local ethics committee of Hospital de Sant Pau, Barcelona, Spain. All research was performed in accordance with relevant guidelines and regulations.

Postmortem human brain samples

Brain samples for immunohistochemical assays were provided by the Neurological Tissue Bank (NTB) of the Biobanc-Hospital Clínic-IDIBAPS and processed as previously described[18] and as internationally recommended[19]. The study group consisted of 10 subjects: 9 EOSAD patients with an age of onset <65 years and the patient treated with Verubecestat. Brain tissue samples from 5 SAD cases and the treated case were processed for AT following previously described[20,21,22] and modified AT methods (Querol-Vilaseca et al. in preparation).

Immunohistochemistry, image acquisition and analysis

Immunohistochemistry was performed on 5-µm-thick consecutive sections of occipital and frontal cortex using the following primary antibodies: mouse monoclonal anti-amyloid beta clone 6F/3D (1:400; DAKO), mouse anti-NAB61 (1:250; a kind gift from Virginia Lee, University of Pennsylvania, Philadelphia, USA), goat anti-synaptophysin (1:100; R&D Systems) and rabbit anti-postsynaptic density protein 95 (PSD-95) clone D27E11 (1:100; Cell Signaling). Reaction was visualized by the EnVision + system peroxidase procedure (DAKO, Glostrup, Denmark). Image acquisition and processing was performed as previously described[22].

Array Tomography

Brain samples for AT were processed using previously described methods[20,21] with minor variations on the fixative step of the protocol (Querol-Vilaseca et al. in preparation). Briefly, according to the standard AT protocol[20,21], fresh brain tissue is fixed in 4% paraformaldehyde (PFA), 2.5% sucrose in PBS for 3 h. Since no fresh brain tissue was available for the patient treated with Verubecestat, we adapted our current AT protocol[21] to perform ultrastructural studies in PFA-fixed samples. Experimental validation of the modified AT protocol is shown in **supplementary figure S1.** We did not find differences in synaptic densities between the same case obtained from PFA-fixed samples or from fresh samples. Fresh and PFA-fixed samples were dehydrated through ethanol and embedded into LR White resin (Electron Microscopy Sciences). 70 nm-thick ribbons of serial-sections were cut using an ultramicrotome (Leica Microsystems) equipped with an Ultra Jumbo Diamond Knife 35° (Diatome) from LR white embedded tissue blocks. The ribbons were stained using the following primary antibodies: mouse anti-NAB61 (1:50; kindly provided by Virginia Lee, University of Pennsylvania, Philadelphia, USA) and goat anti-synaptophysin (1:50; R&D Systems). Then, sections were incubated with secondary fluorescent antibodies Alexa 488, Alexa 555 and Alexa 647 (1:50, Invitrogen). Images of the same region were acquired in consecutive sections using an Olympus BX51 microscope with a 63 1.2NA Plan Apochromat objective (Olympus) controlled with HCImage software (Hamamatsu). For AT

image analysis we used an in-house algorithm developed with MATLAB software (The Math Works, Inc., Natick, MA, USA) as previously described[21,22]. Briefly, image stacks of each channel comprising all 70 nm consecutive sections were first registered using a rigid registration followed by an affine registration of a reference channel. Aligned sections were segmented using an automated mean local thresholding. Additionally, objects that were not in at least two consecutive sections or that were less than 3px were considered background and removed. After identification of three-dimensional structures, the density and size of individual entities were quantified and colocalization between different channels was applied.

Supplementary data

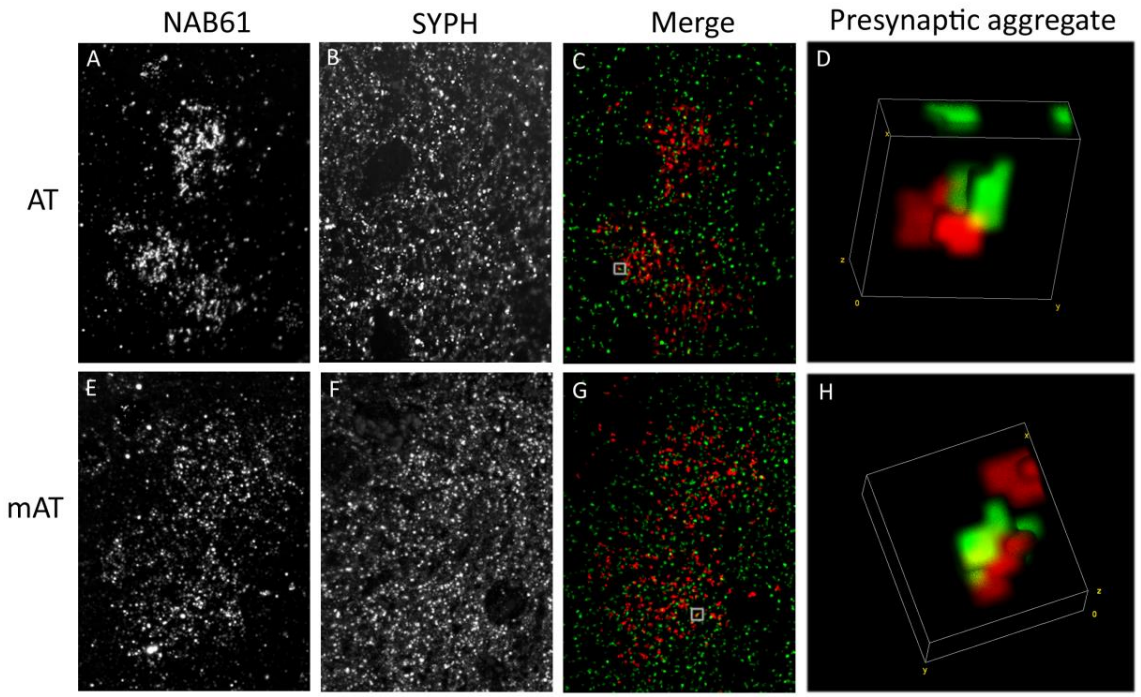

I)

	SYPH density (objects/µm³)	NAB61 density (objects/µm³)	NAB61-SYPH colocalization (%)
AT	0,0007	0,00023	13,68
mAT	0,00075	0,00010	11,61

Supplementary figure S1. Experimental validation of the modified AT protocol. Representative images of the same case using the standard AT protocol for fresh brain samples (A-D) and the modified protocol for PFA-fixed brain samples (E-H). Amyloid plaques were stained with NAB61 antibody (red) and presynaptic terminals with an anti-SYPH antibody (green). Inset of a presynaptic aggregate of non-fibrillar Aβ (D,H). Quantification analysis of 3 plaques per condition show similar SYPH densities and colocalization between NAB61 and SYPH in the samples treated following the standard AT protocol compared with those treated following the modified AT protocol (I).

Supplementary table S1. Neuropathological data of cases included in the study.

Case	Gender	Age at onset	Age at death	APOE genotype	PMI (h)	Thal Aβ phase	Braak NF stage	CERAD
Paraffin-embedded cases								
1	F	51	65	44	18	4	V	frequent
2	F	52	65	33	8	4	VI	frequent
3	F	52	60	44	10,25	4	VI	frequent
4	M	50	63	33	6,5	4	VI	frequent
5	M	56	67	44	4	5	VI	frequent
6	M	54	62	44	6	5	VI	frequent
7	M	52	57	34	4,5	5	VI	frequent
8	F	47	57	34	10	5	VI	frequent
9	M	50	62	33	12,6	5	VI	frequent
10*	M	54	63	33	15	5	VI	frequent
AT cases								
1	F	53	65	NA	17,5	5	VI	frequent
2	M	54	63	33	6,5	5	V	frequent
3	M	51	64	34	18	5	VI	frequent
4	M	52	60	33	16	5	VI	frequent
5	F	60	71	NA	5	5	VI	frequent

CERAD: Consortium to Establish a Registry for Alzheimer's Disease; F: female; M: male; NF: neurofibrillary; PMI: post-mortem interval. * Patient treated with Verubecestat.

Chapter 4: Discussion

In this thesis we combined classical immunoassays, light microscopy techniques and automated computational tools in order to investigate neuroinflammation and abnormal protein accumulation in NDDs. In particular, in study 1, we investigated astrocytic and glial abnormalities in AD and other tauopathies. In study 2, we took advantage of emerging super-resolution techniques and applied and optimized array tomography combined with STED to study human amyloid plaques at a nanoscale level. In study 3, we applied digital methods and AT to quantitative analyse the brain changes in a patient treated with a BACE-1 inhibitor. These three works illustrate how digital tools can be integrated with classical neuropathological methods in the investigation of AD and other NDDs.

YKL-40 (Chitinase 3-like I) is expressed in a subset of astrocytes in Alzheimer's disease and other tauopathies

In study 1, we determined the cellular pattern of YKL-40 expression in the human brain tissue of AD and other primary tauopathies. We also investigated the relationship between YKL-40 expression and tau aggregates in these disorders combining confocal microscopy and automated in-house computational tools to quantify pathology burden.

Growing evidence supports the idea that neuroinflammation plays a key role on disease pathogenesis in dementia and acts as a potential contributor to neurodegeneration[79,80,149]. How and when glial activation mechanisms lead to neuronal damage remains still unclear. Different studies support the idea that sustained activation of microglia and astrocytes may lead to a switch from a neuroprotective to a neurotoxic phenotype[150,151,152,153]. Other studies described inflammaging as the long-term result of chronic physiological stimulation of the innate immune system, which can become damaging during ageing. Thus, they suggested that inflammaging might be the main cause of age-related NDDs[154]. Neuro-inflammaging is associated with a prolonged activation of microglia with secretion of several pro-inflammatory cytokines, such as interleukin 6 (IL-6), tumor necrosis factor α (TNFα) and interleukin 1β (IL-1β); and impaired phagocytic capacities resulting in increased toxic protein accumulation[155,156]. This prolonged pathologic state can lead to a decrease in the number of neurons, neuronal arborization, dendritic spines and cortical volume[157].

The functional role and expression pattern of YKL-40 in the CNS has remained controversial and has not been fully elucidated. Some studies have described that YKL-40 was associated with the macrophage lineage[158,159,160], while others reported an astrocytic expression[91,161,162]. These discrepancies may be due to the fact that YKL-40 expression may vary depending on the disease and the severity of the neuroinflammatory response[96,161]. In study 1, we observed that YKL-40 showed an astroglial cytoplasmic immunoreactivity pattern in postmortem human frontal cortex from healthy controls, AD, PiD, CBD and PSP patients. We did not detect YKL-40 expression in microglia or in neurons. Although YKL-40 was typically found in isolated astrocytes, we occasionally observed focal astrocytic YKL-40 immunoreactivity around blood vessels. Previous studies have suggested that YKL-40 transcription is induced in astrocytes by proinflammatory factors (IL-1β and TNFα) released from macrophages[162]. Interestingly, both cytokines are highly expressed in the microglia of traumatic brain injury (TBI),

Sporadic Creutzfeldt–Jakob disease (sCJD) and AD mouse models[163,164,165]. Moreover, levels of the IL-1β and IL-6 cytokines correlate with YKL-40 expression and are able to up-regulate its levels in *in vitro* primary astrocytes[166]. A recent study also supports that a subtype of reactive astrocytes present in NDDs is induced by secreted cytokines from activated microglia[153] suggesting a strong interaction between microglia and astrocyte activation in chronic inflammatory processes associated with neurodegeneration[167,168]. One possible explanation for our observation of YKL40 positive astrocytes around blood vessels is that perivascular macrophages may induce YKL-40 expression in astrocytes that are in close proximity. After our publication, other studies have supported our results[169,170]. In particular the authors showed YKL-40 expression in perivascular astrocytes in sporadic sCJD and AD cases suggesting that YKL-40 might be implicated in blood vessel conservation and remodelling[169,170].

The functional role of YKL-40 during neuroinflammation is unclear. There is considerable controversy about whether YKL-40 has a neuroprotective or neurotoxic function. On one hand, an *in vivo* study suggested that YKL-40 has a neuroprotective effect as YKL-40 knock-out mice presented more severe neuropathology and prominent gliosis than the wild-type group in a model of controlled cortical impact[171]. These results indicate that YKL-40 modulates the neuroinflammatory response associated with TBI. In agreement with these data, YKL-40 knock-out mice present exacerbated experimental autoimmune encephalomyelitis accompanied by increased lymphocytic and macrophage infiltrates and gliosis compared to wild-type animals[172], suggesting that YKL-40 is necessary for the proper resolution of inflammation. Moreover, *in vitro* studies have shown a dramatic increase of YKL-40 expression during astrocyte differentiation[173]. Other studies based on immunohistochemical techniques suggested that YKL-40 together with stage-specific embryonic antigen-4 (SSEA-4) marker expression represent an unexplored astrogenic lineage[174]. Taking together all these studies, it is possible that YKL-40 expression in astrocytes is crucial for cellular differentiation and proper protective function during the adult time. On the other hand, a very recent study shows a neurotoxic effect of YKL-40 in primary cultured neurons. Exposure of primary cultures of mouse cortical neurons to exogenous YKL-40 resulted in a significant reduction of neurite length and neuronal survival. The authors suggested that YKL-40 has a specific neurotoxic rather than a generalized cytotoxic effect, as they didn't observe a decreased survival in any of the other cell types tested: microglia, astrocytes and splenocytes[175]. Further investigation is needed to solve this controversy. One possibility is that YKL-40 has a neuroprotective role in astrocytes until neuro-inflammaging appears and other mechanisms fail promoting abnormal protein accumulations leading to the YKL-40 neurotoxic shift of function.

Several studies indicate that sustained neuroinflammatory processes can contribute to disease progression in NDDs. In AD, while the relationship between neuroinflammation and amyloid pathogenesis is well established, only a few studies have focused on tau pathology. For that reason, in in our study, we included primary tauopathies: PiD, CBD and PSP, in addition to cases who met clinical and neuropathological criteria for AD to determine the interconnections between YKL-40 and tau. These four tauopathies have in common the abundant deposition of aggregates of hyperphosphorylated tau in the brain. The main difference between AD and the primary tauopathies is that the latter ones do not show amyloid deposits and tau accumulation occurs not only in neurons but also in astrocytes.

This characteristic makes the study of neuroinflammation in these disorders of higher interest. Some studies in animal models have addressed this relationship. One study with transgenic mice overexpressing human tau gene under the glial fibrillary acidic protein (GFAP) promoter showed an age-dependent tau pathology in astrocytes associated with blood-brain-barrier (BBB) and focal neuron loss, highlighting the important role of reactive astrocytes in tauopathies[176]. In study 1, we found that YKL-40 immunoreactivity was independent of tau, since YKL-40 was expressed in a tau negative subset of astrocytes. Whether YKL-40 could be a compensatory response to inhibit tau aggregation or, on the contrary, represents an initial event that facilities tau deposition requires further investigation.

The relationship between neuroinflammation and tau pathology is in constant debate. While some studies revealed that exclusive presence of tau pathology is enough to induce microglia and astroglia activation, others claim that neuroinflammatory responses promote tau pathogenesis[177]. On one hand, studies using different transgenic models of tauopathy showed age-dependent astrogliosis/microglial activation in CNS structures bearing tau pathology at a stage where neuronal loss was absent[178,179,180,181]. In the same direction, colocalization of activated microglial cells and reactive astrocytes with tau oligomers was observed in both mouse models of tauopathy and in AD/FTLD brains[182]. Moreover, misfolded truncated tau has been shown to be sufficient to induce pro-inflammatory cytokines (IL-6, IL-1β, TNFα) in microglial cultures[183]. On the other hand, several studies reported that activation of microglia was observed as an early event prior to NFT formation in mice, promoted tau hyperphosphorylation and aggregation, synaptic loss and behaviour impairment[179,181,184,185].

Recent studies have demonstrated that YKL-40 levels are increased in the CSF of patients with preclinical and prodromal AD[91,186,187,188], which is in agreement with the potential role of astrocytosis in early AD pathogenesis[189]. In addition, increased CSF YKL-40 levels have been reported in multiple AD, FTD and ALS cohorts. A positive correlation between YKL-40, total tau and p-tau has been reported in CSF, suggesting that inflammation and tau-associated neurodegeneration are related pathophysiological processes[98,169,190,191,192, ,193,194]. However, there is a study that suggests that in AD CSF YKL-40 is related to a cerebral structural signature distinct from that related with p-tau associated neurodegeneration at the earliest stages[195]. In study 1, we investigated in detail the potential relationship between tau and YKL-40 in post-mortem brain samples by means of an automated computational tool to quantify YKL-40, tau burden and astrogliosis. The method revealed that total YKL-40 levels were statistically increased in all tauopathies (except PiD) compared with healthy controls. We also found a positive correlation between YKL-40 and tau pathology burden suggesting that inflammation and neurodegeneration are closely related processes in humans. These results are in agreement with studies that investigated YKL-40 levels in CSF of AD and FTD patients[91,93,187,190,193,196,197] and with a recent study that show increased astrocytosis measured with ^{11}C-deuterium-L-deprenyl (^{11}C-DED)-PET tracer in early stages of ADAD patients[198]. Moreover, a recent study in AD human brain samples replicates our results of increased levels of YKL-40 in AD cases compared to controls and MCI. They found that levels of YKL-40 in GM layers I and II and WM, were unchanged in MCI and mild AD, whereas in severe AD, YKL-40 was significantly increased in all cortical layers and WM. They also showed that YKL-40 was expressed only in a subset of GFAP positive astrocytes and not all of them were associated with plaques suggesting that amyloid is

not a necessary precondition for YKL-40 overexpression in astrocytes. Similar to our study they also describe no correlation between YKL-40 and astrogliosis or microglial activation. However, they found an increased expression of GFAP and Iba1 in WM in MCI cases and a positive correlation between WM YKL-40 and Iba1 with cognitive performance during disease progression suggesting that WM inflammation occurs earlier that in the GM and that YKL-40 may play a critical role in WM neuroinflammation associated with cognitive decline in AD[170]. Taking together, all these results suggest that YKL-40 could be a useful marker of neuroinflammation at preclinical stages of NDDs that may mark the astrocytic switch from neuroprotective to neurotoxic phenotype independently of tau. In more advance stages the sustained glial activation could promote tau deposition leading to a vicious circle between inflammation and tau pathology that may contribute to disease progression.

The main limitations of our study were the small sample size, limited to 7-10 cases for group and the descriptive nature of the study that precludes obtaining functional data to better understand the role of YKL-40. In addition, our study lacks early stage cases that could have been interesting for monitoring the YKL-40-tau relationship at the earliest stages. Finally, our study was limited to aggregated tau, and did not investigate oligomeric tau.

In conclusion, study 1 is to our knowledge, the first detailed neuropathologic characterization of YKL-40 expression in human brain tissue. Moreover, the study included tissue samples from healthy controls and four neurodegenerative diseases. By combining confocal microscopy and an automated method to quantify pathology burden, we have shown that the immunoreactivity pattern of YKL-40 in AD and other tauopathies is astroglial. YKL-40 is expressed by a subset of astrocytes that do not contain tau aggregates in non-AD tauopathies. Finally, we found that YKL-40 is associated with tau pathology in neurodegenerative diseases that accumulate tau. These findings could impact on our understanding of this neuroinflammatory marker and its role as potential therapeutic target for early stages in NDDs.

Nanoscale structure of amyloid-β plaques in Alzheimer's disease

In study 2, we demonstrate the potential role of super-resolution microscopy in the neuropathology field by combining two techniques, Array tomography and STED microscopy, to examine the composition of human amyloid β plaques in the brain at a nanometer scale.

In 1992 Hardy and Higgins proposed the amyloid cascade hypothesis in which they postulate that deposition of the Aβ peptide, the main component of the senile plaques, is the primary event on the pathogenesis of AD[199]. Since then, research has been focused intensely on the study of amyloid plaques as one of the main targets for therapeutic approaches for AD. However, the amyloid cascade hypothesis has been questioned by several observations. First, there is lack of correlation between clinical manifestations of the disease and amyloid plaque burden[200]. Second, the presence of Aβ plaques in cognitively normal individuals has been described, meaning that plaque burden does not always equal to cognitive impairment or degeneration, as the individuals of the study did not present memory impairments or changes in brain volume[201,202]. These data promoted the revision of the hypothesis that

the main toxic component of AD are amyloid plaques. An alternative explanation is that smaller and soluble entities, the Aβ oligomers may be more toxic than amyloid plaques. The focus of research shifted when a study published the first evidence of cognitive deficits associated with presence of soluble Aβ oligomers in absence of Aβ plaques[203]. Moreover, another study reported that non-demented individuals had positive biomarkers for amyloidosis measured by 11C Pittsburgh Compound B (PiB)-PET scan demonstrating that presence of larger aggregates did not imply cognitive impairment in those patients[204]. These results suggested that larger aggregates as plaques may not be the main pathogenic cause of neurodegeneration and that Aβ oligomers could better explain the neuronal and synaptic loss observed in AD[205].

Soluble oligomers are Aβ species distinct from monomers or fibrils, and have been identified *in vitro* , in animal models of AD and in AD brains[206]. Several studies in humans and animal models show an early presence of Aβ oligomers prior to plaques[207] and others have suggested a correlation with disease severity [208]. Moreover, some studies have described an inverse correlation between size of Aβ assemblies and their toxicity in multiple *in vitro* and animal models[24,115,209,210]. Aβ oligomer neurotoxicity can be induced by different mechanisms like membrane disruption and ion deregulation by forming pores in the membrane and disrupting their permeability[211,212]. Furthermore, Aβ oligomers also have been implicated in initiating inflammatory processes[149,213]. There is a study that reported that Aβ oligomers bind to a microglial receptor and activates pro-inflammatory pathways, and this receptor was found elevated in AD[214]. However, it is still in debate if oligomers precede inflammation or if inflammation induces oligomer formation.

The characterization of Aβ oligomers in terms of structure, size, conformation, aggregation and neurotoxicity in AD is mainly based on studies *in vitro* and in animal models and using very complex techniques such as ion mobility-based mass spectrometry[215], atomic force microscopy[216,217], solid-state nuclear magnetic resonance[218] and X-ray microdifraction[219]. Multiple Aβ oligomers have been identified in AD brain extracts from humans[220,221,222,223,224,225]. However, it has been really challenging to study and describe these entities in intact human brain samples due to its small size. In our study, we overcome that problem by combining two microscopy techniques, AT and STED, to improve the resolution obtained with conventional confocal microscopy and be able to detect the Aβ oligomers, what we called, non-fibrillar Aβ structures in human amyloid plaques. Using the enhanced resolution of AT-STED we were able to reconstruct a whole human amyloid plaque and examined in detail the nanoscale distribution and size of the non-fibrillar Aβ species. AT-STED allows detection of Aβ structures of at least 100nm, an undetectable size range for immunohistochemical assays due to the resolution limit of light and confocal microscopes (~250 nm)[118,226]. The study revealed that human amyloid plaques consist of a dense core of NAB61 large immunoreactive structures and a peripheral halo of medium and small non-fibrillar Aβ entities. These results are in agreement with a study that used the AT technique to study NAB61 immunoreactivity in an animal model of AD[227].

Several studies have supported the key role of Aβ oligomers in synaptic dysfunction[114,227,228,229,230,231,232,233,234,235]. It has been reported that in transgenic mouse models of AD the onset of synaptic and cognitive dysfunction preceded plaque formation[236,237,238,239]. Moreover, *in vitro* and

in vivo data also indicated that the application of synthetic Aβ oligomers, oligomeric species extracted from AD human brains or from AD mutated cell lines, abolished the formation of new dendritic spines, inhibiting synaptic plasticity and remodelling, thus impairing learning and memory when delivered in the brain of naive mice or rats[225,240,241,242,243,244.]

Taking advantage of super-resolution techniques these past decades has allowed visual observation and description of impaired synapses in presence of Aβ. There is a recent study that used Focused Ion Beam Scanning Electron Microscopy (FIB/SEM) to investigate the relationship between amyloid plaques and the synaptic organization in human AD brains[108]. The main application of AT is to study synapses, and super-resolution microscopy techniques enhances the resolution to achieve a more detailed picture. A study that used AT in AD transgenic mice revealed that oligomeric Aβ interacts directly at the synapse causing dysfunction and spine collapse. They showed that there is a 60% loss of excitatory synapses in the halo of oligomeric Aβ surrounding plaques, suggesting that plaques may be a potential reservoir of oligomeric Aβ, the real synaptotoxic species in the brain of AD patients[227]. In addition, another study characterized the sub-synaptic location of Aβ oligomers using three high-resolution imaging techniques, STORM, immunogold electron microscopy and Förster resonance energy transfer in a mouse model of AD. They observed that different oligomeric Aβ species are present in synaptic terminals by testing different Aβ antibodies[115]. The same group has replicated some of the date in human brain samples. They found that oligomeric Aβ was present at a subset of synapses and that synapse loss around plaques correlates with oligomeric Aβ burden in the neuropil. In addition, they also found that *APOEε4* isoform exacerbates synapse degeneration and synaptic accumulation of oligomeric Aβ in human AD patients[114,228]. In our study we went one step further demonstrating that we were able to detect non-fibrillar Aβ structures two times smaller using AT-STED in human tissue compared to AT alone. Further research is needed to investigate how non-fibrillar Aβ species interact with synapses.

Studies in ADAD have been critical to guide the development of amyloid-based disease-modifying drugs in sporadic AD. Many studies about the pathogenesis of AD rely on transgenic mouse models that overexpress ADAD-associated mutations. The prevailing view about the cause of brain Aβ deposition in ADAD is a chronic increase in the production of Aβ-42 peptide, that over time leads to Aβ oligomer formation, then Aβ fibrillar deposition and finally neurodegeneration[245]. A study carried out in our laboratory showed higher accumulation of APP-CTFs in the brain of ADAD cases than in sporadic AD (SAD) patients and controls. Moreover, we found more severe neuritic component in ADAD than in SAD. These results reinforce the idea of different physiopathological mechanisms underlying the Aβ production/clearance imbalance in SAD and ADAD[246]. In our study, we show preliminary evidence that non-fibrillar Aβ structures were increased in an ADAD case compared to a SAD case in human brain tissue. The significant increase was detected in the smaller non-fibrillar Aβ species. These results suggest that might be a correlation between small Aβ oligomer burden and disease severity, as ADAD patients present early and more aggressive clinical manifestations. These results are also in agreement with a study that showed that Aβ oligomers of high molecular weight are relatively inactive, but when they dissociate to smaller or low molecular weight species they are more bioactive on impairing synapses and activating microglia[210]. Moreover, electrophysiological and biochemical experiments have suggested that soluble Aβ oligomers correlate with disease severity[208,247] and that there is an inverse correlation

between the size of Aβ assemblies and their toxicity in multiple *in vitro* and *in vivo* models[24,115,209]. Interestingly, our findings could not be detected using conventional immunoassays pointing out the importance of implementing super-resolution techniques and computational tools for image processing and analysis for detailed neuropathological studies.

The main limitations of our study are the small sample size for AT-STED due to fact that the requirement of fresh tissue makes these samples extremely scarce. Second, we only used one antibody to detect non-fibrillar Aβ. However, in our hands specific antibodies for oligomeric Aβ suitable for human tissue are exceedingly rare and NAB61 has been extensively characterized[114,227,248.]

In conclusion, as a proof of concept our study shows that the combination of AT and STED can be successfully applied to investigate non-fibrillar Aβ structures in AD human brain. The obtained nanoscale architecture of human amyloid plaques reveals a dense core with a peripheral halo and we provide evidence of higher levels of non-fibrillar Aβ species in ADAD compared to SAD. Additional studies are needed to further investigate the potential relevance of these assemblies in the pathogenesis of the disease. This new tool proposed opens an important door for the neuropathology field allowing the characterization of aggregates or structures at a nanometric scale as potential therapeutic targets.

Reduced non-fibrillar Aβ species in a patient treated with low doses of BACE-1 inhibitor

In study 3, we report the neuropathological findings of a case that participated in a clinical trial with a BACE-1 inhibitor. We demonstrate that Verubecestat may have exerted some effect on non-fibrillar forms of Aβ and synaptic damage.

Inhibition of BACE-1 was proposed as a promising therapeutic strategy for AD. Past attempts using immunotherapy and inhibitors of Aβ or tau aggregation failed, so approaches as the inhibition of the enzyme that promotes the Aβ production gained strength. Several compounds have been developed to target BACE-1 activity, but only a few proceeded to clinical trials. Verubecestat is a BACE-1 inhibitor that was tested in a clinical trial with patients with mild-to-moderate AD. The results showed a 60-80% reduction of Aβ-40 and Aβ-42 in CSF and a modest reduction (~20%) in brain amyloid load, but this reduction was not effective in slowing the clinical progression. In the final report, the authors suggested that because Aβ deposition takes place years before clinical symptoms, treatments targeting amyloid should be implemented early in the disease process[45].

The company also conducted another trial to determine whether Verubecestat could slow disease progression in patients in the prodromal stage of AD[249]. The results showed that cortical amyloid load increased over time in the placebo group and declined in the Verubecestat groups (12 and 40 mg doses) but did not reach threshold for being amyloid-negative. The study also showed a reduction greater than 60% in CSF concentrations of Aβ-42 and related APP metabolites. However, neuropsychological evaluation suggested that cognitive and daily function were worse among patients who received treatment than among those who received placebo. The authors concluded that Verubecestat was acting at its intended target but without a beneficial effect on clinical outcomes. They suggested that patients at

an earlier stage of the disease may be more sensitive to the effects of substantial BACE-1 inhibition, perhaps because of a role of BACE-1 in normal synaptic function[46].

The neuropathological assessment of a case that participated in this clinical trial is of high relevance as may help to understand the impact of the drug on Aβ production/clearance, and other key features, such as synaptic loss. In our study we evaluated post-mortem the non-fibrillar Aβ burden (also referred as oligomeric Aβ) and total Aβ of this case and compared with 9 untreated AD cases. We found that the patient presented the lowest ratio oligomeric/total Aβ of all AD cases included in the study. This result strongly suggests that Verubecestat may be exerting some effect specifically on the non-fibrillar species of Aβ, considered to be those with the highest toxicity[24,39]. These data are in agreement with a recent study that used two-photon microscopy to monitor the impact of pharmacological BACE-1 inhibition on early Aβ plaque deposition in an AD mouse model, demonstrating that treatment slowed down progression of initial Aβ plaque formation but was less effective toward existing plaques[250]. We did not find differences in total Aβ, suggesting that plaques formed by fibrillar Aβ were not affected by the drug and that early Aβ plaques mainly formed by oligomeric species were decreased in the patient treated with Verubecestat. Current evidence suggests that the timing of intervention with BACE-1 inhibitors should be as early as possible in clinical trials to achieve optimal therapeutic efficacy for AD treatment. That may explain the failures of different trials using BACE-1 inhibitors among other factors.

Another aspect to take into account is that BACE-1 has a wide array of substrates, and proper cleavage of these substrates may be necessary for normal neuronal physiology[251,252,253]. In a recent study, the authors showed that the germline BACE-1 knockout (*BACE-1*$^{-/-}$) mice exhibited smaller postnatal size and compromised survival, hypomyelinization, spontaneous seizures and abnormal electroencephalograms, memory deficits, and axon guidance defects among other phenotypes, leading to the conclusion that BACE-1 is crucial during development[254]. To overcome this problem, the same group generated conditional BACE-1 knockout mice to model the effects of BACE-1 inhibition in the mature brain, and mimic the potential effects of a human clinical trial. Several of the neurological phenotypes present in the germline were absent, but organization defects of the mossy fibers in the hippocampus were observed[254,255]. That can be explained because BACE-1 cleavage of Cell Adhesion Molecule L1 Like (CHL1) protein regulates the balance between growth cone extension and collapse for a correct axonal guidance of those fibers[255,256]. An aberrant morphology in an axonal pathway important for learning and memory observed in the conditional BACE-1 knockout mice could explain the adverse effects of cognitive worsening, neuropsychiatric disturbances and hippocampal volume loss in the Verubecestat clinical trial, caused by an over-inhibition of BACE-1 cleavage of CHL1. However, other mechanisms involving different BACE-1 substrates that affect synaptic plasticity or maintenance could also play a role. These observations suggest that the BACE-1 inhibitor dose is critical, and perhaps lower doses able to achieve 50% inhibition might be safer and more effective.

In the same line, it is of a high importance to evaluate the impact of a BACE-1 inhibitor on synaptic morphology and function to avoid potential off-target effects. A study in a mouse AD model showed that Verubecestat altered the formation but not the stability of dendritic spines, suggesting that carefully

dosed inhibitors might be therapeutically effective without affecting the structural integrity of excitatory synapses if given at an early disease stage[257]. In our study, we decided to quantify synapse loss using a pre and a postsynaptic marker, SYPH and PSD-95 respectively, to find a possible correlate of the increased cognitive worsening of the patient. We did not find differences in neither of the markers between the patient and the untreated AD cases included in the study. Interestingly, the immunoreactivity pattern of SYPH was of two types: a neuropil-like pattern and a plaque-like staining. This second pattern was already described in an article where the authors showed that two presynaptic proteins, Vesicle-associated membrane protein 2 (VAMP2) and Synaptosomal-Associated Protein 25 (SNAP-25), colocalized with the core of amyloid plaques and SYPH stain was described as punctate lobular profiles decorating the plaques[258]. Another article provides evidence that BACE-1 is located into vesicles like endosomes in normal hippocampal mossy fiber terminals of both non-transgenic and APP transgenic mouse brains. Moreover, the authors report that BACE-1 colocalized with SYPH in swollen dystrophic presynaptic terminals surrounding plaques. These data suggested that elevated BACE-1 and APP levels in plaque-associated presynaptic dystrophies could increase local peri-plaque Aβ generation and accelerate amyloid plaque growth in AD[259]. In our study we quantify the SYPH plaque-like staining and we found that the patient treated with Verubecestat showed the lowest immunoreactivity, suggesting that BACE-1 inhibition may reduce APP cleavage at the synapses leading to less Aβ accumulation and preventing presynaptic terminal dystrophies.

Synapse loss is the strongest pathological correlate of cognitive decline in AD[33,34]. Evidence shows that Aβ and tau pathological species accumulate at synapses[227,260], disrupt key synaptic machinery[261], and induce spine collapse[262], among others. With the hypothesis that BACE-1 inhibition may promote less Aβ accumulation in synapses, in our study we selected a subset of cases including the patient treated with Verubecestat to quantify synaptic non-fibrillar forms of Aβ. In other words, we investigated if Veruvecestat may promote clearance of synaptic Aβ oligomeric. To test this hypothesis we used the AT technique to achieve nanometric resolutions. The results obtained showed that there were no differences in the quantification of SYPH density between the patient and the untreated cases suggesting no effect on synaptic loss. Interestingly, the presence of non-fibrillar Aβ at the presynaptic terminals was lower in the case treated with Verubecestat than the rest. These data suggested that Verubecestat may also be contributing to the clearance of synaptic non-fibrillar Aβ species.

The main limitation of our study is the sample size as we only had access to one patient treated with Verubecestat. Nonetheless, to our knowledge this is the first neuropathological case reported of a patient who participated in a trial with a BACE-1 inhibitor.

BACE-1 inhibition has proven to be a challenging therapeutic strategy due to the alterations in some physiologic functions promote by different substrates involving BACE-1 activity. However, more research needs to be done to dismiss this option as interpreting all data there is still a chance in lowering the doses and administrating the drug in early stages of the disease. Moreover, another point to treat is finding a way that the BACE-1 inhibitor targets only the enzyme that interacts with APP. May be a small molecule design to target the interaction between APP and BACE-1 is more effective than to target the

active site of the enzyme. Several studies are pursuing the modulation of protein-protein interaction using small-molecules as showed in this review[263].

In conclusion, we observed a reduction of non-fibrillar Aβ forms present in plaques and at synapses in a patient treated with Verubecestat. These data support the notion that BACE-1 inhibition has detectable effects on brain Aβ load but that this approach needs to be refined to avoid off-target effects. A combination therapy of drugs targeting independent mechanisms could be an optimal approach to treat complex disorders as AD.

General discussion

This doctoral thesis highlights the importance of digital neuropathology as a tool for research purposes and clinical interpretation. The three studies included applied conventional immunohistochemisty assays to study the pattern of expression of different markers for a better understanding of the pathologies and the mechanisms involved in different NDDs. We show that these techniques offer greater information than the semi-quantitative methods that still are current practices by many researchers in neuropathological studies and at the brain tissue banks. We have developed automated in-house computational tools to quantify pathology burden that can be of great interest for neuropathologists. A way to transfer these tools to daily practice could be to integrate these tools into brain tissue banks, creating a large quantitative database of all hallmark lesions of each case. Moreover, in this thesis we also provide evidence that it is feasible to implement super-resolution techniques for the study of small structures, such as synapses or small aggregates. Few laboratories worldwide have the possibility to apply this methodology to human samples and to describe in full detail the underlying pathology and ultrastructural alterations in NDDs. A lot of work remains to be done in the field of NDDs. The challenge is to incorporate the current technological advances into our daily practice to meet the current needs, to achieve its maximal potential and to accelerate the development of effective therapies for these disorders.

Chapter 5: Conclusions

In this thesis, digital neuropathology and super-resolution techniques has been implemented for the study of different mechanisms involved in neurodegenerative diseases.

The main conclusions of this thesis are:

1. YKL-40 immunoreactivity pattern in AD and other tauopathies is mainly astroglial. YKL-40 is expressed by a subset of astrocytes that do not contain tau aggregates in non-AD tauopathies. YKL-40 inflammatory marker is associated with tau pathology in neurodegenerative diseases that accumulate tau.

2. The combination of array tomography and STED can be successfully applied to investigate non-fibrillar Aβ structures in AD human brain. The nanoscale architecture of human amyloid plaques reveals a dense core of large Aβ structures and a peripheral halo of medium and small non-fibrillar Aβ entities. ADAD present higher levels of non-fibrillar Aβ species compared to SAD.

3. Treatment with low-dose Verubecestat may have exerted some effect on brain non-fibrillar forms of Aβ and synaptic derangement.

Chapter 6: References

1. Alzheimer's Disease International. World Alzheimer Report 2019, Attitudes to dementia. *Alzheimer's Dis Int London*. Published online 2019:1-15.

2. Kovacs GG. Molecular pathological classification of neurodegenerative diseases: Turning towards precision medicine. *Int J Mol Sci*. 2016;17(2).

3. Kovacs GG. Current Concepts of Neurodegenerative Diseases. *EMJ Neurol*. 2014;1(July):78-86.

4. Kovacs GG. Introduction: Classification of Neurodegenerative Diseases. In: Kovacs GG, Ed. Neuropathology of Neurodegenerative Diseases: A Practical Guide. *Cambridge University Press: Cambridge, UK,* 2015; pp. 1–8.

5. Bertram L & Tanzi RE. The genetic epidemiology of neurodegenerative disease. *J Clin Invest*. 2005;115(6):1449-1457.

6. Barnes DE & Yaffe K. The Projected Impact of Risk Factor Reduction on Alzheimer's Disease Prevalence. *Lancet Neurol*. 2011;10(9):819-828.

7. Erkkinen MG, Kim M & Geschwind MD. Clinical Neurology and Epidemiology of the Major Neurodegenerative Diseases. *Cold Spring Harb Perspect Biol*. 2018;10(4)::a033118.

8. Mayeux R & Stern Y. Epidemiology of Alzheimer Disease. *Cold Spring Harb Perspect Med*. 2012;2(8):a006239.

9. Galton CJ, Patterson K, Xuereb JH & Hodges JR. Atypical and typical presentations of Alzheimer's disease: a clinical, neuropsychological, neuroimaging and pathological study of 13 cases. *Brain*. 2000;123(3):484-498.

10. Villemagne VL *et al.* Amyloid β deposition, neurodegeneration, and cognitive decline in sporadic Alzheimer's disease: A prospective cohort study. *Lancet Neurol*. 2013;12(4):357-367.

11. Frisoni GB, Winblad B & O'Brien JT. Revised NIA-AA criteria for the diagnosis of Alzheimer's disease: A step forward but not yet ready for widespread clinical use. *Int Psychogeriatrics*. 2011;23(8):1191-1196.

12. Reisa A *et al*. Toward defining the preclinical stages of Alzheimer's disease: Recommendations from the National Institute on Aging- Alzheimer's Association workgroups on diagnostic guidelines for Alzheimer's disease. *Alzheimer's Dement*. 2011;7(3):280-292.

13. Albert MS *et al.* The diagnosis of mild cognitive impairment due to Alzheimer's disease: Recommendations from the National Institute on Aging- Alzheimer's Association workgroups on diagnostic guidelines for Alzheimer's disease. *Focus (Madison)*. 2013;11(1):96-106.

14. McKhann GM *et al.* The diagnosis of dementia due to Alzheimer's disease: Recommendations from the National Institute on Aging- Alzheimer's Association workgroups on diagnostic guidelines for Alzheimer's disease. *Alzheimers Dement*. 2011;7(3):263-269.

15. Serrano-Pozo A, Frosch MP, Masliah E and Hyman BT. Neuropathological alterations in Alzheimer disease. *Cold Spring Harb Perspect Med*. 2011;1(1):1-24.

16. Atri A. The Alzheimer's Disease Clinical Spectrum: Diagnosis and Management. *Med Clin North Am*. 2019;103(2):263-293.

17. Masters CL *et al.* Alzheimer's disease. *Nat Rev Dis Prim*. 2015;1:1-18.

18. Selkoe DJ & Hardy J. The amyloid hypothesis of Alzheimer's disease at 25 years. *EMBO Mol Med*. 2016;8:595-608.

19. Müller UC, Deller T & Korte M. Not just amyloid: Physiological functions of the amyloid precursor protein family. *Nat Rev Neurosci*. 2017;18(5):281-298.

20. Xu H, Greengard P & Gandy S. Regulated formation of Golgi secretory vesicles containing Alzheimer β- amyloid precursor protein. *J Biol Chem*. 1995;270(40):23243-23245.

21. Kinoshita A *et al*. Demonstration by FRET of BACE interaction with the amyloid precursor protein at the cell surface and in early endosomes. *J Cell Sci*. 2003;116(16):3339-3346.

22. Haass C, Kaether C, Thinakaran G & Sisodia S. Trafficking and proteolytic processing of APP. *Cold Spring Harb Perspect Med*. 2012;2(5):1-25.

23. Reiss AB *et al*. Amyloid toxicity in Alzheimer's disease. *Rev Neurosci*. 2018;29(6):613-627.

24. Sengupta U, Nilson AN & Kayed R. The Role of Amyloid-β Oligomers in Toxicity, Propagation, and Immunotherapy. *EBioMedicine*. 2016;6:42-49.

25. Kent SA, Spires-Jones TL & Durrant CS. The Physiological Roles of Tau and Aβ: Implications for Alzheimer's Disease Pathology and Therapeutics. *Acta Neropathol.* 2020;140:417-447.

26. Crook R *et al.* A variant of Alzheimer's disease with spastic paraparesis and unusual plaques due to deletion of exon 9 of presinilin 1. *Nat Med*. 1998;4(4):452-455.

27. Tabira T, De Chui H, Nakayama H, Kuroda S & Shibuya M. Alzheimer's disease with spastic paresis and cotton wool type plaques. *J Neurosci Res*. 2002;70(3):367-372.

28. Boon BDC *et al*. The coarse-grained plaque: a divergent Aβ plaque-type in early-onset Alzheimer's disease. *Acta Neuropathol*. 2020; doi: 10.1007/s00401-020-02198-8

29. Brettschneider J, Del Tredici K, Lee VM & Trojanowski JQ. Spreading of pathology in neurodegenerative diseases: a focus on human studies. *Nat Rev Neurosci*. 2015;16(2):109-120.

30. Morsy A & Trippier PC. Current and Emerging Pharmacological Targets for the Treatment of Alzheimer's Disease. *J Alzheimer's Dis*. 2019;72(s1):S145-S176.

31. Kimura T, Ishiguro K & Hisanaga SI. Physiological and pathological phosphorylation of tau by Cdk5. *Front Mol Neurosci*. 2014;7:1-10.

32. Hooper C, Killick R & Lovestone S. The GSK3 hypothesis of Alzheimer's disease. *J Neurochem*. 2008;104(6):1433-1439.

33. DeKosky ST & Scheff SW. Synapse loss in frontal cortex biopsies in Alzheimer's disease: Correlation with cognitive severity. *Ann Neurol*. 1990;27(5):457-464.

34. Terry RD *et al.* Physical Basis of Cognitive Alterations in Alzheimer's Disease: Synapse hss Is the Major Correlate of Cognitive Impairment. *Ann Neurol*. 1991;30:572-580.

35. DeKosky ST, Scheff SW & Styren SD. Structural correlates of cognition in dementia: Quantification and assessment of synapse change. *Neurodegeneration*. 1996;5(4):417-421.

36. Montine TJ *et al*. National Institute on Aging-Alzheimer's Association guidelines for the neuropathologic assessment of Alzheimer's disease: a practical approach. *Acta Neuropathol*. 2012;123(1):1-11.

37. Kovacs GG. Molecular pathology of neurodegenerative diseases: Principles and practice. *J Clin Pathol*. 2019;72(11):725-735.

38. Gilling KE, Jatzke C, Hechenberger M & Parsons CG. Potency, voltage-dependency, agonist concentration-dependency, blocking kinetics and partial untrapping of the uncompetitive N-methyl-d-aspartate (NMDA) channel blocker memantine at human NMDA (GluN1/GluN2A) receptors. *Neuropharmacology*. 2009;56(5):866-875.

39. Ono K & Yamada M. Low-n oligomers as therapeutic targets of Alzheimer's disease. *J Neurochem*. 2011;117(1):19-28.

40. Gervais F *et al*. Targeting soluble Aβ peptide with Tramiprosate for the treatment of brain amyloidosis. *Neurobiol Aging*. 2007;28(4):537-547.

41. Aisen PS, *et al.* Tramiprosate in mild-to-moderate Alzheimer's disease - A randomized, double-blind, placebo-controlled, multi-centre study (the alphase study). *Arch Med Sci*. 2011;7(1):102-111.

42. Doody RS *et al*. A phase 3 trial of semagacestat for treatment of Alzheimer's disease. *N Engl J Med*. 2013;369(4):341-350.

43. Coric V *et al*. Safety and tolerability of the γ-secretase inhibitor avagacestat in a phase 2 study of mild to moderate Alzheimer disease. *Arch Neurol*. 2012;69(11):1430-1440.

44. Gilman S *et al*. Clinical Effect of AB immunization(AN1792) in patients with AD in an interrupted trial. *Neurology* 2005;64;1553-1562.

45. Egan MF *et al.* Randomized trial of verubecestat for mild-to-moderate Alzheimer's disease. *N Engl J Med*. 2018;378(18):1691-1703.

46. Egan MF *et al.* Randomized trial of verubecestat for prodromal Alzheimer's disease. *N Engl J Med*. 2019;380(15):1408-1420.

47. Lovestone S *et al.* A phase II trial of tideglusib in alzheimer's disease. *J Alzheimer's Dis*. 2015;45(1):75-88.

48. Heneka MT *et al.* Neuroinflammation in Alzheimer ' s Disease. *Lancet Neurol*. 2015;14(4):388-405.

49. Bronzuoli MR, Iacomino A, Steardo L & Scuderi C. Targeting neuroinflammation in Alzheimer's disease. *J Inflamm Res*. 2016;9:199-208.

50. Jiang C, Li G, Huang P, Liu Z & Zhao B. The Gut Microbiota and Alzheimer's Disease. *J Alzheimer's Dis*. 2017;58(1):1-15.

51. Kovacs GG. Tauopathies. *Handbook of Clinical Neurology.* 2017;145:355-368

52. Bang J, Spina S & Miller BL. Non-Alzheimer's dementia 1: Frontotemporal dementia. *Lancet*. 2015;386(10004):1672-1682.

53. Goedert M, Spillantini MG, Jakes R, Rutherford D & Crowther RA. Multiple isoforms of human microtubule-associated protein tau: sequences and localization in neurofibrillary tangles of Alzheimer's disease. *Neuron*. 1989;3(4):519-526.

54. Hutton M *et al.* Association of missense and 5'-splice-site mutations in tau with the inherited dementia FTDP-17. *Nature*. 1998;393:702-705.

55. Poorkaj P et al. Tau is a candidate gene for chromosome 17 frontotemporal dementia. *Ann Neurol*. 1998;43(6):815-825.

56. Spillantini MG *et al.* Mutation in the tau gene in familial multiple system tauopathy with presenile dementia. *Proc Natl Acad Sci U S A*. 1998;95(13):7737-7741.

57. Ghetti B *et al.* Invited review: Frontotemporal dementia caused by microtubule-associated protein tau gene (MAPT) mutations: A chameleon for neuropathology and neuroimaging. *Neuropathol Appl Neurobiol*. 2015;41(1):24-46.

58. Kovacs GG. Invited review: Neuropathology of tauopathies: Principles and practice. *Neuropathol Appl Neurobiol*. 2015;41(1):3-23.

59. Kovacs GG. Astroglia and Tau: New Perspectives. *Front Aging Neurosci*. 2020;12(April):1-14.

60. Hodges JR *et al.* Survival in frontotemporal dementia. *Neurology*. 2003;61(3):349-354.

61. Knopman DS & Roberts RO. Degeneration in the US Population. *J Mol Neurosci*. 2011;45(3):330-335.

62. Olney NT, Spina S & Miller BL. Frontotemporal Dementia. *Neurol Clin*. 2017;35(2):339-374.

63. Irwin DJ. Tauopathies as Clinicopathological Entities David. *Park Relat Disord*. 2016;22(0 1):S29-S33.

64. Gorno-Tempini ML *et al.* Classification of primary progressive aphasia and its variants. *Neurology*. 2011;76(11):1006-1014.

65. Respondek G *et al.* Which ante-mortem clinical features predict progressive supranuclear palsy pathology? *Physiol Behav*. 2017;176(1):139-148.

66. Höglinger GU, Respondek G & Kovacs GG. New classification of tauopathies. *Rev Neurol (Paris)*. 2018;174(9):664-668.

67. Irwin DJ *et al*. Deep Clinical and Neuropathological Phenotyping of Pick's Disease. *Physiol Behav*. 2016;176(10):139-148.

68. Dickson DW. Pick's Disease: A Modern Approach. *Brain Pathol*. 1998;8(2):339-354.

69. Dugger BN & Dickson DW. Pathology of neurodegenerative diseases. *Cold Spring Harb Perspect Biol*. 2017;9(7):1-22.

70. Zhukareva V *et al*. Sporadic Pick's disease: A tauopathy characterized by a spectrum of pathological τ isoforms in gray and white matter. *Ann Neurol*. 2002;51(6):730-739.

71. Buée L, Bussière T, Buée-Scherrer V, Delacourte A, Hof PR. Tau protein isoforms, phosphorylation and role in neurodegenerative disorders. *Brain Res Rev*. 2000;33(1):95-130.

72. Lee VMY, Goedert M & Trojanowski JQ. Neurodegenerative tauopathies. *Annu Rev Neurosci*. 2001;24:1121-1161.

73. Dickson DW *et al.* Office of rare diseases neuropathologic criteria for corticobasal degeneration. *J Neuropathol Exp Neurol*. 2002;61(11):935-946.

74. Josephs KA *et al.* Neuropathological background of phenotypical variability in frontotemporal dementia. *Acta Neuropathol*. 2011;122(2):137-153.

75. Josephs KA *et al.* Clinicopathologic analysis of frontotemporal and corticobasal degenerations and PSP. *Neurology*. 2006;66(1):41-48.

76. Litvan I *et al.* Validity and reliability of the preliminary NINDS neuropathologic criteria for progressive supranuclear palsy and related disorders. *J Neuropathol Exp Neurol*. 1996;55:97-105.

77. Dickson DW. Neurodegeneration the molecular pathology of dementia and movement disorders. Neurodegeneration: the molecular pathology of dementia and movement disorders. *Oxford: Wiley-Blackwell;* 2011. p. 1–5.

78. Josephs KA. Corticobasal Ganglionic Degeneration. *Blue Books of Neurology.* 2010;34:375-396.

79. Labzin LI, Heneka MT & Latz E. Innate Immunity and Neurodegeneration. *Annu Rev Med*. 2018;69:437-449.

80. Heneka MT, Kummer MP & Latz E. Innate immune activation in neurodegenerative disease. *Nat Rev Immunol*. 2014;14(7):463-477.

81. Verkhratsky A & Nedergaard M. Physiology of astroglia. *Physiol Rev*. 2018;98(1):239-389.

82. Ferrer I. Diversity of astroglial responses across human neurodegenerative disorders and brain aging. *Brain Pathol*. 2017;27(5):645-674.

83. Perez-Nievas BG & Serrano-Pozo A. Deciphering the astrocyte reaction in Alzheimer's disease. *Front Aging Neurosci*. 2018;10:1-23.

84. Colonna M & Butovsky O. Microglia function in the central nervous system during health and neurodegeneration. *Annu Rev Immunol*. 2017;35:441-468.

85. González-Reyes RE, N et al,. Involvement of astrocytes in Alzheimer's disease from a neuroinflammatory and oxidative stress perspective. *Front Mol Neurosci*. 2017;10:1-20.

86. Ransohoff RM. How neuroinflammation contributes to neurodegeneration. *Science*. 2016;353(6301):777-783.

87. Renkema GH *et al.* Chitotriosidase a chitinase, and the 39-kDa human cartilage glycoprotein, a chitin-binding lectin, are homologues of family 18 glycosyl hydrolases secreted by human macrophages. *Eur J Biochem*. 1998;251(1-2):504-509.

88. Hakala BE, White C & Recklies AD. Human cartilage gp-39, a major secretory product of articular chondrocytes and synovial cells, is a mammalian member of a chitinase protein family. *J Biol Chem*. 1993;268(34):25803-25810.

89. Johansen J. Studies on serum YKL-40 as a biomarker in diseases with inflammation, tissue remodelling, fibroses and cancer. *DanMed Bull*. 2006;53:172–209.

90. Kawada M, Hachiya Y, Arihiro A & Mizoguchi E. Role of mammalian chitinases in inflammatory conditions. *Keio J Med*. 2007;56(1):21-27.

91. Craig-Schapiro R *et al.* YKL-40: A Novel Prognostic Fluid Biomarker for Preclinical Alzheimer's Disease. *Biol Psychiatry*. 2010;68(10):903-912.

92. Mattsson N *et al.* Cerebrospinal fluid microglial markers in Alzheimer's disease: Elevated chitotriosidase activity but lack of diagnostic utility. *NeuroMolecular Med*. 2011;13(2):151-159.

93. Alcolea D *et al.* Relationship between β-Secretase, Inflammation and Core Cerebrospinal Fluid Biomarkers for Alzheimer's Disease. *J Alzheimer's Dis*. 2014;42(1):157-167.

94. Alcolea D *et al.* CSF sAPPβ, YKL-40, and neurofilament light in frontotemporal lobar degeneration. *Neurology*. 2017;89(2):178-188.

95. Mañé-Martínez MA *et al.* Glial and neuronal markers in cerebrospinal fluid in different types of multiple sclerosis. *J Neuroimmunol*. 2016;299:112-117.

96. Cantó E *et al.* Chitinase 3-like 1 plasma levels are increased in patients with progressive forms of multiple sclerosis. *Mult Scler J*. 2012;18(7):983-990.

97. Comabella M *et al.* Cerebrospinal fluid chitinase 3-like 1 levels are associated with conversion to multiple sclerosis. *Brain*. 2010;133(4):1082-1093.

98. Illán-Gala I *et al.* CSF sAPPβ, YKL-40, and NfL along the ALS-FTD spectrum. *Neurology*. 2018;91(17):E1619-E1628.

99. West MJ, Slomianka L & Gundersen HJG. Unbiased stereological estimation of the total number of neurons in the subdivisions of the rat hippocampus using the optical fractionator. *Anat Rec*. 1991;231(4):482-497.

100. Armstrong RA & Cairns NJ. Spatial patterns of the tau pathology in progressive supranuclear palsy. *Neurol Sci*. 2013;34(3):337-344.

101. Armstrong RA, Cairns NJ & Lantos PL. Clustering of cerebral cortical lesions in patients with corticobasal degeneration. *Neurosci Lett*. 1999;268(1):5-8.

102. Byrne UTE, Ross JM, Faull RLM & Dragunow M. High-throughput quantification of Alzheimer's disease pathological markers in the post-mortem human brain. *J Neurosci Methods*. 2009;176(2):298-309.

103. Samaroo HD *et al.* High throughput object-based image analysis of β-amyloid plaques in human and transgenic mouse brain. *J Neurosci Methods*. 2012;204(1):179-188.

104. Tang Z *et al*. Interpretable classification of Alzheimer's disease pathologies with a convolutional neural network pipeline. *Nat Commun*. 2019;10(1):1-14.

105. Irwin DJ *et al*. Semi-Automated Digital Image Analysis of Pick's Disease and TDP-43 Proteinopathy. *J Histochem Cytochem*. 2016;64(1):54-66.

106. Gray EG. Electron Microscopy of synaptic contacts on dendirte spines of the cerebral cortex.

Nature. 1959;183:1592-1593.

107. De Robertis E. Electron microscope observations on the submicroscopic organization of the retinal rods. *J Biophys Biochem Cytol*. 1956;2(3):319-330.

108. Blazquez-Llorca L, Merchán-Pérez Á, Rodríguez JR, Gascón J & DeFelipe J. FIB/SEM technology and Alzheimer's disease: Three-dimensional analysis of human cortical synapses. *J Alzheimer's Dis*. 2013;34(4):995-1013.

109. Kopeikina KJ *et al.* Tau accumulation causes mitochondrial distribution deficits in neurons in a mouse model of tauopathy and in human Alzheimer's disease brain. *Am J Pathol*. 2011;179(4):2071-2082.

110. Henstridge CM *et al.* Synapse loss in the prefrontal cortex is associated with cognitive decline in amyotrophic lateral sclerosis. *Acta Neuropathol*. 2018;135(2):213-226.

111. Long BR, Robinson DC & Zhong H. Subdiffractive microscopy: techniques, applications, and challenges Background: Diffraction limit in biological imaging. *Wiley Interdiscip Rev Syst Biol Med*. 2014;6(2):151-168.

112. O'Rourke NA, Weiler NC, Micheva KD & Smith SJ. Deep molecular diversity of mammalian synapses: Why it matters and how to measure it. *Nat Rev Neurosci*. 2012;13(6):365-379.

113. Micheva KD & Smith SJ. Array Tomography: A New Tool for Imaging the Molecular Architecture and Ultrastructure of Neural Circuits. *Neuron*. 2007;55(1):25-36.

114. Koffie RM *et al.* Apolipoprotein E4 effects in Alzheimer's disease are mediated by synaptotoxic oligomeric amyloid-β. *Brain*. 2012;135(7):2155-2168.

115. Pickett EK *et al.* Non-Fibrillar Oligomeric Amyloid-β within Synapses. *J Alzheimer's Dis*. 2016;53(3):787-800.

116. Colom-Cadena M *et al.* Synaptic phosphorylated α-synuclein in dementia with Lewy bodies. *Brain*. 2017;140(12):3204-3214.

117. Hell SW & Wichmann J. Breaking the diffraction resolution limit by stimulated emission: stimulated-emission-depletion fluorescence microscopy. *Opt Lett*. 1994;19(11):780

118. Schermelleh L, Heintzmann R & Leonhardt H. A guide to super-resolution fluorescence microscopy. *J Cell Biol*. 2010;190(2):165-175.

119. Merino D, Mallabiabarrena A, Andilla J, Artigas D, Zimmermann T & Loza-Alvarez P. STED imaging performance estimation by means of Fourier transform analysis. *Biomed Opt Express*. 2017;8(5):2472.

120. Tam J & Merino D. Stochastic optical reconstruction microscopy (STORM) in comparison with stimulated emission depletion (STED) and other imaging methods. *J Neurochem*.

2015;135(4):643-658.

121. Willig KI, Rizzoli SO, Westphal V, Jahn R & Hell SW. STED microscopy reveals that synaptotagmin remains clustered after synaptic vesicle exocytosis. *Nature*. 2006;440(7086):935-939.

122. Singh H *et al.* Visualization and quantification of cardiac mitochondrial protein clusters with STED microscopy. *Mitochondrion*. 2012;12(2):230-236.

123. Gad AKB *et al.* Rho GTPases link cellular contractile force to the density and distribution of nanoscale adhesions. *FASEB J*. 2012;26(6):2374-2382.

124. Urban NT, Willig KI, Hell SW & Nägerl UV. STED nanoscopy of actin dynamics in synapses deep inside living brain slices. *Biophys J*. 2011;101(5):1277-1284.

125. Benda A, Aitken H, Davies DS, Whan R & Goldsbury C. STED imaging of tau filaments in Alzheimer's disease cortical grey matter. *J Struct Biol*. 2016;195(3):345-352.

126. Rust MJ, Bates M & Zhuang X. Stochastic optical reconstruction microscopy (STORM) provides sub-diffraction-limit image resolution. *Nat Methods*. 2006;3(10):793-795.

127. Heilemann M *et al.* Subdiffraction-resolution fluorescence imaging with conventional fluorescent probes. *Angew Chemie - Int Ed*. 2008;47(33):6172-6176.

128. Endesfelder U & Heilemann M. Direct Stochastic Optical Reconstruction Microscopy (dSTORM). *Methods Mol Biol*. 2015;1251:109-133.

129. Dudok B *et al.* Cell-specific STORM superresolution imaging reveals nanoscale organization of cannabinoid signaling. Nat Neurosci. 2015; 18(1): 75–86.

130. Barna L *et al*. Correlated confocal and super-resolution imaging by VividSTORM. *Nat Protoc*. 2016;11(1):163-183.

131. Dani A, Huang B, Bergan J, Dulac C & Zhuang X. Superresolution Imaging of Chemical Synapses in the Brain. *Neuron*. 2010;68(5):843-856.

132. MacGillavry HD, Song Y, Raghavachari S & Blanpied TA. Nanoscale scaffolding domains within the postsynaptic density concentrate synaptic ampa receptors. *Neuron*. 2013;78(4):615-622.

133. Nair D *et al.* Super-resolution imaging reveals that AMPA receptors inside synapses are dynamically organized in nanodomains regulated by PSD95. *J Neurosci*. 2013;33(32):13204-13224.

134. Specht CG *et al.* Quantitative nanoscopy of inhibitory synapses: Counting gephyrin molecules and receptor binding sites. *Neuron*. 2013;79(2):308-321.

135. Tang A-H *et al*. A transsynaptic nanocolumn aligns neurotransmitter release to receptors.

Nature. 2016;536:210-214.

136. Sakamoto H *et al.* Synaptic weight set by Munc13-1 supramolecular assemblies. *Nat Neurosci*. 2018;21(1):41-55.

137. Hainsworth AH, Lee S, Patel A, Poon WW & Knight AE. Super-resolution imaging of subcortical white matter using stochastic optical reconstruction microscopy (STORM) and super-resolution optical fluctuation imaging (SOFI). *Neuropathol Appl Neurobiol*. 2018;44(4):417-426.

138. Begemann I & Galic M. Correlative light electron microscopy: Connecting synaptic structure and function. *Front Synaptic Neurosci*. 2016;8:1-12.

139. Booth DG, Beckett AJ, Prior IA & Meijer D. SuperClem: An accessible correlative light and electron microscopy approach for investigation of neurons and glia in vitro. *Biol Open*. 2019;8(5).

140. Burel A *et al.* A targeted 3d em and correlative microscopy method using sem array tomography. *Dev*. 2018;145(12).

141. De Boer P, Hoogenboom JP & Giepmans BNG. Correlated light and electron microscopy: Ultrastructure lights up! *Nat Methods*. 2015;12(6):503-513.

142. Kopek BG, Shtengel G, Xu CS, Clayton DA & Hess HF. Correlative 3D superresolution fluorescence and electron microscopy reveal the relationship of mitochondrial nucleoids to membranes. *Proc Natl Acad Sci U S A*. 2012;109(16):6136-6141.

143. Lees RM, Peddie CJ, Collinson LM, Ashby MC & Verkade P. Correlative Two-Photon and Serial Block Face Scanning Electron Microscopy in Neuronal Tissue Using 3D near-Infrared Branding Maps. *Methods in Cell Biology* . 2017;140:245-276.

144. Smith D & Starborg T. Serial block face scanning electron microscopy in cell biology: Applications and technology. *Tissue Cell*. 2019;57:111-122.

145. Perkovic M *et al.* Correlative Light- and Electron Microscopy with chemical tags. *J Struct Biol*. 2014;186(2):205-213.

146. Smith SJ. Q&A: Array tomography. *BMC Biol*. 2018;16(1):98.

147. Collman F *et al*. Mapping synapses by conjugate light-electron array tomography. *J Neurosci*. 2015;35(14):5792-5807.

148. Bloss EB *et al*. Structured Dendritic Inhibition Supports Branch-Selective Integration in CA1 Pyramidal Cells. *Neuron*. 2016;89(5):1016-1030.

149. Minter MR, Taylor JM & Crack PJ. The contribution of neuroinflammation to amyloid toxicity in Alzheimer's disease. *J Neurochem*. 2016;136(3):457-474.

150. Zamanian JL *et al.* Genomic analysis of reactive astrogliosis. *J Neurosci*. 2012;32(18):6391-6410.

151. Ugbode C *et al*. Astrocytic transporters in Alzheimer's disease. *Biochem J*. 2017;474(3):333-355.

152. Liddelow SA & Barres BA. Reactive Astrocytes: Production, Function, and Therapeutic Potential. *Immunity*. 2017;46(6):957-967.

153. Liddelow SA *et al.* Neurotoxic reactive astrocytes are induced by activated microglia. *Nature*. 2017;541(7638):481-487.

154. Franceschi C *et al.* Inflamm-aging. An evolutionary perspective on immunosenescence. *Ann N Y Acad Sci*. 2000;908:244-254.

155. Rawji KS *et al*. Immunosenescence of microglia and macrophages: Impact on the ageing central nervous system. *Brain*. 2016;139(3):653-661.

156. Spittau B. Aging microglia-phenotypes, functions and implications for age-related neurodegenerative diseases. *Front Aging Neurosci*. 2017;9:1-9.

157. Yankner BA, Lu T & Loerch P. The Aging Brain Bruce. *Annu Rev Pathol Dis*. 2008;3:67-97.

158. Johansen JS *et al.* Serum YKL-40 concentrations in patients with rheumatoid arthritis: Relation to disease activity. *Rheumatology*. 1999;38(7):618-626.

159. Junker N, Johansen JS, Andersen CB & Kristjansen PEG. Expression of YKL-40 by peritumoral macrophages in human small cell lung cancer. *Lung Cancer*. 2005;48(2):223-231.

160. Létuvé S *et al.* YKL-40 Is Elevated in Patients with Chronic Obstructive Pulmonary Disease and Activates Alveolar Macrophages. *J Immunol*. 2008;181(7):5167-5173.

161. Bonneh-Barkay D, Wang G, Starkey A, Hamilton RL & Wiley CA. In vivo CHI3L1 (YKL-40) expression in astrocytes in acute and chronic neurological diseases. *J Neuroinflammation*. 2010;7:1-8.

162. Bonneh-Barkay D *et al*. Astrocyte and macrophage regulation of YKL-40 expression and cellular response in neuroinflammation. *Brain Pathol*. 2012;22(4):530-546.

163. Dalgard CL *et al.* The cytokine temporal profile in rat cortex after controlled cortical impact. *Front Mol Neurosci*. 2012;5:1-10.

164. Llorens F *et al.* Subtype and regional-specific neuroinflammation in sporadic creutzfeldt-jakob disease. *Front Aging Neurosci*. 2014;6:198.

165. López-González I *et al*. Neuroinflammatory signals in alzheimer disease and APP/PS1 transgenic mice: Correlations with plaques, tangles, and oligomeric species. *J Neuropathol*

Exp Neurol. 2015;74(4):319-344.

166. Bhardwaj R *et al.* RelB/p50 complexes regulate cytokine-induced YKL-40 expression1. *J Immunol*. 2015;194(6):2862-2870.

167. Lian H *et al*. Astrocyte-microglia cross talk through complement activation modulates amyloid pathology in mouse models of alzheimer's disease. *J Neurosci*. 2016;36(2):577-589.

168. Schwab C & McGeer PL. Inflammatory aspects of Alzheimer disease and other neurodegenerative disorders. *Handb Infect Alzheimer's Dis*. 2017;13:27-37.

169. Llorens F et al. YKL-40 in the brain and cerebrospinal fluid of neurodegenerative dementias. *Mol Neurodegener*. 2017;12(1):1-21.

170. Moreno-Rodriguez M, Perez SE, Nadeem M, Malek-Ahmadi M & Mufson EJ. Frontal cortex chitinase and pentraxin neuroinflammatory alterations during the progression of Alzheimer's disease. *J Neuroinflammation*. 2020;17(1):1-15.

171. Wiley CA *et al.* Role for mammalian chitinase 3-like protein 1 in traumatic brain injury. *Neuropathology*. 2015;35(2):95-106.

172. Bonneh-Barkay D, Wang G, LaFramboise WA, Wiley CA & Bissel SJ. Exacerbation of Experimental Autoimmune Encephalomyelitis in the Absence of Breast Regression Protein-39/Chitinase 3-like-1. *J Neuropathol Exp Neurol*. 2012;71(11):948-958.

173. Singh SK, Bhardwaj R, Wilczynska KM, Dumur CI & Kordula T. A complex of nuclear factor I-X3 and STAT3 regulates astrocyte and glioma migration through the secreted glycoprotein YKL-40. *J Biol Chem*. 2011;286(46):29893-29903.

174. Brøchner CB & Møllgård K. SSEA-4 and YKL-40 positive progenitor subtypes in the subventricular zone of developing human neocortex. *Glia*. 2016;64(1):90-104.

175. Matute-Blanch C *et al.* Chitinase 3-like 1 is neurotoxic in primary cultured neurons. *Sci Rep*. 2020;10(1):1-6.

176. Forman MS *et al.* Transgenic mouse model of tau pathology in astrocytes leading to nervous system degeneration. *J Neurosci*. 2005;25(14):3539-3550.

177. Laurent C, Buée L & Blum D. Tau and neuroinflammation: What impact for Alzheimer's Disease and Tauopathies? *Biomed J*. 2018;41(1):21-33.

178. Laurent C *et al.* Hippocampal T cell infiltration promotes neuroinflammation and cognitive decline in a mouse model of tauopathy. *Brain*. 2017;140(1):184-200.

179. Maphis N *et al.* Reactive microglia drive tau pathology and contribute to the spreading of pathological tau in the brain. *Brain*. 2015;138(6):1738-1755.

180. Bellucci A *et al*. Induction of inflammatory mediators and microglial activation in mice transgenic for mutant human P301S tau protein. *Am J Pathol*. 2004;165(5):1643-1652.

181. Yoshiyama Y *et al.* Synapse Loss and Microglial Activation Precede Tangles in a P301S Tauopathy Mouse Model. *Neuron*. 2007;53(3):337-351.

182. Nilson AN *et al.* Tau oligomers associate with inflammation in the brain and retina of tauopathy mice and in neurodegenerative diseases. *J Alzheimer's Dis*. 2017;55(3):1083-1099.

183. Kovac A *et al*. Misfolded Truncated Protein τ Induces Innate Immune Response via MAPK Pathway. *J Immunol*. 2011;187(5):2732-2739.

184. Lee DC *et al.* LPS- induced inflammation exacerbates phospho-tau pathology in rTg4510 mice. *J Neuroinflammation*. 2010;7:1-16.

185. Bhaskar K *et al.* Regulation of tau pathology by the microglial fractalkine receptor. *Neuron*. 2010;68(1):19-31.

186. Olsson B *et al.* Microglial markers are elevated in the prodromal phase of Alzheimer's disease and vascular dementia. *J Alzheimer's Dis*. 2013;33(1):45-53.

187. Antonell A *et al.* Cerebrospinal fluid level of YKL-40 protein in preclinical and prodromal Alzheimer's disease. *J Alzheimer's Dis*. 2014;42(3):901-908.

188. Kester MI *et al.* Cerebrospinal fluid VILIP-1 and YKL-40, candidate biomarkers to diagnose, predict and monitor Alzheimer's disease in a memory clinic cohort. *Alzheimer's Res Ther*. 2015;7(1):1-9.

189. Verkhratsky A, Parpura V, Pekna M, Pekny M & Sofroniew M. Glia in the pathogenesis of neurodegenerative diseases. *Biochem Soc Trans*. 2014;42(5):1291-1301.

190. Janelidze S *et al*. CSF biomarkers of neuroinflammation and cerebrovascular dysfunction in early Alzheimer disease. *Neurology*. 2018;91(9):e867-e877.

191. Zhang H *et al.* Cerebrospinal fluid phosphorylated tau, visinin-like protein-1, and chitinase-3-like protein 1 in mild cognitive impairment and Alzheimer's disease. *Transl Neurodegener*. 2018;7(1):1-12.

192. Thompson AG *et al*. Cerebrospinal fluid macrophage biomarkers in amyotrophic lateral sclerosis. *Ann. Neurol.* 2018;83(2):258-268..

193. Alcolea D *et al.* Elevated YKL-40 and low sAPPβ:YKL-40 ratio in antemortem cerebrospinal fluid of patients with pathologically confirmed FTLD. *J Neurol Neurosurg Psychiatry*. 2019;90(8):180-186.

194. Baldacci F *et al*. The neuroinflammatory biomarker YKL-40 for neurodegenerative diseases: advances in development. *Expert Rev Proteomics*. 2019;16(7):593-600.

195. Gispert JD *et al.* CSF YKL-40 and pTau181 are related to different cerebral morphometric patterns in early AD. *Neurobiol Aging*. 2016;38:47-55.

196. Alcolea D *et al.* Amyloid precursor protein metabolism and inflammation markers in preclinical Alzheimer disease. *Neurology*. 2015;85(7):626-633.

197. Irwin DJ, Trojanowski JQ & Grossman M. Cerebrospinal fluid biomarkers for differentiation of frontotemporal lobar degeneration from Alzheimer's disease. *Front Aging Neurosci*. 2013;5:1-11.

198. Vilaplana E *et al.* Cortical microstructural correlates of astrocytosis in autosomal-dominant Alzheimer disease. *Neurology*. 2020;94(19):e2026-e2036.

199. Hardy JA & Higgins GA. Alzheimer's Disease: The Amyloid Alzheimer's disease. *Science (80-)*. 1992;256:184-185.

200. Hardy, J & Selokoe D. The Amyloid Hypothesis of Alzheimer 's Disease. *Amyloid Int J Exp Clin Investig*. 2002;297(5580):353-357.

201. Sloane JA *et al.* Lack of correlation between plaque burden and cognition in the aged monkey. *Acta Neuropathol*. 1997;94(5):471-478.

202. Erten-Lyons D *et al.* Factors associated with resistance to dementia despite high Alzheimer disease pathology. *Neurology*. 2009;72(4):354-360.

203. Lublin AL & Gandy S. Amyloid-β oligomers: Possible roles as key neurotoxins in Alzheimer's disease. *Mt Sinai J Med*. 2010;77(1):43-49.

204. Petersen RC *et al.* Criteria for Mild Cognitive Impairment Due to Alzheimer's Disease in the Community. *Ann Neurol.* 2013; 74(2): 199–208

205. Haass C & Selkoe DJ. Soluble protein oligomers in neurodegeneration: Lessons from the Alzheimer's amyloid β-peptide. *Nat Rev Mol Cell Biol*. 2007;8(2):101-112.

206. Kayed R *et al.* Common structure of soluble amyloid oligomers implies common mechanism of pathogenesis. *Science (80-)*. 2003;300(5618):486-489.

207. Cline EN, Bicca MA, Viola KL & Klein WL. The Amyloid-β Oligomer Hypothesis: Beginning of the Third Decade. *J Alzheimer's Dis*. 2018;64(s1):S567-S610.

208. Tomic JL, Pensalfini A, Head E & Glabe CG. Soluble fibrillar oligomer levels are elevated in Alzheimer's disease brain and correlate with cognitive dysfunction. *Neurobiol Dis*. 2009;35(3):352-358.

209. Viola KL & Klein WL. *Amyloid β Oligomers in Alzheimer's Disease Pathogenesis, Treatment, and Diagnosis*. Vol 129.; 2015.

210. Yang T, Li S, Xu H, Walsh DM & Selkoe DJ. Large soluble oligomers of amyloid β-protein from

alzheimer brain are far less neuroactive than the smaller oligomers to which they dissociate. *J Neurosci*. 2017;37(1):152-163.

211. Kayed R & Lasagna-Reeves CA. Molecular mechanisms of amyloid oligomers toxicity. *J Alzheimer's Dis*. 2013;33(SUPPL. 1):1-12.

212. Serra-Batiste M *et al*. Aβ42 assembles into specific β-barrel pore-forming oligomers in membrane-mimicking environments. *Proc Natl Acad Sci U S A*. 2016;113(39):10866-10871.

213. Paranjape GS, Gouwens LK, Osborn DC & Nichols MR. Isolated amyloid-β(1-42) protofibrils, but not isolated fibrils, are robust stimulators of microglia. *ACS Chem Neurosci*. 2012;3(4):238-247.

214. Walker D, Lue LF, Paul G, Patel A & Sabbagh MN. Receptor for Advanced Glycation Endproduct Modulators: A New Therapeutic Target in Alzheimer's Disease. *Expert Opin v estig Drugs*. 2015;24(3):393-399.

215. Thomas P, Summer B, Krenn V & Thomsen M. Allergy diagnostics in suspected metal implant intolerance. *Orthopade*. 2013;42(8):602-606.

216. Ungureanu AA, Benilova I, Krylychkina O, et al. Amyloid beta oligomers induce neuronal elasticity changes in age-dependent manner: A force spectroscopy study on living hippocampal neurons. *Sci Rep*. 2016;6(April):1-13.

217. Economou. NJ, Giammona MJ, Thanh D. Do XZ, Teplow DB, Buratto SK, Bowers MT. Amyloid β-protein assembly and Alzheimer's disease: Dodecamers of Aβ42, but not of Aβ40, seed fibril formation Nicholas. *J Am Chem Soc*. 2016;138(6):1772-1775.

218. Wei Qiang1, † W-MY, Jun-Xia Lu1, † JC, & Robert Tycko. Structural variation in amyloid-β fibrils from Alzheimer's disease clinical subtypes. *Nature*. 2017;541(7636):217-221.

219. Liu J *et al.* Amyloid structure exhibits polymorphism on multiple length scales in human brain tissue. *Sci Rep*. 2016;6(September):1-11.

220. Ding Y *et al.* Amyloid Beta Oligomers Target to Extracellular and Intracellular Neuronal Synaptic Proteins in Alzheimer's Disease. *Front Neurol*. 2019;10:1-16.

221. Lasagna-Reeves CA, Glabe CG & Kayed R. Amyloid-β annular protofibrils evade fibrillar fate in Alzheimer disease brain. *J Biol Chem*. 2011;286(25):22122-22130.

222. Lesné SE *et al.* Brain amyloid-β oligomers in ageing and Alzheimer's disease. *Brain*. 2013;136(5):1383-1398.

223. Lu JX *et al.* XMolecular structure of β-amyloid fibrils in alzheimer's disease brain tissue. *Cell*. 2013;154(6):1257.

224. Noguchi A *et al.* Isolation and characterization of patient-derived, toxic, high mass Amyloid β-

protein (Aβ) assembly from Alzheimer disease brains. *J Biol Chem*. 2009;284(47):32895-32905.

225. Shankar GM *et al.* Amyloid β-Protein Dimers Isolated Directly from Alzheimer Brains Impair Synaptic Plasticity and Memory. *Nat Med*. 2008;14(8):837-842.

226. Pawley J. Handbook of Biological Confocal Microscopy. *Springer Sci + Bus Media*. 2006.

227. Koffie RM *et al.* Oligomeric amyloid β associates with postsynaptic densities and correlates with excitatory synapse loss near senile plaques. *Proc Natl Acad Sci U S A*. 2009;106(10):4012-4017.

228. Jackson RJ *et al.* Clusterin accumulates in synapses in Alzheimer's disease and is increased in apolipoprotein E4 carriers. *Brain Commun*. 2019;1(1):1-12.

229. Li S *et al.* Soluble Oligomers of Amyloid β Protein Facilitate Hippocampal Long-Term Depression by Disrupting Neuronal Glutamate Uptake. *Neuron*. 2009;62(6):788-801.

230. Li S *et al.* Soluble a β oligomers inhibit long-term potentiation through a mechanism involving excessive activation of extrasynaptic NR2B-containing NMDA receptors. *J Neurosci*. 2011;31(18):6627-6638.

231. Muckle L & Sekloe D. Neurotoxicity of Amyloid β -Protein : Synaptic and Network. *Cold Spring Harb Perspect Med*. Published online 2012:1-17.

232. Klein WL. Synaptotoxic amyloid-β oligomers: A molecular basis for the cause, diagnosis, and treatment of Alzheimer's disease? *J Alzheimer's Dis*. 2013;33(SUPPL. 1).

233. Spires TL *et al.* Dendritic spine abnormalities in amyloid precursor protein transgenic mice demonstrated by gene transfer and intravital multiphoton microscopy. *J Neurosci*. 2005;25(31):7278-7287.

234. Spires-Jones TL *et al.* Impaired spine stability underlies plaque-related spine loss in an Alzheimer's disease mouse model. *Am J Pathol*. 2007;171(4):1304-1311.

235. Spires-Jones TL *et al.* Passive immunotherapy rapidly increases structural plasticity in a mouse model of Alzheimer disease. *Neurobiol Dis*. 2009;33(2):213-220.

236. Holcomb L *et al.* Accelerated Alzheimer-type phenotype in transgeic mice carrying both mutant amyloid precursor protein and presenilin 1 transgenes. *Nat Med*. 1998:97-100.

237. Hsia AY *et al.* Plaque-independent disruption of neural circuits in Alzheimer ' s. *Neurobiology*. 1999;96:3228-3233.

238. Mucke L *et al*. High-Level Neuronal Expression of Aβ1–42 in Wild-Type Human Amyloid Protein Precursor Transgenic Mice: Synaptotoxicity without Plaque Formation. *J Neurosci*. 2000;20(11):4050-4058.

239. Balducci C *et al.* Cognitive deficits associated with alteration of synaptic metaplasticity precede plaque deposition in AβPP23 transgenic mice. *J Alzheimer's Dis*. 2010;21(4):1367-1381.

240. Cleary JP *et al.* Natural oligomers of the amyloid-β protein specifically disrupt cognitive function. *Nat Neurosci*. 2005;8(1):79-84.

241. Lesné S *et al.* A specific amyloid-β protein assembly in the brain impairs memory. *Nature*. 2006;440(7082):352-357.

242. Poling A *et al.* Oligomers of the amyloid-β protein disrupt working memory: Confirmation with two behavioral procedures. *Behav Brain Res*. 2008;193(2):230-234.

243. Balducci C *et al.* Synthetic amyloid-β oligomers impair long-term memory independently of cellular prion protein. *Proc Natl Acad Sci U S A*. 2010;107(5):2295-2300.

244. Freir DB *et al.* Aβ oligomers inhibit synapse remodelling necessary for memory consolidation. *Neurobiol Aging*. 2011;32(12):2211-2218.

245. Bateman RJ *et al.* Autosomal-dominant Alzheimer's disease: A review and proposal for the prevention of Alzheimer's disease. *Alzheimer's Res Ther*. 2011;2(6):1-13.

246. Pera M *et al.* Distinct patterns of APP processing in the CNS in autosomal-dominant and sporadic Alzheimer disease. *Acta Neuropathol*. 2013;125(2):201-213.

247. McLean CA *et al.* Soluble pool of Aβ amyloid as a determinant of severity of neurodegeneration in Alzheimer's disease. *Ann Neurol*. 1999;46(6):860-866.

248. Lee EB *et al.* Targeting amyloid-β peptide (Aβ) oligomers by passive immunization with a conformation-selective monoclonal antibody improves learning and memory in Aβ precursor protein (APP) transgenic mice. *J Biol Chem*. 2006;281(7):4292-4299.

249. Dubois B *et al.* Revising the definition of Alzheimer's disease: A new lexicon. *Lancet Neurol*. 2010;9(11):1118-1127.

250. Peters F *et al.* BACE1 inhibition more effectively suppresses initiation than progression of β-amyloid pathology. *Acta Neuropathol*. 2018;135(5):695-710.

251. Barão S, Moechars D, Lichtenthaler SF & De Strooper B. BACE1 Physiological Functions May Limit Its Use as Therapeutic Target for Alzheimer's Disease. *Trends Neurosci*. 2016;39(3):158-169.

252. Yan R & Vassar R. Targeting the β secretase BACE1 for Alzheimer's disease therapy. *Lancet Neurol*. 2014;13(3):319-329.

253. Yan R. Physiological functions of the β-site amyloid precursor protein cleaving enzyme 1 and 2. *Front Mol Neurosci*. 2017;10:1-12.

254. Vassar R. Editorial: Implications for BACE1 Inhibitor Clinical Trials: Adult Conditional BACE1 Knockout Mice Exhibit Axonal Organization Defects in the Hippocampus. *J Prev Alzheimer's Dis*. 2019;6(2):78-84.

255. Ou-Yang MH *et al.* Axonal organization defects in the hippocampus of adult conditional BACE1 knockout mice. *Sci Transl Med*. 2018;10(459).

256. Hitt B *et al.* β-Site amyloid precursor protein (APP)-cleaving enzyme 1 (BACE1)-deficient mice exhibit a close homolog of L1 (CHL1) loss-of-function phenotype involving axon guidance defects. *J Biol Chem*. 2012;287(46):38408-38425.

257. Blume T *et al.* BACE1 Inhibitor MK-8931 Alters Formation but Not Stability of Dendritic Spines. *Front Aging Neurosci*. 2018;10(July):1-7.

258. Hadley KC *et al.* Determining composition of micron-scale protein deposits in neurodegenerative disease by spatially targeted optical microproteomics. *Elife*. 2015;4(September2015):1-21.

259. Kandalepas PC *et al*. The Alzheimer's β-secretase BACE1 localizes to normal presynaptic terminals and to dystrophic presynaptic terminals surrounding amyloid plaques. *Acta Neuropathol*. 2013;126(3):329-352.

260. Tai HC *et al*. The synaptic accumulation of hyperphosphorylated tau
oligomers in alzheimer disease is associated with dysfunction of the ubiquitin-proteasome system. *Am J Pathol*. 2012;181(4):1426-1435.

261. Zhou L *et al.* Tau association with synaptic vesicles causes presynaptic dysfunction. *Nat Commun*. 2017;8(May):1-13.

262. Wei W *et al*. Amyloid beta from axons and dendrites reduces local spine number and plasticity. *Nat Neurosci*. 2010;13(2):190-196.

263. Mabonga L & Kappo AP. Protein-protein interaction modulators: advances, successes and remaining challenges. *Biophys Rev*. 2019;11(4):559-581.